Studies on heme-based redox enzymes from *Aspergillus terreus* MTCC 6324 and their potential applications for bioelectronic devices

A Thesis

Submitted by

Preety Vatsyayan

For the award of the degree

of

Doctor of Philosophy

Department of Biotechnology

Indian Institute of Technology Guwahati

Guwahati-781039, Assam, India.

June 2010

Dedicated to my beloved Parents

Department of Biotechnology

INDIAN INSTITUTE OF TECHNOLOGY GUWAHATI

STATEMENT

I do hereby declare that the matter embodied in this thesis is the result of investigations carried out by me in the Department of Biotechnology, Indian Institute of Technology Guwahati, India, under the guidance of Prof. Pranab Goswami.

In keeping with the general practice of reporting scientific observations, due acknowledgements have been made wherever the work described is based on the findings of other investigators.

June, 2010. Preety Vatsyayan

DEPARTMENT OF BIOTECHNOLOGY

Indian Institute of Technology Guwahati
Guwahati 781 039, Assam, INDIA

Dr. Pranab Goswami,
Professor

Tel: +91-(0)361 2582202
Fax:+91-(0)361 2582249/2690762
Email: **pgoswami@iitg.ernet.in**

Date: 10.06.2010

CERTIFICATE

This is to certify that the thesis entitled "**Studies on heme-based redox enzymes from *Aspergillus terreus* MTCC 6324 and their potential applications for bioelectronic devices**", that is being submitted by **Ms. Preety Vatsyayan (Roll No. 06610606)** for the award of degree of Doctor of Philosophy is an authentic record of the results obtained from the research work carried out under my supervision in the Department of Biotechnology, Indian Institute of Technology Guwahati, India.

The results embodied in this thesis have not been submitted to any other University or Institute for the award of any degree.

June, 2010.

(Pranab Goswami)

(Research Supervisor)

ACKNOWLEDGEMENTS

First of all, I want to acknowledge my thesis supervisor Prof. Pranab Goswami for his constant support and guidance throughout the years of my work. I sincerely thank him for giving me an opportunity to work in his lab, his valuable time and suggestions which aided a lot in completing my work on time.

I would also like to thank my Doctoral Committee members, Dr. Utpal Bora, Dr. K. Pakshirajan and Dr. Anil Verma for helping me in improving my work with their critical suggestions.

I am grateful to other faculty members, office staff and my colleagues from Dept. of Biotechnology for their constant support and help. My special acknowledgements are to Head (Prof. P. Mahanta) and staff members of Center for Energy for accommodating me so well and allowing me to work there for last one year. Besides, I also want to thank members from other Departments (Chemistry, especially Dr. Mrs. Papori Goswami; and Chemical Engineering), and Central Instrumentation Facility (CIF) for allowing me to utilize their facilities time to time.

I thank Dept. of Science and Technology (DST), Ministry of Human Resource and Development (MHRD), Gov. of India and Indian Institute of Technology Guwahati for providing all the financial assistances to carry out my research smoothly.

I would like to express my gratitude to my colleagues from our research group Lepakshi di, Kiran, Urmila, Seraj, Sandip, Shushovan, Madhuri, Mitun, Ankana, Vishwa and Reddy for their help and suggestions. A special mention to Lepakshi di, Kiran, Urmila and Sandip who were always there for me with their unconditional support.

My heartiest thanks to my friends in hostel Priyanka, Vigya, Mithilesh, Urmila and Rachana who made my stay here a pleasant trip.

I want to thank my family for showing their constant support and believe in me and God for giving me the courage to complete my work. A special thanks to Shantanu (Nishu) for being with me from last few months of thesis writing.

Preety Vatsyayan

June 2010

ABSTRACT

The cytochrome P450 monooxygenase (CYP) activity in the cells of *Aspergillus terreus* MTCC 6324 was localized in the cytosol of *n*-hexadecane grown cells, while, it was apparently distributed in light mitochondrial and microsomal fractions of glucose grown cells. The substrate specificities of CYP present in all these locations were similar irrespective of the substrates used for the growth. CYP activities with different category of substrates namely, alkanes, alkane derivatives, alcohols, aromatic compounds, organic solvents, and steroids were detected in the cells. High specific activity of CYP was observed when methanol (5.60±0.20 U mg^{-1}), acetone (7.76±0.20 U mg^{-1}), DMSO (9.70±0.50 U mg^{-1}), *n*-hexadecane (4.39±0.05 U mg^{-1}) and *n*-octadecane (4.23±0.10 U mg^{-1}) were used as substrates. Significant CYP activity was also detected when naphthalene (3.80±0.20 U mg^{-1}) was used as substrate. The CYP catalysis of *n*-hexadecane had followed both terminal and sub terminal oxidations. Heme staining of the microsomal fraction containing CYP and other proteins in SDS–PAGE showed single heme protein band with corresponding molecular weight of 110 kDa. A high level of cellular large catalase (CAT) was also detected in the cells during growth of *A. terreus* on *n*-hexadecane, with total activity 17×10^6 U gm^{-1} dry cell-mass. A 160-fold purification with specific activity of around 66×10^5 U mg^{-1} protein in comparison to the original crude extract was achieved. The native protein molecular mass was 368±5 kDa with subunit molecular mass nearly 90 kDa, which indicates that the native CAT protein is a homotetramer. The isoelectric pH (*pI*) of the purified CAT was 4.2. Peptide mass fingerprinting studies confirmed its identity as catalase B (large catalase). The heme was identified as heme b by ESI-MS/MS. CAT was active in a broad range of pH 4.0 to 12.0 and temperatures 25ºC to 90ºC. The catalytic efficiency (K_{cat}/K_m) of

4.7×10^8 M^{-1} s^{-1} and alkaline pH stability ($t_{½}$ at pH 12.0 ~15 months) of CAT are considerably higher than most of the extensively studied catalases from different sources. The storage stability ($t_{½}$) of CAT at physiological pH 7.5 and 4°C was nearly 30 months. These high activity and stability under broad thermal and pH conditions are construed as the attractive properties of CAT for potential industrial applications. The stability of CAT, however, decreased with decreasing pH and eventually lost at pH 3.0. The highest stability ($t_{½}$) in the acidic range was at pH 6.0 and it was 38% less than the lowest $t_{½}$ obtained in the alkaline pH range. The intensity of the Soret peak (405 nm) of the heme integrated CAT incubated at pH 12.0, 4.0, and 3.0 were decreased by 10%, 32% and 51%, respectively, from the value obtained at pH 7.5 where the highest CAT stability was recorded. Typical cyclic voltammetric peaks for Fe^{3+}/Fe^{2+} redox couple of CAT immobilized on GCE/MWCNT-NF/PEI with formal potential ($E°$) -0.45 V (vs. Ag/AgCl reference) were detected at pH 7.5. Negative and positive shifts of $E°$ towards alkaline- and acidic-pH, respectively, were detected. A significant increase in redox current of CAT in the acidic pH range was observed. This upsurge current is attributed to the increased electron transfer between the electrode and the heme released on the surface of the electrode as a result of its disintegration from the insulating protein matrix. The heme isolated from CAT at acidic pH was again reconstituted with apo-CAT only at alkaline denaturing condition to a detectable Soret peak and CAT activity. These findings revealed that the acidic pH promotes disintegration of the heme prosthetic group in the CAT protein and is suggested to destabilize CAT under acidic environment. CAT was also found to be exceptionally stable at wide range of temperatures with $t_{½}$ of 15 days at 40°C, 20 h at 60°C and 42 minutes at 80°C. The CAT activity was completely lost when boiled. The thermal dissociation rate of the heme from protein matrix at 80ºC was 3.14 ± 0.20 h^{-1} for first 5 min followed by 0.39 ± 0.07 h^{-1}. Considering these bright properties of

CAT, a detailed investigation on the direct electrochemistry and electro-catalytic properties of CAT immobilized on MWCNT-NF/PEI modified GCE was carried out to explore its bioelectronics application potential. The surface coverage of CAT immobilized on GCE/MWCNT-NF/PEI was approximately 2.1×10^{-10} mol cm^{-2}. The electron transfer rate constant (*Ks*) of 1.05±0.2 s^{-1} was observed for the bioelectrode, indicating facilitation of the electron transfer between CAT and GCE. Assembly of CAT and PEI layer over MWCNT/NF composite showed a considerable decrease in the overall charge transfer resistance (R_{ct}). GCE/MWCNT-NF/CAT/PEI exhibited a remarkable electro-catalytic activity toward the reduction of hydrogen peroxide (H_2O_2). The apparent Michaelis–Menten constant (K_m´) for the fabricated bioelectrode, was calculated as 3 mM H_2O_2. The biosensor response increased linearly with H_2O_2 concentrations from 10 µM to 5 mM. The response time for steady state current and detection limit were ~2 s and 1 µM H_2O_2, respectively. A high operational and storage stability was observed for the self assembled bioelectrode. Thus, an efficient electrical conductivity between the redox centre of CAT and electrode was confirmed following the current immobilization method which was further adapted to immobilize microsomal CYP from *A. terreus* to investigate its direct electrochemistry and electro-catalytic properties. A pair of well defined and nearly reversible cyclic voltammetric peaks for Fe^{3+}/Fe^{2+} redox couple of CYP immobilized on MWCNT-NF/PEI modified GCE, with $E°$ of about -0.53 V (vs. Ag/AgCl reference electrode) in pH 8.0 buffer was observed under deoxygenated condition. In the presence of oxygen and substrate, the redox potential of the bioelectrode was shifted to -0.475 V. Electro-catalytic current with *n*-hexadecane and inhibition studies with PBO confirmed the involvement of $Fe^{3+/2+}$ system of CYP in the redox process. The bioelectrode exhibited a remarkable electro-catalytic activity towards the *n*-hexadecane substrate. The current response

increased linearly from 1 µM to 100 µM of substrate with detection limit 0.1 µM *n*-hexadecane. The IC_{50} for PBO was 2.7 µM. The surface coverage of CYP immobilized on MWCNT-NF/PEI modified GCE was approximately 3.45×10^{-10} mol cm^{-2}, suggesting enzyme monolayer formation. The *Ks* was 1.0±0.2 s^{-1}, indicating facilitation of the electron transfer between CYP and GCE. A significant positive shift in the redox potential of CYP in the presence of oxygen and substrate is one of the interesting finding, which supports the theory of thermodynamic switch present in CYP catalytic systems. The results have established the potentials of CYP and CAT from *A. terreus* for their applications in bioelectronic devices, such as biosensors/bio-fuel cells.

CONTENTS

LIST OF FIGURES

LIST OF TABLES

LIST OF SCHEMES

ABBREVIATIONS

×*g* ……	Relative centrifugal force
AFM ……...	Atomic force microscopy
Apo-CAT …….	Apo-catalase
BLAST ……	Basic local alignment search tool
BOM ……	Biological oxygen monitor
BSA …….	Bovine serum albumin
CAT …….	Large catalase from *A. terreus*
CBB …….	Coomassie brilliant blue
$CDCl_3$ ……..	Deuterated chloroform
CO ……...	Carbon monoxide
CV ……...	Cyclic voltammetry
CYP …….	Cytochrome P450 monooxygenase
DET ……	Direct electron transfer
DPV ……	Differential pulse voltammetry
DMSO ……	Dimethyl sulfoxide
DTT …….	Dithiothretol
EC ……	Enzyme commission
EDTA ……..	Ethylenediamine tetraacetic acid
EDX …….	Energy dispersive X-ray spectroscopy
EIS ……...	Electrochemical impedance spectroscopy
EPR ……..	Electron paramagnetic resonance spectroscopy
ESI-MS ……	Electrospray ionization- mass spectroscopy
FAD …….	Flavin adenine dinucleotide
$FADH_2$ …….	Flavin adenine dinucleotide (reduced)
FMN ……	Flavin mononucleotide
FPLC ……...	Fast performance liquid chromatography
FTIR ……	Fourier transform infrared spectroscopy
GCE …….	Glassy carbon electrode

HIC ……..	Hydrophobic interaction chromatography
HPLC ……...	High performance liquid chromatography
HRP …….	Horseradish peroxidase
LC-MS/MS ……..	Liquid chromatography-tandem mass spectroscopy
MTCC ……..	Microbial type culture collection
MWCNT ……..	Multiwalled carbon nanotubes
$NAD(P)^+$ ……..	Nicotinamide adenine dinucleotide phosphate (oxidized)
NAD(P)H ……	Nicotinamide adenine dinucleotide phosphate (reduced)
NAD^+ ……..	Nicotinamide adenine dinucleotide (oxidized)
NCP …….	NAD(P)H cytochrome P450 reductase
NF ……	Nafion®
NMR ……	Nuclear magnetic resonance spectroscopy
PAS ……..	Periodic acid Schiff
PBO …….	Piperonyl butoxide
PEI ……...	Polyethyleneimine
PMSF ……...	Phenyl methane sulphonyl fluoride
R_f …….	Retention factor
RH ……...	Alkane
ROH ……	Alcohol
ROS …….	Reactive oxygen species
SCAO ……..	Short chain alcohol oxidase
SDS-PAGE ……..	Sodium dodecyl sulfate-polyacrylamide gel electrophoresis
SEC ……..	Size exclusion chromatography
SPB ……..	Sodium phosphate buffer
$t_{½}$ ……..	Half-life
TCA …….	Trichloro acetic acid
TLC …….	Thin layer chromatography
tris ……	Tris(hydroxymethyl)aminomethane
UV-Vis ……	UV-Vis spectroscopy

Chapter1

Introduction

Redox enzymes are biological catalysts, which can carry out oxidation and reduction of a substrate or a group of substrates with the addition or removal of a proton (H^+) or electron (e^-). Enzymes mostly included in this class are dehydrogenases, oxidases, monooxygenases, dioxygenases, peroxidases, catalases etc. The diverse chemical transformations (typically oxidation, monooxygenation, peroxidation etc.) catalyzed by these enzymes make them prime targets for exploitation by the emerging biotechnology industries (Heuvel et al. 2001; Beilen and Funhoff 2005). Furthermore, the potentials of these redox enzymes for direct electron transfer to electrodes have already attracted much interest of the researchers for their applications in the construction of bioelectrodes for biosensor and biofuel cell development (Ikeda 1992; Azevedo et al. 2005; Bistolas et al. 2005; Jiang et al. 2008). Among these, heme- based redox enzymes constitute an extensively exploited group for biotechnological applications due to their efficient catalysis, diversity of biotransformation, potent redox centers and fast electron transport kinetics. Besides, their strong affinity towards oxygen and reactive oxygen species, large spectral changes associated with the heme-protein interactions and direct electron transfer capacity of their heme-Fe^{3+}/Fe^{2+} redox center, make them an efficient tool for mechanistic and structure- function studies. Thus, the heme- based redox enzymes have attracted the interests of the researchers for their both practical and theoretical implications. Searching novel sources of these enzymes is a continuing thrust with a hope of exploring enzymes bearing novel characteristics or improved catalytic properties (viz. stability, specificity, catalytic efficiency, substrate range etc.). Fungi of

the genus *Aspergillus* are widespread and abundant in terrestrial ecosystem due to their capability to utilize a wide variety of carbon substrates for growth and survival (Britton 1984; Dashti et al. 2008). Hence the presence of novel enzymes in the metabolic pathways involved in the degradation of such diverse substrates in the cells of *Aspergillus* strains may be argued. Through the work done in our laboratory during recent past, a novel broad substrate specific alcohol oxidase has already been isolated from *Aspergillus terreus* and its novel functional and protein chemical characteristics have been reported (Kumar and Goswami 2006, 2008). The findings on these novel functional properties of the alcohol oxidase prompted us to believe the existence of other redox enzymes bearing novel catalytic properties that co-ordinate the function of alcohol oxidase for completing the metabolic task safely, during degradation of such broad range of substrates by this fungus. In this regard, cytochrome P450 monooxygenase and catalase have drawn our attention. Cytochrome P450 monooxygenase is the foremost enzyme involved in the oxy-functionalization of substrates like aliphatic hydrocarbons to corresponding alcohols, while catalase is expected to be produced to neutralize large amounts of H_2O_2 formed during oxidations of the generated alcohols by alcohol oxidase. We have however, restricted our studies on some critical functional and biochemical analysis and based on these finding, we have extended our work for the fabrication of enzyme electrodes for biosensor/biofuel cell applications.

Major objectives of the work

- Isolation of two different heme- based redox enzymes, namely cytochrome P450 monooxygenase and catalase from *Aspergillus terreus* MTCC 6324 and their characterization with respect to their functional properties including substrate specificities and optimum conditions for activities.
- Protein-chemical characteristics, stability, reconstitution and inhibition studies of the isolated redox enzymes.
- Development of suitable electroactive and biocompatible matrix for immobilization of enzymes on electronic units.
- Characterization of the fabricated bioelectrodes and to evaluate their potentials for biosensor/biofuel cell applications.

To accomplish these objectives the studies in this thesis have been divided into the following experimental chapters starting from chapter 2 to chapter 6. The literature reviews are included in each chapter for better focus on the state-of-art of the individual section of the research work:

Chapter 2: Isolation, protein-chemical and functional characterization of cytochrome P450 monooxygenase (CYP) from *Aspergillus terreus*

This chapter describes the isolation and sub-cellular localization of CYP during growth of the *A. terreus* MTCC 6324 on different substrates. The broad substrate specificities and optimum

physical and chemical parameters for enzyme activity and stability are also presented. Terminal and sub-terminal modes of CYP catalysis have also been elucidated in this chapter.

Chapter 3: Isolation, purification, protein-chemical and functional characterization of catalase (CAT) from *Aspergillus terreus*

In this chapter a cellular large catalase (CAT) of distinct kinetic properties and stability was isolated, purified and characterized from a hydrocarbon degrading *A. terreus* MTCC 6324.

Chapter 4: Stability and heme dissociation studies of CAT

This chapter includes the investigation on the stability of isolated CAT over a wide range of pH and temperature conditions. The stability of the heme in the protein matrix under the broad pH range was investigated following absorption spectroscopy as well as electrochemical studies. Further studies on the separation of heme from the CAT protein and its reconstitution with the generated apo-CAT to a functionally active CAT were conducted. The stability of the heme-protein integration was also analyzed at high temperature and presented in this chapter.

Chapter 5: Fabrication and characterization of CAT bioelectrode

The studies in this chapter include the fabrication of the CAT bioelectrode on GCE using MWCNT-NF/PEI matrix and determination of redox potential of CAT. The bioelectrode was further characterized for its electron conductivity, resistance to charge transfer, bio-electrocatalysis and stability for its application as biosensor.

Chapter 6: Fabrication and characterization of CYP bioelectrode

In this chapter, the fabrication of CYP bioelectrode and its direct electrochemistry were studied. Further investigation was carried out to understand the bio-electrocatalytic response of the CYP bioelectrode towards *n*-hexadecane substrate and the findings on these studies are also incorporated in this chapter.

Chapter 2

Isolation, protein-chemical and functional characterization of cytochrome P450 monooxygenase (CYP) from *Aspergillus terreus*

2.1. Overview

Microbial monooxygenase/hydroxylase enzymes involved in the metabolism of endogenous and xenobiotic compounds have potential application in many areas such as, bioremediation of petroleum hydrocarbon contaminations (Mfincnerovfi and Augustin 1994) organic synthesis, and production of pharmaceutically and other industrially useful compounds (Beilen and Funhoff 2005; Bistolas et al. 2005). The microbial sources for these enzymes are mostly reported from several bacterial species (Britton 1984), and yeasts such as *Candida sp.* (Scheller et al. 1996). Searching novel source of these enzymes is a continuing thrust with a hope of exploring enzymes of unusual catalytic properties. Research on filamentous fungi for the monooxygenases has not yet received adequate attention as revealed from the limited literature available on the area. *Fusarium oxysporum* (Nakayama and Shoun 1994; Nakayama et al. 1996) and *Cladosporium resinae* (Goswami and Cooney 1999) are some of the fungi only where progress is recorded to a greater extent. The filamentous fungus that belongs to the species *Aspergillus* is wide spread in nature and utilizes substrates of diverse chemical character. Since, monooxygenases are the foremost enzymes involved in the microbial metabolism of many such

substrates, the fungal cells of *Aspergillus* is likely to hold enzymes such as, cytochrome P450 monooxygenase (CYP), with novel catalytic properties having potential industrial applications.

We report here the presence of CYP activities with broad substrate specificities in the cells of *Aspergillus terreus*. The localization of these enzymes in the sub-cellular sites during growth of the fungi in different substrates is also presented in this chapter.

2.2. Literature Review

Cytochrome P450 was initially reported as a microsomal membrane-bound heme-protein without known physiological functions and was characterized by a unique 450 nm optical absorption peak of its carbon monoxide-bound form, which was originally reported as the spectrum of a novel "microsomal carbon monoxide-binding pigment" (Klingenberg 1958). The term "cytochrome P450" first appeared in literature in 1962 with full accounts of the work published in 1964 by Omura and Sato (1962, 1964a, 1964b). Elucidation of its function as the oxygenase in 1963 by Estabrook and his coworkers (Estabrook et al. 1963) triggered rapid expansion of research on this hemoprotein (Omura 1999).

Cytochrome P450 monooxygenase (CYP) (EC 1.14.x.x) forms a large family of heme enzymes that catalyzes a diverse chemical reactions such as epoxidation, hydroxylation and heteroatom oxidation (Scheme 2.2.1). The enzymes are involved in the metabolism of many drugs and xenobiotics and are responsible for bioactivation (Poulos 1995; Lewis 1996; Ortiz de Montellano and De Voss 2005).

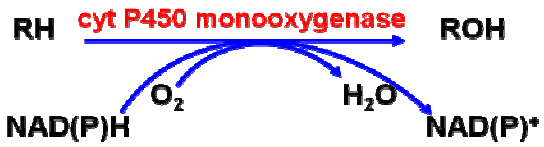

Scheme 2.2.1. Reaction depicting the CYP catalysis.

The catalytic cycle of CYP is initiated by substrate (RH) binding to the native, predominantly low spin, hexacoordinate, ferric form I, converting it to the high spin, pentacoordinate ferric complex II (Scheme 2.2.2). One electron reduction of II yields the high-spin, pentacoordinate ferrous complex III. Complex III subsequently binds dioxygen (O_2) to form a `semistable' low spin, hexacoordinate ferrous-O_2 adduct IV. Species I-IV of the P450 cycle and the low spin, hexacoordinate ferrous-CO inhibitor complex V have been isolated and well characterized. It is hypothesized that such species as a low spin, ferric peroxycomplex VI, and oxyferryl (Fe^{IV}=O) intermediate VII, are further formed. Oxygen atom transfer from VII to the substrate yields oxidized product (ROH) and regenerates state I. In the presence of external oxygenation agents, such as peroxides, the complex II may directly yield state VII *via* a `shunt' pathway. Species I, II and VII are neutral, while the overall charge of species III, IV and V is -1 and of species VI is -2 (White and Coon 1980; Andersson and Dawson 1991).

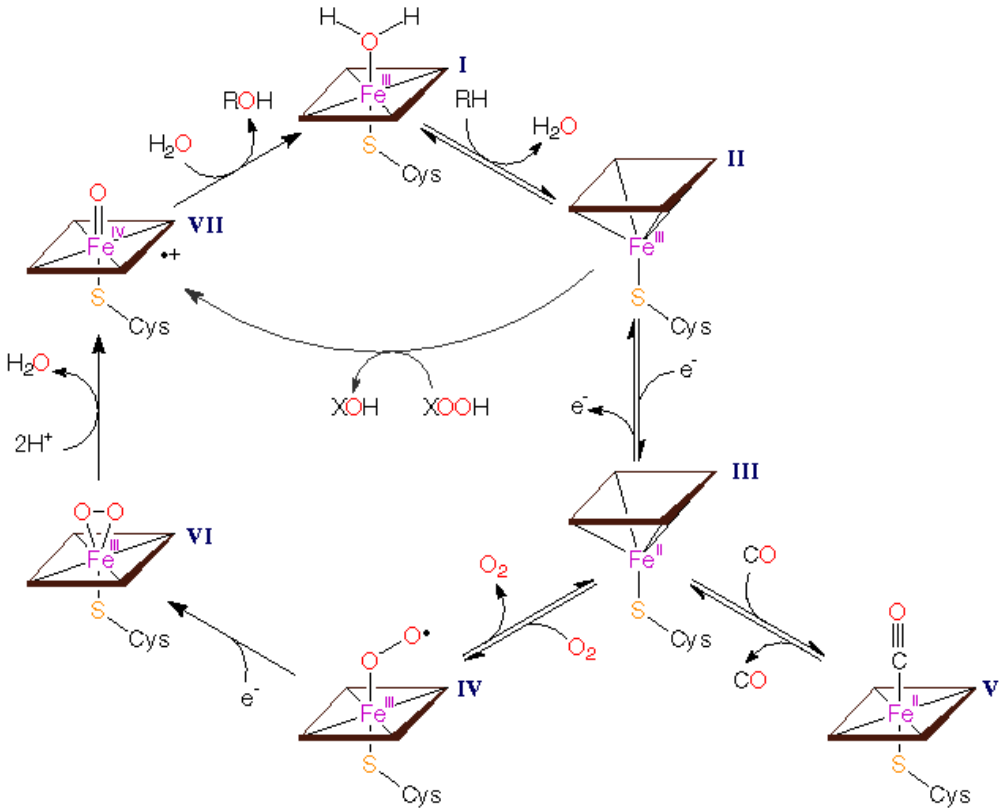

Scheme 2.2.2. Reaction cycle depicting the mechanism of CYP catalysis.

(Adapted from http://metallo.scripps.edu/promise/CYTOCHROMES.html)

In eukaryotic system, the CYP catalysis requires another component, NAD(P)H cytochrome P450 reductase (NCP) which catalyzes the transfer of electrons from NAD(P)H to the CYP catalytic cycle. NCP belongs to the diflavin reductase family (Smith et al. 1994). The diflavin reductases are thought to have evolved through the fusion of FMN- and FAD-containing flavoproteins, flavodoxin, and ferredoxin reductase, respectively (Porter and Kasper 1986). NCP has a membrane anchoring region, the FMN-binding domain, and the FAD- and NAD(P)H-binding domains joined by a linker region that supposedly allows for efficient electron transfer (Wang et al. 1997). The electroactive component of P450 enzymes is an iron-protoporphyrin IX

(heme), which is bound with the rest of the protein with thiol group of cystein, so called heme-thiolate enzyme. The structural elements that form the active-site region (or pocket) controlling the substrate specificity, can vary substantially giving P450s a diverse substrate range (Poulos 2005).

CYP have pivotal roles in primary and secondary metabolic pathways and drug degradation and bioremediation of toxic wastes. They have long been the focus of chemists and biochemists because of their extraordinary ability to introduce oxygen into non-activated carbon– hydrogen bonds, regio- and stereo-selectively. Some of these enzymes have a narrow substrate spectrum, for example, P450s involved in anabolic pathways, such as the synthesis of steroids in mammals or secondary metabolites in plants, whereas other P450s (for instance, microsomal-derived) are involved in detoxification of xenobiotics, convert many different substrates (Guengerich 1991). Bacterial CYP often show higher stability, activity and better expression rates in recombinant hosts, however the substrate spectra and reactions catalyzed by eukaryotic P450s are often more amenable to industrial applications (Urlacher and Eiben 2006).

Many different forms of CYP are present in all eukaryotic organisms, namely, animals, plants and fungi, and that some prokaryotes also have CYP (Stoilov et al. 2001). CYP of eukaryotic organisms are all bound to the membranes of endoplasmic reticulum (Nakayama and Shoun 1994; Scheller et al. 1996) or cell membrane (Schnuck et al. 1983), whereas most bacterial P450s are water-soluble such as cytochrome $P450_{cam}$.

Purification of a soluble bacterial P450, $P450_{cam}$ of *Pseudomonas putida,* was achieved in 1970 (Dus et al. 1970), but the membrane-bound P450s of animal and plant sources were difficult to purify in the beginning mainly due to their instability to solubilization treatments with detergents. Lately, some of the successes have been achieved with the reconstitution of purified

CYP in phospholipid membrane (Lu et al. 1972; Coon 2005) but still the process is cumbersome and is unable to recover the complete activity of CYP which involves other components such as, NCP for its activity.

CYP are involved in oxidation of a variety of substrates including long chain alkanes, fatty acids, steroids, drugs, aromatic hydrocarbons etc. (Mfincnerovfi and Augustin 1994; Omura 1999). The broad substrate specificities of CYP from different sources have been widely reported (Coon 2005), mostly from bacteria (Lentz et al. 2004), yeast (Eschenfeldt et al. 2003), plant (Zhu et al. 2006) and mammals (Ito et al. 2006), while there are other reports on highly specific CYP (Dus et al. 1970). CYP capable of both terminal and sub-terminal oxidations of long chain alkanes have been reported from bacteria and yeast (Beilen and Funhoff 2005) while, the same has not been studied adequately from filamentous fungi.

2.3. Experimental approaches

2.3.1. Organism and culture conditions

The fungal strain *Aspergillus terreus* used in this investigation was isolated from the oil contaminated soil sample, collected from an oil field of Assam, by enrichment culture using *n*-hexadecane as the sole source of carbon as described by our research group elsewhere (Kumar and Goswami 2006; Kumar et al. 2010). The purification of the fungi was done in fungal agar plates (Fig. 2.6.1A). The pure colonies formed on the plates were transferred to fungal agar slants and incubated at 28°C. The organism was maintained on fungal agar slants with periodic transfer to a new slant following every 15 days. The pure fungal strain was identified as *A.*

terreus and submitted to the Microbial Type Culture Collection (MTCC), Chandigarh with accession number 6324. The organism was cultivated in 500-ml Erlenmeyer flasks containing 2% *n*-hexadecane/glucose in 50 ml of basal medium (Bushnell and Haas 1941) of the following compositions (g l^{-1}): $MgSO_4$.$7H_2O$, 0.2; NH_4NO_3, 1.0; $CaCl_2$, 0.02; KH_2PO_4, 1.0; K_2HPO_4, 1.0; and yeast extract, 1.0. The pH of the medium was adjusted to 5.8 and the flasks were incubated at 28°C under static condition (Fig. 2.6.1B).

2.3.2. Preparation of microsomes

The procedure for microsomes preparation was similar as described by Kumar and Goswami (2006). The cells were harvested from the early stationary phase of growth of the static culture. The harvested cells were separated from the culture broth and then washed with tris HCl buffer and *n*-hexane (only for *n*-hexadecane grown cells) to prepare substrate-free cell mass following the procedure described by Goswami and Cooney (1999). The cells were suspended in 50 mM tris HCl buffer (pH 8.0) containing EDTA (10 mM); $MgCl_2$ (1 mM), and PMSF (1 mM) and then disrupted by using mechanical cell disruptor (Constant Systems, UK) at 30 kpsi. The cell homogenate formed after disruption was then immediately mixed with DTT (1 mM) and then centrifuged at 10,000×g for 10 min to pellet the undisrupted cells and nuclei. The supernatant (Sup-1) was collected and subjected to 20,000×g for 20 min to pellet light mitochondrial fraction (LMF). The supernatant (Sup-2) collected was again centrifuged at 114,000×g for 1 h 30 min (Beckman Ultracentrifuge, USA) to sediment the microsomal fraction (MF). The MF was separated and suspended in 50 mM tris HCl buffer (pH 8.0). The supernatant

(Sup-3) formed was retained for enzymatic study. All the steps in the procedure were performed at 4°C, unless specified.

2.3.3. Assay of CYP

The CYP activity was assayed by measuring the substrate dependent oxygen consumption in BOM (model 53 YSI, USA) using Clark-type oxygen electrode with a partial modification of the method described earlier (Kumar and Goswami 2006). 3 µl of emulsified substrate containing 25 mM of *n*-hexadecane and triton X-100 (0.2 mg ml^{-1} final concentration) in tris HCl buffer (50 mM, pH 8.0) was sonicated for 30 s and taken in each tube of BOM. 100 µl of NADH (0.33 mM final concentration) was added as cofactor before the addition of enzyme. A Parallel reaction containing all the components of reaction mixture except the substrate was used as control to nullify any endogenous oxygen consumption during the assay. One unit (U) of enzyme activity is the amount of enzyme that consumes 1 µmol O_2 in 1 min at 30°C.

2.3.4. Assay of NCP

NADH cytochrome P450 reductase (NCP) activity was assayed by measuring its NADH cytochrome c reductase activity as described elsewhere (Imai 1976). The reaction mixture for determination of NCP activity contained 20 µM cytochrome c (equine heart, Sigma), 0.5 mM EDTA and 1 mM NADH in SPB (50 mM, pH 7.5). The reaction was started with the addition 10 µl of microsomal enzyme preparation. The rate of cytochrome c reduction was calculated from the A_{550} change using an extinction coefficient (ε = 21 mM^{-1} cm^{-1}).

2.3.5. Determination of substrate specificity of CYP

Substrate specificity was determined by using 25 mM of the test substrates in the reaction mixture instead of *n*-hexadecane as described earlier. In case of volatile substrates such as methanol, ethanol, propanol, acetone, benzene, toluene and benzyl alcohol, 100 mM of the test substrates were used and then the CYP activity was measured by BOM as described earlier.

2.3.6. Determination of pH and temperature optima and stability of CYP

In order to determine pH and temperature optima, the enzyme reactions were carried out in different test pH buffers and different test temperatures, respectively and the CYP activity was measured by BOM. For determination of pH stability, the enzyme samples were incubated in test pH buffers for minimum 30 min to maximum 96 h at 4°C and then residual activity of CYP was determined by BOM at 30°C in tris HCl buffer (50 mM, pH 8.0). Similarly, for determination of temperature stability enzyme samples were incubated at different test temperatures in circulating water bath for different time periods followed by measurement of residual activity of CYP by BOM as described earlier.

Protein estimation was done following the Bradford's method using BSA as standard (Bradford 1976).

2.3.7. CO difference spectra

Establishment of monooxygenase from *A. terreus* as cytochrome P450 monooxygenase was achieved by analyzing CO difference spectra following a partial modification of the original method described elsewhere (Estabrook and Werringloer 1978). Microsomal sample containing 1.5–2 mg of protein in 1 ml of phosphate buffer (pH 7.4) containing 20% glycerol, in a stoppered cuvette was gently sparged with carbon monoxide for 1–2 min, at which time several fine grains of solid sodium dithionite were added. Sparging was continued for 1–2 min more, and the cuvette was stoppered. Spectra (410–500 nm) were recorded on a Cary 100 UV–Vis (Varian, USA) to record the maximum development of difference spectra at 450 nm.

2.3.8. Inhibitor study for CYP

Microsomal sample was incubated for 5 min with taxifolin at concentrations of 0–900 µM, before the addition to the reaction mixture containing *n*-hexadecane as substrate. The CYP activity was then measured by BOM as described earlier. A control experiment without inhibitor was carried simultaneously to calculate the effect of inhibitor concentration in terms of residual activity of the CYP.

2.3.9. Solubilization and reconstitution of enzyme system

Solubilization of microsomal fraction containing CYP and NCP was initiated by addition of a 10% (w/v) sodium cholate solution to give a final concentration of 0.8% (w/v) and was carried out for 30 min at 4°C. After ultracentrifugation (100,000×g, 60 min, 4°C) both supernatant and pelleted fractions were checked for activities of both the enzymes.

Reconstitution of both the CYP and NCP present in the supernatant was carried out by a slight modification of method described elsewhere (Scheller et al. 1994), where phospholipids extracted from the fungal cells (hexadecane grown *A. terreus*) by standard chloroform–methanol (2:1) method (Folsch et al. 1957) were used for reconstitution of enzymes in membrane. Sodium cholate was removed from enzyme sample containing phopholipid by dialyzing it against 10 mM of potassium–phosphate buffer (pH 7.3), containing 20% glycerol, 0.5 mM DTT and 1 mM EDTA, 5 µM FAD and 0.5% sodium cholate for around 15 h at 4°C.

2.3.10. Product analyses

A total 30 ml of the reaction mixture in a 50 ml cotton plugged Erlenmeyer flask containing test substrates, *n*-hexadecane or ethanol, 1 ml of the microsomal enzyme (5 mg of protein ml^{-1}) and 0.33 mM of NADH in tris HCl buffer (pH 8.0) was shaken in water bath at 30°C for 8 h. The final concentration of *n*-hexadecane in the reaction mixture was 100 mM, which was prepared by emulsifying 1 ml of *n*-hexadecane in the reaction mixture containing triton X-100 (0.2 mg ml^{-1} final concentration) using ultrasonicator followed by addition of the enzyme solution. A control without *n*-hexadecane was also run and analyzed to avoid any interference in the product analysis caused by the triton X-100 or its degraded product. The final concentration of ethanol in the reaction mixture was 95% (v/v) prepared by mixing 28.5 ml of absolute ethanol (Merck) in 30 ml of the reaction mixture. Additional enzyme (1 ml) and NADH (0.33 mM) were added in the reaction mixture intermittently after every 2 h during the reaction period. After completion of reaction, the products of *n*-hexadecane were extracted with dichloromethane in separating funnel and then purified by silica gel column using solvent

mixture of hexane and ethyl acetate at different ratios starting from 10:0 to 8:2. The purified products were then analyzed by TLC using solvent mixture of hexane and ethyl acetate at 8:2 ratios. Spots were developed in iodine chamber. Purified products were analyzed by FTIR (Perkin-Elmer) and NMR (Varian model 400 MHz). For analysis of product using ethanol as substrate, the reaction mixture at the end of the reaction was first filtered through a 0.45 µm Millipore filter. The residual ethanol from the filtrate was then removed as much as possible by vacuum evaporation. The concentrated fraction of the reaction mixture was then absorbed in a small amount of dry silica (column chromatographic grade) and then dried overnight at room temperature. The sample-absorbed silica gel was then loaded on the top of a silica gel column and then eluted by using solvent mixture of hexane and ethyl acetate at different ratios starting from 10:0 to 8:2. Finally, the column was washed with methanol to elute any remaining product in the column. Products were then analyzed by TLC, FTIR and NMR as described earlier.

2.3.11. Heme staining in SDS–PAGE

SDS–PAGE analysis of the protein was done following the method of Laemmli (1970) by using 5% stacking and 10% separating gels of thickness 0.75 mm at constant 20 mA and 30 mA current for stacking and resolving gel, respectively, for 1 h. Before loading, samples were denatured for around 2 h at 40°C in reducing sample buffer. Heme staining of proteins separated by SDS–PAGE was carried out using *o*-dianisidine as substrate (Schulz et al. 2000). The gel was incubated for 10 min in 10% TCA. After extensive washing with water, the gel was stained using 20 mg of *o*-dianisidine dissolved in 20 ml of 50 mM trisodium citrate buffer (pH 4.4) containing 0.7% H_2O_2. The exact replica of the same gel was also stained with CBB R 250. The standard

protein markers used to determine the approximate molecular weight of the sample protein were carbonic anhydrase (29 kDa), glyceraldehyde 3-phosphate dehydrogenase (36 kDa), chicken ovalbumin (45 kDa) and BSA (66 kDa).

2.4. Results and discussion

The localization of CYP from *A. terreus* was found to be growth substrate specific, as the CYP activity in the *n*-hexadecane grown cells was localized mostly in the cytosolic fraction, whereas, for glucose grown cells the activity was distributed between MF and LMF (Table 2.7.1). The corresponding activities in MF and LMF were 53.4% and 43.4%, respectively, as compared to the original activity in the crude extract. Although, CYP in the glucose grown cells was detected both in LMF and MF, analysis of NADPH cytochrome c reductase, a marker enzyme for microsomal membrane fraction (Fleisher 1974), in the LMF suggest that large amount of MF was co-precipitated along with the LMF during the separation of LMF at 20,000×g. Notably, centrifugal force of 20,000×g is usually considered as standard protocol for selective separation of LMF during cellular fractionation (Okado-Matsumoto and Fridovich 2001). The functional distinctions of the CYP present in these two locations could not be identified. Although, on the basis of the marker enzyme analysis MF may be indicated as the primary site of CYP in the glucose-grown cells, further investigations, particularly, on the *in situ* metabolic liability of the CYP in the cells are necessary to arrive at a conclusion. Reports on the location of the CYP in microsomes (Nakayama and Shoun 1994; Scheller et al. 1996) or cell membrane fractions (Schnuck et al. 1983) are available. However, distribution of CYP with similar enzymatic activities in different sub-cellular sites is intriguing. The CYP activity in the *n*-

hexadecane grown cells was mostly detected in the supernatant (Table 2.7.1) and was largely associated with the lipid layer floating on the supernatant. Sup-1 of *n*-hexadecane grown cells contains seven-fold more lipid (4.4 g%) than the glucose grown cells (0.62 g%). However, the level of CYP activity in the sup-1 of *n*-hexadecane grown cells (1.6±0.07 U mg^{-1}) was nearly three-fold less than the corresponding activity obtained in the sup-1 of glucose grown cells (5.0±0.09 U mg^{-1}). The highly hydrophobic integral membrane bound CYP enzyme was probably detached by the low-density lipid to the top during disruption of the cells and centrifugation. Since, the membrane fraction is essential for the enzyme activity as revealed by the membrane solubilization experiment, so detachment of the enzyme from the membrane fraction may substantially reduce the enzyme activity in the sub-cellular fractions of *n*-hexadecane grown cells. NCP activity was found associated with the corresponding fractions containing CYP activity.

Analyses of the cofactor requirement, optimum temperature and pH (Fig. 2.6.2), specificities to different substrates (Table 2.7.2) implied that the CYP from all the locations were similar. The specific CYP activity in the glucose grown cells (6.8±0.12 U mg^{-1}) was nearly 3.5-folds the activity obtained in *n*-hexadecane grown cells (2.2±0.07 U mg^{-1}), hence, glucose-grown cells were considered for further studies of the enzyme activities.

The CYP activity was detected over a wide range of substrates those belong to aliphatic and aromatic hydrocarbons, steroids, short chain and long chain alcohols, organic solvents, and derivatives of aliphatic hydrocarbons. Among all these substrates highest activity was detected with the organic solvents, namely, acetone (7.76±0.20 U mg^{-1}) and DMSO (9.70±0.50 U mg^{-1}) (Table 2.7.2). Next higher CYP activity was detected with long chain alkanes, namely, *n*-hexadecane (4.39±0.05 U mg^{-1}) and *n*-octadecane (4.23±0.01 U mg^{-1}) followed by methanol

(5.60±0.20 U mg^{-1}). Within the groups of aromatic compounds, naphthalene (3.80±0.20 U mg^{-1}) showed highest CYP activity. The enzyme also showed high activity towards branched chain alkane like pristane. Considerable CYP activity was also detected with the substrates void of terminal methyl groups such as 12-hydroxydodecanoic acid, 1,12-dichlorododecane, and 1,16-hexadecanediol (Table 2.7.2), which demonstrated that CYP from *A. terreus* could catalyze sub-terminal oxidations. However, terminal oxidation seems to be the primary mechanism as revealed from the higher catalytic rate with the corresponding alkanes (Table 2.7.2). Besides these we have also demonstrated the CYP activity towards unusual substrates such as, steroids, and aromatic hydrocarbons. CYP involved in the metabolism of aromatic hydrocarbons are reported from different microbial sources including fungi (Mfincnerovfi and Augustin 1994). Although CYP hydroxylations of cholesterol and testosterone are common in higher eukaryotic systems, reports on the specific CYP those catalyze these steroids are not known from microbial system.

The CYP activity was obtained only when NADH was used as co-factor. No other compounds checked such as, NAD, NADP, NADPH, FMN, FAD, and $FADH_2$ could serve as co-factor of the enzyme which confirms the presence of only one NADH dependent monooxygenase or hydroxylase in the MF.

The optimum pH for CYP activity was found to be pH 7.0 (Fig. 2.6.2A). The CYP activity vanished completely below pH 5.0 and above pH 11.0. Similarly, the optimum temperature for CYP activity was observed at 37°C (Fig. 2.6.2B). Activity decreased drastically when the temperature of the reaction mixture was increased to 40°C. Below 37°C, the enzyme activity decreased but the rate of decrease was comparatively less than at higher temperatures. From a range of pH 6.0–11.0 chosen to study the stability, CYP was highly stable at pH 7.0 and

above. Within pH 7.0–8.0 activity was intact for 2 days and with a minor reduction in activity the enzyme was stable up to 4 days. CYP was comparatively less stable at acidic pH and above pH 10.0. Around 50% of the enzyme activity was retained even after 2 days within pH 9.0–10.0. Stability of CYP reduced substantially at pH 11.0 and pH 6.0 (Fig. 2.6.3A). The stability of the CYP diminished steadily with the increase in the temperature within the studied temperature range of 25°C–40°C. At 25°C the activity was intact up to nearly 1 h following which the activity went down and diminished to 50% of the original activity at 0 h (Fig. 2.6.3B). The optimum temperature for CYP activity was 37°C, which is albeit higher as compared to temperature range of 25–30°C commonly reported from other fungal and bacterial sources. Reports on the stability of CYP from other sources are limited. The stability of the enzyme at different temperature ranging from 25 to 40°C shows the expected pattern for enzyme stability, being most stable at 25°C followed by decreasing stability with increasing temperatures. The CYP is most stable at and around physiological pH (7.0–8.0) as nearly 95% of the original activity was retained even up to four days. This property of enzyme may be promising for its applications in areas, where stability of the enzyme is an important process criterion.

CYP from *A. terreus* belongs to cytochrome P450 family as revealed from the prominent absorption peak of the dithionite reduced CYP CO adduct at 450 nm in the CO difference spectra (Fig. 2.6.4). The result was further confirmed by the strong inhibition of the CYP activity by taxifolin. Inhibition was 17.4±5% at 100 µM, 52.2±5% at 300 µM, and 78.4±5% at 600 µM. At or above 900 µM, there was complete inhibition of the enzyme activity. The IC_{50} of 300 µM was estimated for the taxifolin inhibition of the CYP activity. Taxifolin, which is a flavonoid, is known specific inhibitor of cytochrome P450 (Haraguchi et al. 1996). The mechanism of taxifolin inhibition has been explained to a certain extent (Nagao et al. 2000). The IC_{50} of 300

μM of taxifolin inhibition was found to be comparatively higher than the CYP inhibition reported by other taxifolin like flavonoids (Kim et al. 2000).

Sodium cholate at a concentration of 0.8% (w/v) could solubilize the enzymes CYP and NCP from the microsomal membrane as no activities of these enzymes were retained in the sodium cholate treated MF or LMF of the glucose grown cells. Reconstitution of the NCP activity from the solubilized fractions could be achieved, while, the same condition was not effective to reconstitute the CYP in the solubilized fractions. Loss of CYP activity after membrane solubilization with sodium cholate confirms that it is an integral membrane bound enzyme and membrane system is essential for its function.

In order to understand the mode of initial oxidation of long chain alkanes catalyzed by the microsomal membrane bound CYP, the product of the CYP catalyzed reaction using *n*-hexadecane as substrate was analyzed. The product was identified as 1-hexadecanal-8-one. The spectral data of the purified product obtained by using *n*-hexadecane as substrate are as follows: ^{1}H NMR ($CDCl_3$, 400 MHz): d 0.877 (3H, t, CH_3), 1.25–1.29 (12H, m, CH_2), 1.56 (6H, br, CH_2), 2.31 (6H, m, CH_2CO), 11.2 (1H, s, CHO). IR (neat): 2925, 2857, 1741, 1791, 1459, 1374 cm^{-1}. Similarly, the product of CYP catalyzed oxidation of ethanol was also analyzed and the product was identified as glycolic acid. The spectral data of the purified product obtained by using ethanol as substrate are as follows: ^{1}H NMR ($CDCl_3$, 400 MHz): d 2.02 (1H, s, –OH), 4.42 (2H, s, CH_2), 10.92 (1H, s, COOH). IR (KBr): 3393, 1614 cm^{-1}. The melting point of 79°C obtained for the ethanol-oxidized product was also matched with the standard melting point (75–79°C) of glycolic acid. Presence of ketone and aldehyde groups in the CYP catalyzed product of *n*-hexadecane substrate further supports the association of both sub-terminal and terminal oxidation mechanisms. Long chain- and secondary-alcohol oxidases present in the MF of *A. terreus*, as

reported from our laboratory (Kumar and Goswami 2006), might further oxidize the primary- and secondary-alcohol generated by the CYP catalysis of long chain alkanes resulting in the formation of products containing functional groups, aldehyde and ketone, respectively. The presence of secondary alcohol oxidase in the MF indirectly supports the existence of sub-terminal oxidation mechanism for *n*-alkanes. Sub-terminal oxidation of long chain alkanes by bacteria and yeast has been reported (Beilen and Funhoff 2005), while, the same has not been studied adequately from filamentous fungi. The microsomal ethanol-oxidizing enzyme, namely, alcohol dehydrogenase, has been widely reported from microorganisms and higher eukaryotes, which convert ethanol to acetaldehyde and eventually to acetic acid. However, biocatalytic oxidation of methyl groups present in ethanol and in other organic solvent is rare as revealed from the literature available in referred journals. The only information available with us at the time of reporting was of acetone monooxygenase, present in the rat and rabbit microsomes (Koops and Casazza 1985). It may be mentioned that these solvents are commonly used to solubilize hydrophobic substrates to assay CYP. Glycolic acid, as detected by us, from ethanol substrate probably formed as a result of sequential catalytic action of CYP, short chain alcohol oxidase (SCAO) (Kumar and Goswami 2006) and other enzyme(s) present in the MF of *A. terreus* as shown in Scheme 2.4.1.

Scheme 2.4.1. Proposed scheme for stepwise conversion of ethanol to glycolic acid in the cells of *A. terreus*.

Between the two enzymes, namely, CYP and NCP that constitute the monooxygenase redox system commonly found in eukaryotes, the specificity of the enzyme is frequently attributed to CYP, which endures the substrate binding sites (White and Coon 1980). Broad substrate specificities of the CYP present in the membrane fraction in the cells of *A. terreus* prompted us to examine the possibility of existence of isoforms of this cytochrome P450 protein following the heme staining method. Molecular weights of the microsomal heme protein(s) including the CYP were examined by heme staining of the SDS–PAGE of the microsomal proteins. Appearance of single green band upon staining indicates the presence of only one heme protein in the microsomes (Fig. 2.6.5). The approximate molecular weight of the heme containing protein was nearly 110 kDa when compared with the R_f values of the standard protein markers ran parallel in the same gel and stained separately with CBB R250. Detection of single band upon heme staining the microsomal samples in SDS–PAGE inferred the lack of plurality of the heme-containing protein in the MF. Which, however, call for further investigation using sensitive method, as the sensitivity of the SDS–PAGE may not be sufficient to differentiate the isoforms of closer molecular weight. The approximate molecular weight of 110 kDa measured by us was closer to the report from *Fusarium oxysporum*, which was 118 kDa (Nakayama et al. 1996). The appearance of green band after heme staining was due to the formation of semiquinone radical, the intermediate formed during the partial oxidation of *o*-dianisidine in acidic medium by enzymes containing heme in presence of H_2O_2 (Claiborne and Fridovich 1979).

2.5. Conclusions

The CYP activity in the cells of *A. terreus* was localized in the cytosol of *n*-hexadecane grown cells, while, it was apparently distributed in light mitochondrial and microsomal fractions of glucose grown cells. The substrate specificities of CYP present in all these locations were similar irrespective of the substrates used for the growth. CYP activities with different category of substrates namely, alkanes, alkane derivatives, alcohols, aromatic compounds, organic solvents, and steroids were detected in the cells. High specific activity of CYP was observed when methanol (5.60±0.20 U mg^{-1}), acetone (7.76±0.20 U mg^{-1}), DMSO (9.70±0.50 U mg^{-1}), *n*-hexadecane (4.39±0.05 U mg^{-1}) and *n*-octadecane (4.23±0.10 U mg^{-1}) were used as substrates. Microbial CYP active on methanol, acetone and DMSO substrates is appeared not to be widely known as evidenced from the available literature. Significant CYP specific activity was also detected when naphthalene (3.80±0.20 U mg^{-1}) was used as substrate. The CYP catalysis of *n*-hexadecane had followed both terminal and sub terminal oxidations. Heme staining of the microsomal fraction containing CYP and other proteins in SDS–PAGE showed single heme protein band with corresponding molecular weight of 110 kDa.

2.6. Figures

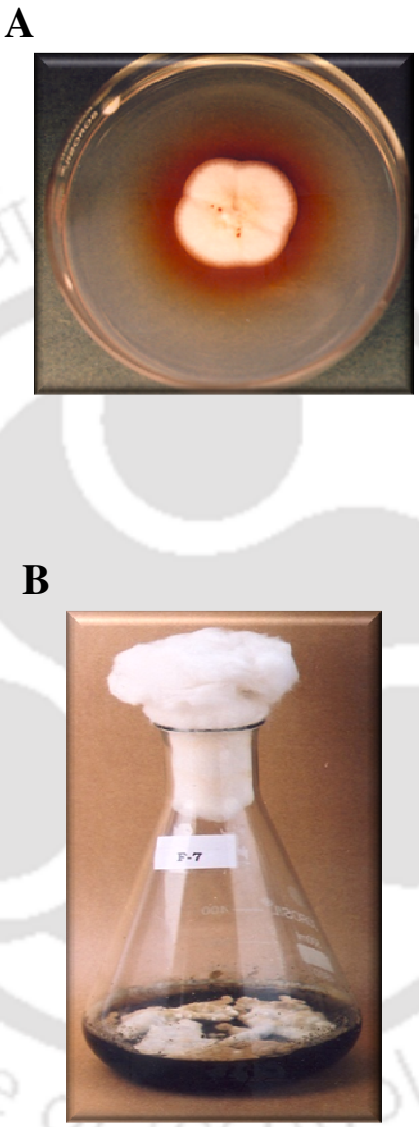

Fig. 2.6.1. Growth of *A. terreus* MTCC 6324 **(A)** on fungal agar and **(B)** in culture broth containing *n*-hexadecane as carbon source.

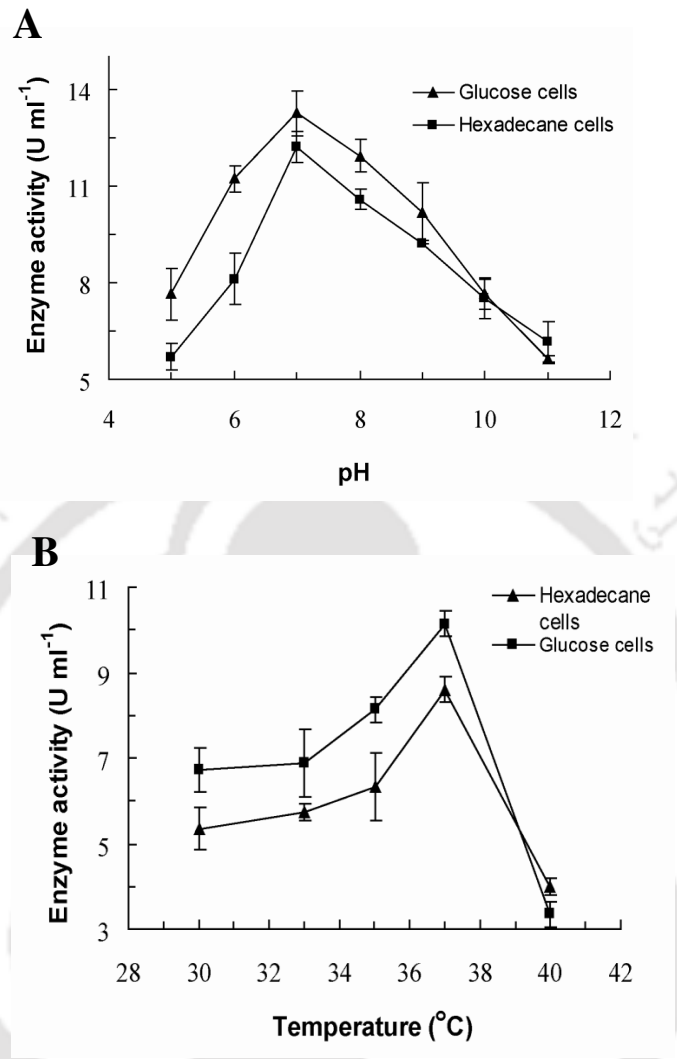

Fig. 2.6.2. pH and temperature optima of the CYP from *A. terreus*. **(A)** The pH optimum, the buffer systems used were acetate buffer (pH 5.0), phosphate buffer (pH 6.0 and 7.0), tris buffer (pH 8.0), ethanolamine buffer (pH 9.0), piperazine buffer (pH 10.0 and 11.0) each at a concentration of 50 mM. **(B)** The temperature optimum. For better comparison the pH and temperature optima of the *n*-hexadecane grown cells were consciously amplified to three times of their original values. Each datum point represents the average of the analysis of triplicate values, with the range indicated with error bars.

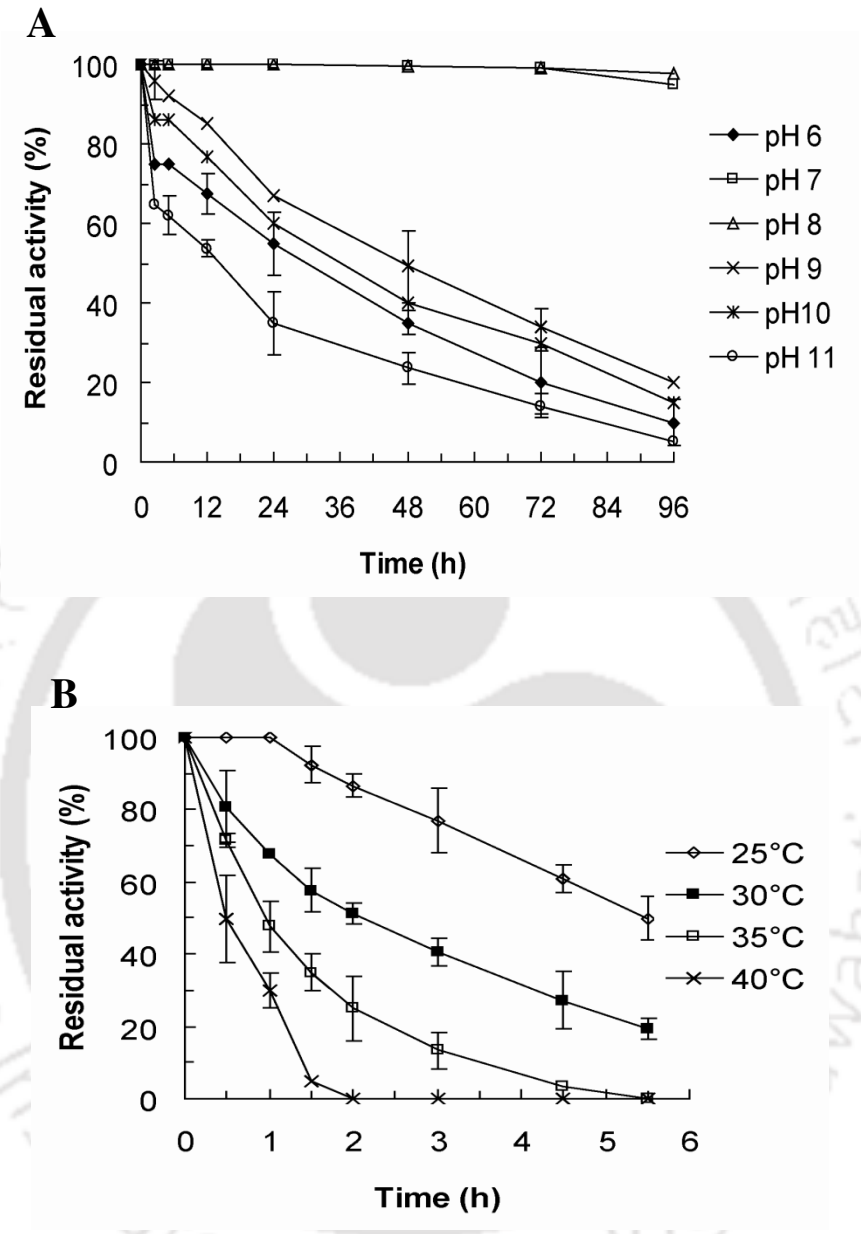

Fig. 2.6.3. pH and temperature stability of CYP from *A. terreus*. **(A)** The pH stability; the buffer systems used were phosphate buffer (pH 6.0 and 7.0), tris buffer (pH 8.0), ethanolamine buffer (pH 9.0), piperazine buffer (pH 10.0 and 11.0), each at a concentration of 50 mM. **(B)** The temperature stability. Each datum point represents the average of the analysis of triplicate values, with the range indicated with error bars. 100% activity corresponds to 27.2±0.17 μM min^{-1} ml^{-1}.

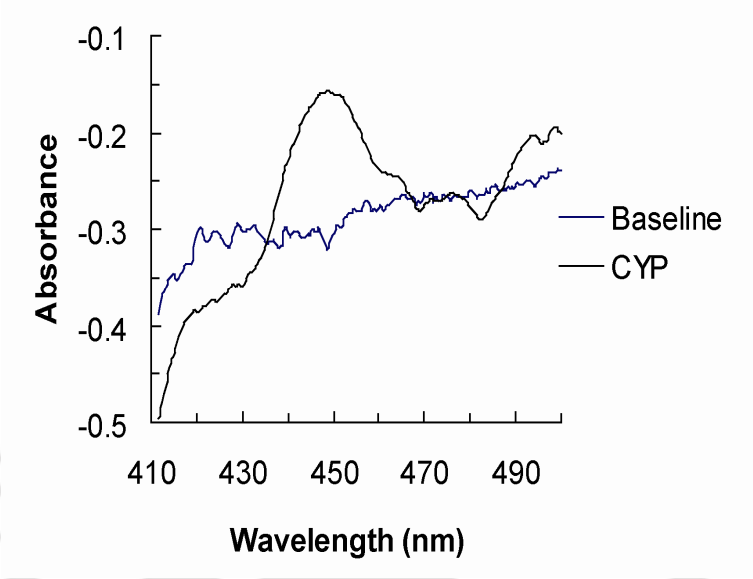

Fig. 2.6.4. CO difference spectra of CYP from *A. terreus*.

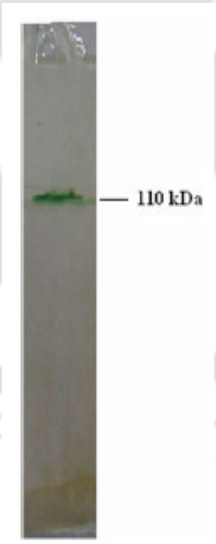

Fig. 2.6.5. Heme staining of microsomal fraction of glucose grown cells. The approximate molecular weight is calculated by simultaneously staining a part of the similar gel containing standard molecular markers with CBB R 250 and comparing their R_f values.

2.7. Tables

Table 2.7.1. Localization of CYP in the cellular fractions of *A. terreus.*

	CYP activity							
	n-hexadecane grown cells				Glucose grown cells			
Fraction	Protein (mg)	Total activity (U)	Sp act (U mg^{-1} of protein)	% DA	Protein (mg)	Total activity (U)	Sp act (U mg^{-1} of protein)	% DA
Crude extract	102.0± 4.04	183.4±7.23	1.8±0.08	100	141.2±2.77	1032±20.31	7.3±0.11	100
Sup-1	56.0±2.22	91.7±3.35	1.6±0.07	50.0	75.8±1.61	381.7±7.36	5.0±0.09	36.9
Pellet-1	21.5±0.83	24.5± 0.96	1.1±0.04	13.4	28.9±0.39	156.8±3.05	5.4±0.10	15.2
Sup-2	23.3±0.89	61.2±2.42	2.6±0.08	66.7	61.2±2.61	204.1±4.84	3.3±0.03	53.4
LMF	1.0±0.05	2.4± 0.10	2.3±0.09	2.6	10.2±0.18	165.5±3.16	16.2±0.34	43.4
Sup-3	12.7±0.52	58.7±2.30	4.6±0.17	95.9	43.2±2.15	nil	nil	nil
MF	2.2±0.10	4.9±0.19	2.2±0.07	8.0	16.3±0.3	110.0±2.15	6.8±0.12	53.9

Each value represents the mean ± standard error at $p < 0.05$. Sp act: Specific activity, DA: Distribution of activity in fractions.

Table 2.7.2. CYP activity from *A. terreus* with different substrates.

Substrate	Specific activity (U mg^{-1})	
	n-hexadecane grown cells	Glucose grown cells (MF)
Alkanes		
n-octane	trace	0.49±0.05[e]
n-dodecane	0.30±0.02[d]	0.98±0.04[d]
n-hexadecane	1.28±0.01[b]	4.39±0.05[a]
n-octadecane	1.40±0.05[a]	4.23±0.01[b]
n-docosane	0.81±0.08[c]	2.60±0.50[c]
n-tetracosane	0.32±0.02[d]	0.98±0.04[d]
Aliphatic Alcohols		
Methanol	1.86±0.02[a]	5.60±0.20[a]
Ethanol	1.30±0.14[b]	3.88±0.50[b]
n-propanol	0.57±0.10[c]	2.02±0.10[c]
n-butanol	trace	0.40±0.11[h]
n-heptanol	0.60±0.04[c]	1.80±0.05[d]
n-octanol	trace	0.48±0.03[h]
n-decanol	trace	0.59±0.03[g]
n-undecanol	trace	0.40±0.05[h]
n-dodecanol	trace	trace
n-tetradecanol	0.38±0.02[d]	1.14±0.02[e]
n-hexadecanol	0.35±0.01[d]	1.07±0.01[e]
n-eicosanol	0.38±0.06[d]	1.16±0.01[e]
n-docosanol	trace	0.76±0.04[f]

Branched alkanes		
Pristane	0.88±0.03	2.69±0.13
Aromatic compounds		
Benzene	trace	0.80±0.06[c]
Toluene	0.40±0.23[b]	1.20±0.05[b]
Phenol	0.33±0.02[c]	0.90±0.05[c]
Naphthalene	1.26±0.02[a]	3.80±0.20[a]
Benzyl alcohol	trace	0.48±0.04[d]
Steroids		
Cholesterol	trace	0.71±0.08[b]
Testosterone	0.38±0.01	1.19±0.05[a]
Organic Solvents		
Acetone	2.58±0.20[b]	7.76±0.20[b]
DMSO	3.23±0.10[a]	9.70±0.50[a]
Derivatives of alkane		
12-hydroxydecanoic acid	trace	0.49±0.04
1,12-dichlorododecane	trace	0.49±0.02
1,16-hexadecanediol	trace	0.49±0.01

Each value represents the mean±standard error; with no common letter in a column for a group of substrates are significantly different at $p < 0.05$.

Chapter 3

Isolation, purification, protein-chemical and functional characterization of catalase (CAT) from *Aspergillus terreus*

3.1. Overview

The importance of catalase in different industrial niches like, biosensors (Campanella et al. 1998; Campanella et al. 2001; Mello and Kubota 2007; Modrzejewska et al. 2007; O'Brien et al. 2007), therapeutics (Day 2004), food and textile (Akertek and Tarhan 1995) etc. is tremendously growing as revealed from the volume of publications on these areas since recent past. Catalase (EC 1.11.1.6) is a heme-containing antioxidant enzyme known for its ability to degrade hydrogen peroxide (H_2O_2) into water and oxygen (Zamocky and Koller 1999). The degradation occurs in two-steps: the first step involves reduction of a H_2O_2 molecule into water with the concomitant oxidation of the catalase heme Fe^{3+} to oxyferryl species (Fe^{4+}=O), while the second step involves oxidation of a second molecule of H_2O_2 into water and oxygen with the associated reduction of the oxyferryl species that regenerates the heme Fe^{3+}.

Catalases are ubiquitous enzymes present in archaea, bacteria, fungi, plants, and animals. They are monophyletic in origin and are grouped into three clades: clade 1 in green algae and plants; clade 2 in archaea, bacteria, and fungi; and clade 3 in archaea, bacteria, fungi, and animals (Klotz and Loewen 2003). Clades 1 and 3 are composed of 55 to 69 kDa subunits, while clade 2 enzymes are formed by larger subunits of nearly 75 to 86 kDa (Diaz et al. 2009). In

bacteria, the large catalases described are from *E. coli* (HPII or KatE), *Bacillus subtilis* (KatE), *Bacillus firmus* (KatE), *Mycobacterium avium* (KatE), *Pseudomonas putida* (CatC), and *Xanthomonas oryzae* (KatX) (Klotz et al. 1997), whereas, from fungi they are mostly reported from *Neurospora crassa* (Cat-1 and Cat-3) (Diaz et al. 2001), *Penicillium vitale* (Vainshtein et al. 1986), *Claviceps* (CPCAT1) (Garre et al. 1998) and *Aspergillus* species namely, *A. nidulans* (CatA and CatB) (Navarro et al. 1996; Kawasaki et al. 1997; Calera et al. 2000), *A. fumigatus* (CatA and CatB) (Lopez-Medrano et al. 1995; Takasuka et al. 1999) and *A. niger* (CatR) (Fowler et al. 1993; Switala and Loewen 2002). The works on biochemical characterization of large catalases from the *Aspergillus* species are mostly limited to *A. nidulans* (Calera et al. 2000), *A. fumigatus* (Lopez-Medrano et al. 1995) and *A. niger* (Switala and Loewen 2002).

Fungi, *A. terreus* are widespread and abundant in terrestrial ecosystem due to their capability to utilize a wide variety of carbon substrates for growth and survival (Britton 1984; Dashti et al. 2008). Investigations on large catalases from *A. terreus* are not yet known from the reported literatures. In this chapter we describe a cellular large catalase (CAT) of distinct kinetic properties and stability, isolated and purified from *A. terreus* MTCC 6324.

3.2. Literature Review

The early history of catalases goes back to the 19th century when they became one of the first sources of valuable information about the nature and behavior of enzymes. Loew (1901) was the first who named H_2O_2-degrading enzyme catalase, but it took further 22 years until Warburg (1923) demonstrated that the active center of catalase contains iron, as concluded from the characteristic inhibition with cyanide. In 1927, Wieland and Franke offered a simple

explanation for the `catalase function' in cells, according to which H_2O_2 was acting as a hydrogen donor for a hypothetical catalyst, which in hydrogenated form reduced another molecule of H_2O_2 to water (Wieland and Franke 1927). Stern (1936) demonstrated that in all then known catalases protoporphyrin IX was the active group, and the first crystals of beef liver catalase (BLC) were obtained a year later (Sumner and Dounce 1937). In 1947, the pioneering work of Chance led to the discovery of the primary complex formed between catalase and H_2O_2 (compound I, $Por^{\cdot+}$–Fe^{IV}=O, Chance 1947). In addition to compound I, Chance (1949) discovered a further derivative named compound II (Por–Fe^{IV}=O) which was independently observed by other investigators (Lemberg and Foulkes 1948).

The First prokaryotic catalase was obtained from *Micrococcus luteus* by Herbert and Pinsent (1948). In the next decade more species became available for detailed analysis (Deutsch 1951; Galston et al. 1952; Clayton 1959). In the course of various sequencing projects a broad spectrum of catalase sequences from organisms of all kingdoms appeared in the public databases (e.g. Schroeder et al. 1982; Hartig and Ruis 1986; Cohen et al. 1988; von Ossowski et al. 1991; Buzy et al. 1995; Guan and Scandalios 1995). The sequences of about more than 80 true catalases, 16 catalase-peroxidases and one manganese catalase are available in public databases and a number of three-dimensional structures of catalases are solved to high resolution. With this broad range of species in hand one can systematically analyze the structure-function relationships and follow the evolutionary history of H_2O_2 dismutating enzymes. From these data although it became clear that this large group of oxidoreductases is not homogenous.

The first attempt to classify the various enzymes with significant catalatic activity was made by Goldberg and Hochman, who suggested the division of all existing catalases into three subgroups: typical, atypical and catalase-peroxidases (Goldberg and Hochman 1989). Currently

more than 90 catalase sequences appear to belong to one of three distinct subgroups: two of them are heme containing, namely typical (sometimes known as true) catalases and catalase-peroxidases. The third group is (non-heme) manganese catalases. The most characteristic feature of catalases-peroxidases is their bifunctional catalytic behavior. Members of this subgroup are found in all three living kingdoms, although in eukaryotes they were detected lately (Levy et al. 1992; Fraaije et al. 1996). Their molecular weight varies from 120 to 340 kDa and in general they are homodimers (Obinger et al. 1997; Nagy et al. 1997), although homotetramers were also reported (Hochman and Shemesh 1987; Hochman and Goldberg 1991). Until recently three manganese catalases were known, one from lactic acid bacteria (Beyer and Fridovich 1985) and two from thermophilic organisms (Barynin et al. 1986; Kagawa et al. 1999). These enzymes are sometimes referred to as pseudocatalases (Kono and Fridovich 1983; Allgood and Perry 1986) due to the fact that they utilize manganese ions (instead of ferric heme) in their active sites. The species from *Lactobacillus plantarum* was cloned and sequenced (Igarashi et al. 1996). The focus of this section is however the heme containing typical/true catalases.

Catalase (EC 1.11.1.6) is a highly conserved heme-containing antioxidant enzyme known for its ability to degrade H_2O_2 into water and oxygen (Scheme 3.2.1).

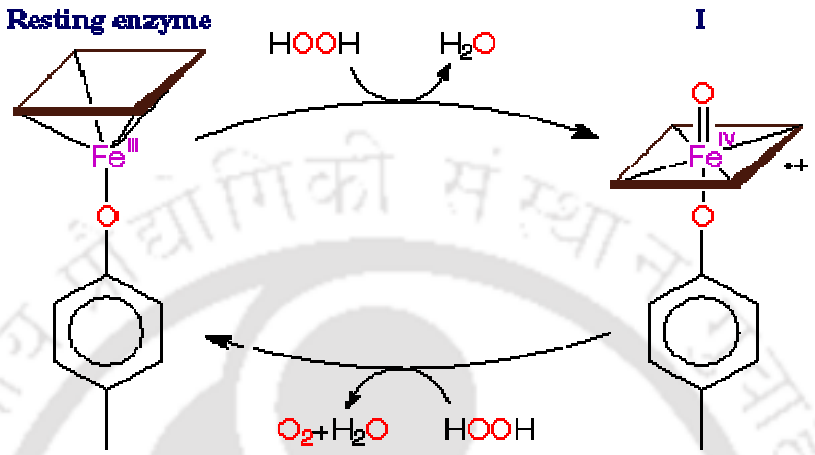

Scheme 3.2.1. Reaction cycle depicting the catalase catalysis.

(Adapted from http://metallo.scripps.edu/promise/CATALASE.html)

Most of these hydroperoxidases are homotetramers, 200-340 kDa in size with four prosthetic heme groups. In the majority of cases ferric protoporphyrin IX was found, but in some representatives heme d resides in the active center, formed autocatalytically from protoheme IX (Bravo et al. 1997). Characteristic physical features include their distinct electronic spectrum with rather strong absorbance in the Soret band, reflected by R_z values around 1 (Reinheitszahl ratio, A_{406} nm/A_{280} nm), irreversible inhibition by the suicide inhibitor 3-amino-1,2,4-triazole and the fact that their ferric heme group cannot readily be reduced with sodium dithionite. In addition to a very efficient catalatic reaction mode (4×10^7 M^{-1} s^{-1}, for human erythrocyte catalase; Schonbaum and Chance 1976) they can also catalyze 2-electron peroxidation of short-chain aliphatic alcohols at reasonable rates (Sichak and Dounce 1986). Genes coding for typical

catalases were isolated and sequenced from more than 75 organisms. The currently best analyzed representatives come from: bovine liver (Schroeder et al. 1982), *Saccharomyces cerevisiae* (Cohen et al. 1988), *Escherichia coli* (von Ossowski et al. 1991), maize (Guan and Scandalios 1995) and *Proteus mirabilis* (Buzy et al. 1995). The conserved core of typical catalases comprises about 390 amino acids (from residue 70 to 460, numbering for yeast catalase A; Klotz et al. 1997) spanning four structural domains. The highest degree of homology is found in the area around the essential distal histidine, and around the proximal heme-ligand tyrosine (Zamocky et al. 1997). The tertiary structure of the β-barrel, and to some extent also the wrapping domain, which harbor the above-mentioned essential residues with their surroundings is highly conserved in all currently resolved structures of typical catalases.

Catalase from different sources usually hold the properties namely, hydrophobic and glycoprotein nature (Calera et al. 2000), low acidic isoelectric pH (*pI*) (Brown-Petersen and Salin 1993; Ro et al. 2003; Eremin et al. 2004) and broad pH and temperature optima (Chandlee et al. 1983; Amo et al. 2002; Monti et al. 2003; Kang et al. 2006). However, the stability and catalytic efficiency of catalases varies significantly among different sources (Calera et al. 2000; Switala and Loewen 2002; Diaz et al. 2001, 2005).

3.3. Experimental approaches

3.3.1. Organism and culture conditions

The culture conditions of *A. terreus* MTCC 6324 used in this study have been described in section 2.2.1.

3.3.2. Purification of CAT

The fungal mycelia were harvested from the early stationary phase of growth (72 hours) and were disrupted at 30 kpsi using mechanical cell disruptor (Constant Systems, UK). The disrupted cell homogenate was centrifuged successively at 10,000×g for 10 min and 20,000×g for 20 min to pellet undisrupted cell mass and light mitochondrial fractions. The supernatant thus obtained was initially adjusted to 50% $(NH_4)_2SO_4$ saturation to precipitate the contaminating proteins. After removing the precipitated protein by centrifugation at 10,000×g for 30 min, the supernatant was finally adjusted to 80% $(NH_4)_2SO_4$ saturation to precipitate the CAT protein and centrifuged at 10,000×g for 30 min. The pellet was resuspended in 50 mM SPB containing 1 M $(NH_4)_2SO_4$ and loaded on a Phenyl Sepharose 6 Fast Flow HIC column (1.5×25 cm) connected to FPLC (AKTA prime plus, GE), pre-equilibrated with 50 mM SPB (pH 7.5) containing 1 M $(NH_4)_2SO_4$. The fractions were eluted from the column using 50 mM SPB (pH 7.5) containing a decreasing step gradient of $(NH_4)_2SO_4$ (0.75 M, 0.5 M, and 0.25 M). The final fraction was eluted with 50 mM SPB (pH 7.5). Fractions containing the CAT activity were pooled, dialyzed, concentrated and then loaded on Hiprep Sephacryl S-300 HR (1.6×60 cm, 50 µm) SEC column pre-equilibrated with 50 mM SPB (pH 7.5) to be eluted with the same buffer and flow rate. CAT containing fractions were pooled and concentrated. The lyophilized purified CAT was stored at -20ºC and was used for further characterization after re-suspension in 50 mM SPB (pH 7.5).

3.3.3. Molecular weight determination and electrophoresis

Molecular weight of purified native CAT was determined by SEC (Hiprep Sephacryl S-300 HR, 1.6×60 cm, 50 µm) using the FPLC (AKTA prime plus, GE). The gel filtration

molecular weight standards used were thyroglobulin (669 kDa), apoferritin (443 kDa), β–amylase (200 kDa), alcohol dehydrogenase (150 kDa), and carbonic anhydrase (29 kDa) (Sigma).

Native and SDS-PAGE analyses of the purified CAT protein were done following the method of Laemmli (1970) using 7% and 10% separating gels, respectively with 5% stacking gel and thickness of 0.75 mm. The gels were stained with CBB R 250 (Merck, India). Zymogram analysis of the native PAGE was done by incubating the gel in 10 mM H_2O_2 for 10 min. The SDS-PAGE protein markers used were carbonic anhydrase (bovine erythrocyte, 29 kDa), fumarase (porcine heart, 48.5 kDa), serum albumin (bovine, 66 kDa), phosphorylase b (rabbit muscle, 97.4 kDa), β-galactosidase (*E. coli*, 116 kDa) (Sigma). Glycostaining of the protein band in SDS-PAGE was done following the method of Segrest and Jackson (1972) using PAS reagent. The gel was fixed overnight in 100-200 ml of PAS fixative solution (40% ethanol and 5% glacial acetic acid in distilled water). The gel was then treated with the 0.7% periodic acid solution (in 5% acetic acid) for 2-3 hours, followed by treatment with 0.2% sodium metabisulfite solution (in 5% acetic acid) for 2-3 hours with one solution change after 30 min. The gel after clearing was put in tube and the tube was filled with Schiff reagent (Merck). After development of color in 12-18 hours at room temperature, the gel was stored at 4°C.

The *pI* was determined by isoelectric focusing, using immobiline 127 pH gradient gel strips of 3-11 and 4-7 linear range (GE healthcare, Sweden) following the instruction manual supplied with the Multiphor II gel apparatus (Hoefer, Pharmacia). The *pI* markers used were *A. niger* amyloglucosidase (3.6), soybean trypsin inhibitor (4.6), bovine milk β-lactoglobulin A (5.1), bovine erythrocytes carbonic anhydrase II (5.9), human erythrocytes carbonic anhydrase I

(6.6) and horse heart myoglobin (6.8, 7.2), lens culinaris lectin (8.2, 8.6, 8.8), and bovine pancreas trypsinogen (9.3).

3.3.4. Peptide mass fingerprinting

The protein identification work was carried out at ProtTech, Inc. (USA) by using the nano LC-MS/MS peptide sequencing technology. Each protein gel band was destained, cleaned, and digested in-gel with sequencing grade modified trypsin. The resulting peptide mixture was analyzed by a LC-MS/MS system, in which a HPLC with a reverse phase C_{18} column (75 µm inner diameter) was coupled on-line with an ion trap mass spectrometer. The mass spectrometric data acquired were used to search the most recent non-redundant protein database with ProtTech's proprietary software suite. The output from the database search was manually validated before reporting.

3.3.5. Enzyme assay and kinetics

The CAT activity was assayed by the method of Beers and Sizer (1952) with a partial modification. The activity was assayed using 50 mM SPB (pH 7.5) and 4.9 mM H_2O_2 (ε_{240} = 43.6 M^{-1} cm^{-1}). Initial reaction rate was determined spectrophotometrically (Cary 100Bio, Varian) by measuring the decrease of absorbance at 240 nm. One unit (U) of enzyme activity is the amount of enzyme that consumes 2 µmol H_2O_2 in one minute at room temperature. The substrate saturation kinetics was measured with H_2O_2 concentrations in a range of 0.05 to 75 mM

and enzyme preparation bearing specific CAT activity 30.74×10^5 U mg^{-1} protein. The apparent Michaelis–Menten constant (K_m) for H_2O_2, was calculated from the Lineweaver-Burk plot.

3.3.6. pH and temperature optima and stability of CAT

To measure pH optima, the enzyme reactions were carried out in different pH buffers namely, trisodium citrate (pH 2.5 to 4.0), sodium acetate (pH 5.0), sodium phosphate (pH 6.0 to 7.5), tris (pH 8.0), ethanolamine (pH 9.0), and sodium phosphate (pH 10.0 to 12.5) each at a concentration of 50 mM. For pH stability measurement the enzyme samples were incubated for different time periods in the aforementioned pH buffers at 4ºC and the residual CAT activity was determined at room temperature in SPB (50 mM, pH 7.5). The temperature optima were determined by carrying out the enzyme reactions at different temperatures and the CAT activity was measured spectrophotometrically. For determination of temperature stability, enzyme samples were incubated at different temperatures (4ºC to 80ºC) in circulating water bath (Julabo SW22, Germany) for different time periods followed by measurement of residual activity of CAT at room temperature in SPB (50 mM, pH 7.5).

The $t_{½}$ was calculated from the value of 0.693/k, where 'k' is the first order rate constant. The value of 'k' was calculated from the slope of a curve obtained by plotting ln a_0/a_t vs time (t), where a_0 is the initial CAT activity and a_t is the residual CAT activity obtained after incubating CAT for different time periods at said pH and temperatures.

3.3.7. Heme isolation from CAT and identification

Extraction of heme from the purified CAT was carried out by 2-butanone/HCl method (Teale 1959). Ice cold salt free purified CAT preparation was adjusted with 0.1 N HCl to pH 2.5,

followed by addition of equal volume of ice cold 2-butanone. The mixture was shaken for short time and was allowed to stand at 4°C. Ketone fraction containing heme was concentrated by rotary evaporator (Roteva, Equitron). Dissociated heme was further characterized by ESI-MS (Q-TOF Premier, Waters) following the method of Sana et al. (2008) and FTIR (Perkin-Elmer). All mass spectrometric measurements were recorded using ESI in the positive mode using the following conditions: nebulizer gas flow (N_2), 2 l min^{-1}; capillary voltage, 4 kV; temperature of the ESI probe, 100°C; curve; CDL temperature, 350°C; deflection voltage, 55 V; detector gain, 1.7 V; collision energy, 5. For scan measurements, a mass range from 100 to 1000 *m/z* was chosen; the integration time was 1 s. High resolution mass spectra was calculated based on the calibration of the instrument with standard leucine enkaphalin using a lock mass *m/z* 556.2771. The spectra obtained were processed and analyzed with the MassLynx V4.1 integrated software.

Protein was estimated by Bradford's method using BSA as standard (Bradford 1976) and carbohydrate was estimated by anthrone method using glucose as standard (Mokrasch 1953).

3.4. Results and discussion

A very high CAT activity was detected in the vegetative cells of *A. terreus* during its growth on *n*-hexadecane (2% v/v) substrate. A total activity of 17×10^6 U gm^{-1} dry cell-mass was obtained in the cells harvested from the late exponential phase (90 h) of growth in *n*-hexadecane substrate. This activity in the corresponding glucose-grown cells was 4.25×10^6 U gm^{-1} dry cell-mass. The average CAT activity from late log phase to late exponential phase was 9.5×10^6 U gm^{-1} dry cell mass in *n*-hexadecane grown cells. The overall CAT activity decreased in the stationary

phase of the growth of fungus. The high level of cellular CAT reported here is rare and is not known from the cells grown on hydrocarbon substrates. Such increased level of CAT activity in the *n*-hexadecane grown cells is likely to be linked to the metabolism of this hydrocarbon substrate in the cells of fungal mycelia. The initial oxidation of *n*-hexadecane by *A. terreus* produces hexadecanol as decribed in the section 2.4. The hexadecanol is further oxidized by a long chain alcohol oxidase with concomitant generation of H_2O_2 as by product (Kumar and Goswami 2006). It is expected that this high level of CAT produced in the cells of *A. terreus* rapidly neutralizes the harmful H_2O_2 continuously generated as byproduct in the cells during metabolism of the aforesaid substrates. It is also reported that other large catalases are less sensitive to oxidative damage by H_2O_2 (Diaz et al. 2001; Switala and Loewen 2002). Thus, induction of such high level of CAT may be attributed to the cellular defense mechanism against the oxidative stress caused by H_2O_2 formed during metabolism of *n*-hexadecane. Notably, except the level of activity, other properties of CAT as described later in this section were alike to the one produced in the glucose grown cells of *A. terreus* (results not separately shown).

CAT was isolated and purified successively by differential centrifugation, $(NH_4)_2SO_4$ precipitation, HIC and SEC. A 160-fold purification with specific activity of 66×10^5 U mg^{-1} protein with an overall yield of 47% in comparison to the original crude extract was achieved (Table 3.7.1). The homogeneity of the purified protein was demonstrated by single protein band in native PAGE (Fig. 3.6.1A, lanes 1 and 2). The molecular weight of CAT determined by SDS–PAGE of the purified protein sample (Fig. 3.6.1B, lanes 1 and 2) was nearly 90 kDa. The native protein molecular mass determined by SEC was 368±5 kDa (Fig. 3.6.2), which indicates that the native CAT protein is a homotetramer. The purity of CAT was further demonstrated by the high optical purity ratio (R_z, A_{405}/A_{280}) of 0.8±0.05 (A_{405} is the characteristic absorbance of protein-

bound heme; Eriksson et al. 1971). A distinct but low intensity peak at around 600 nm attributed to the tyrosine-linked heme coordination complex for CAT (Hargrove et al. 1994), was also detected in the same spectrum (Fig. 3.6.3A). A low temperature EPR spectrum showed the presence of high spin ferric iron in the purified CAT (Fig. 3.6.3B). The *pI* determined by isoelectric focusing of the purified CAT was found to be 4.2±0.1.

The SDS-PAGE separated protein band of the purified CAT was subjected to peptide mass finger printing studies to validate the preliminary identification of the enzyme as described above and also to understand the molecular characteristics of CAT to the possible extent. As anticipated, the enzyme had the highest similarity with the catalase B precursor protein from the strain NIH 2624 of *A. terreus* (Accession code: XP_001216098, www.ncbi.nlm.nih.gov). The calculated molecular weight of 77,768 Da of the precursor protein was less than the one experimentally measured by us for CAT (~90 kDa). The higher molecular weight of CAT than the precursor protein has been attributed to the glyco-moiety of CAT as CAT was identified as glycoprotein based on the PAS staining of the protein band in SDS-PAGE. The protein to carbohydrate ratio 3.33 of the purified CAT determined experimentally was, however, found marginally higher than the ratio required to compute with the calculated molecular weight of the protein to account for the molecular weight of CAT measured by SDS-PAGE. BLAST analysis of peptide fragments from CAT shows the conserved domains for proximal heme binding and tetramer interface (Fig. 3.6.4). Fig. 3.6.5A and B, are the LC-MS/MS spectra of amino acid residues of aforesaid domains respectively. Multiple sequence alignment of proximal heme binding residues of CAT with catalases from different source organisms showed the presence of conserved positions for tyrosine (Y) and arginine (R) (Table 3.7.2). The conserved arginine residue in the heme binding domain is known to involve in the catalytic mechanism of many

catalases (Carpena et al. 2005). It is known that phenolic side chain of the conserved tyrosine acts as the fifth heme iron ligand, the other four being the nitrogens of the porphyrin ring.

The heme was isolated from the purified CAT and the molecular mass of 616 of the isolated heme was determined by ESI-MS (Fig. 3.6.6A), which is similar to the reported molecular mass of heme b (Sana et al. 2008). The isolated heme was further characterized for its functional groups -OH, $-CH_3$, $-CH_2-$, and -C=O by FTIR spectrum (Fig. 3.6.6B). Many variants of heme namely, heme-b, -d, and -derivatives of heme have been reported in catalases. Notably, the presence of only heme d in large catalases from *Aspergillus* has been described so far (Switala and Loewen 2002). Thus, this finding on the presence of heme b in the large catalase from *A. terreus* is interesting and warrant further investigation to understand the exact role of these two types of heme (b and d) in the large catalases, though heme in general is known as the catalytic center of these redox enzymes.

CAT activity with increasing H_2O_2 concentration (within 0.05 to 75 mM H_2O_2) followed Michaelis-Menten kinetics with apparent K_m of 14.15 mM as calculated from the Lineweaver-Burk plot with a linear equation, y=4.265x+0.301 and correlation coefficient (R^2) of 0.9949 (Fig. 3.6.7). A high catalytic efficiency (K_{cat}/K_m) of 4.7×10^8 M^{-1} s^{-1} was deduced from the catalytic turnover number (K_{cat}) of 6.65×10^6 s^{-1} and apparent K_m of CAT.

CAT was active in a broad range of pH 4.0 to 12.0 and temperature 25ºC to 90ºC (Fig. 3.6.8A and B). However, a variation in the CAT activity was observed within this pH range, where, the activity was increased with the increasing pH. The activity of CAT was drastically lost outside this pH range and when boiled. The stability ($t_{½}$) of the CAT activity at pH 7.5 was nearly 30 months and was found to be exceptionally stable at alkaline pH. The $t_{½}$ of CAT at pH 12.0 was ~15 months. The stability of CAT diminished steadily with the increasing temperature

from 25ºC to 80ºC with $t_{½}$ of 54 days and 42 min at 25ºC and 80ºC, respectively. CAT was highly stable when stored at 4ºC and pH 7.5, as more than 98% of the initial CAT activity was retained even after one month and a $t_{½}$ of nearly 30 months was calculated.

Although, many of the basic properties like acidic *pI*,, glycoprotein nature, binding to hydrophobic column and broad pH and temperature optima, of the isolated CAT from *A. terreus* are similar to the widely studied large catalases reported from other sources, certain properties of CAT were found to be rare. The catalytic efficiency and stability near extreme alkaline pH of CAT are considerably higher than most of the extensively studied catalases from different sources (Calera et al. 2000; Switala and Loewen 2002; Monti et al. 2003; Ogawa et al. 2004). The high catalytic efficiency reported by us is only comparable to the durable large catalase (Cat-1) from *N. crassa* (Diaz et al. 2001). Similarly, the thermal stability of CAT at 80ºC is exceptional among the mesophiles, and is comparable with the catalase from few thermophilic origins (Amo et al. 2002; Thompson et al. 2003) and Cat-1 from *N. crassa* (Diaz et al. 2001). High stability at 4ºC and room temperature is also interesting feature of the isolated CAT. Such significantly high activity and stability under broad thermal and pH conditions are construed as the attractive properties of CAT for potential industrial applications in areas like, biosensors, therapeutics, textile and food industries where the enzyme is required to work in a broad pH and temperature range for long periods. The present findings also suggest *n*-alkane, an easily available carbon source from natural resources, as efficient substrate for CAT production by *A. terreus*. Further studies on the optimization of the catalase production using this substrate may provide a suitable process to meet the industrial requirements for this redox enzyme.

3.5. Conclusions

A hydrocarbon degrading *A. terreus* MTCC 6324 produces high level of cellular large catalase during growth on *n*-hexadecane, with total activity 17×10^6 U gm^{-1} dry cell-mass. A 160-fold purification with specific activity of around 66×10^5 U mg^{-1} protein in comparison to the original crude extract was achieved. The native protein molecular mass was 368±5 kDa with subunit molecular mass nearly 90 kDa, which indicates that the native CAT protein is a homotetramer. The *pI* of the purified CAT was 4.2. Peptide mass fingerprinting studies confirmed its identity as catalase B (large catalase). The heme was identified as heme b by ESI-MS. CAT was active in a broad range of pH 4.0 to 12.0 and temperatures 25ºC to 90ºC. The catalytic efficiency (K_{cat}/K_m) of 4.7×10^8 M^{-1} s^{-1} and alkaline pH stability ($t_{½}$ at pH 12.0 ~15 months) of CAT are considerably higher than most of the extensively studied catalases from different sources. The storage stability ($t_{½}$) of CAT at physiological pH 7.5 and 4°C was nearly 30 months. These high activity and stability under broad thermal and pH conditions are construed as the attractive properties of CAT for potential industrial applications.

3.6. Figures

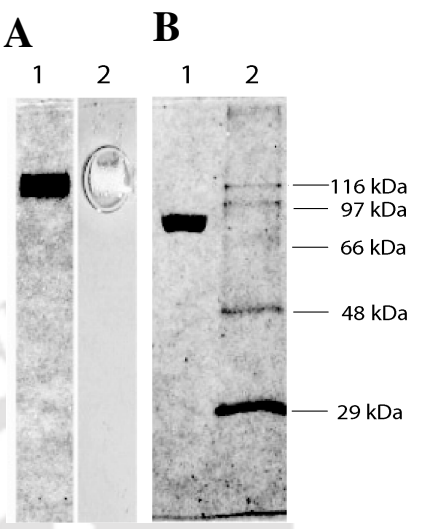

Fig. 3.6.1. PAGE analysis of purified CAT. **(A)** Native PAGE: lane 1, CBB staining of CAT and lane 2, activity staining of CAT (loaded 10 µg purified protein). **(B)** SDS-PAGE: lane 1, CBB staining of CAT protein and lane 2, CBB staining of standard molecular markers.

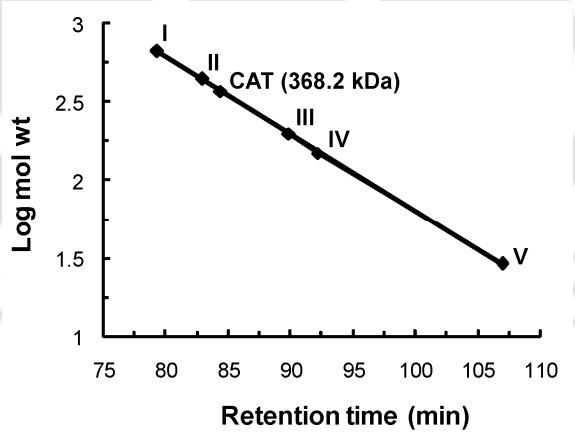

Fig. 3.6.2. Determination of molecular weight of native CAT by SEC (Hiprep Sephacryl S-300 HR, 1.6×60 cm, 50 µm, GE). Molecular weight standards were: I. thyroglobulin (669 kDa), II. apoferritin (443 kDa), III. β-amylase (200 kDa), lV. alcohol dehydrogenase (150 kDa) and V. carbonic anhydrase (29 kDa) (Sigma).

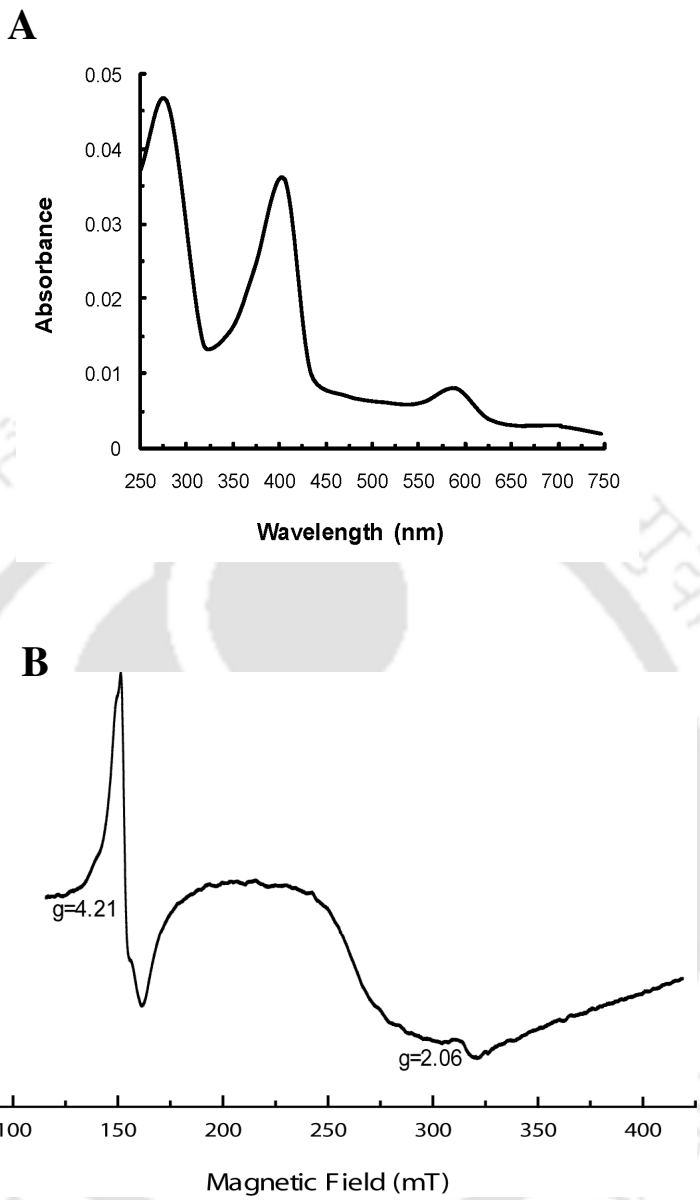

Fig. 3.6.3. (A) UV-Vis spectrum of purified CAT. The protein concentration was 15 µg ml^{-1} in 50 mM SPB (pH 7.5). The data was recorded at a scan rate of 100 nm min^{-1}. **(B)** Low-temperature EPR spectrum of purified CAT. Measurement conditions: protein concentration, 15 µg ml^{-1} in 10 mM SPB (pH 7.5); microwave frequency, 9.063 GHz; microwave power, 20 mW; modulation amplitude 4 G; modulation frequency, 100 kHz; time constant 0.3 s.

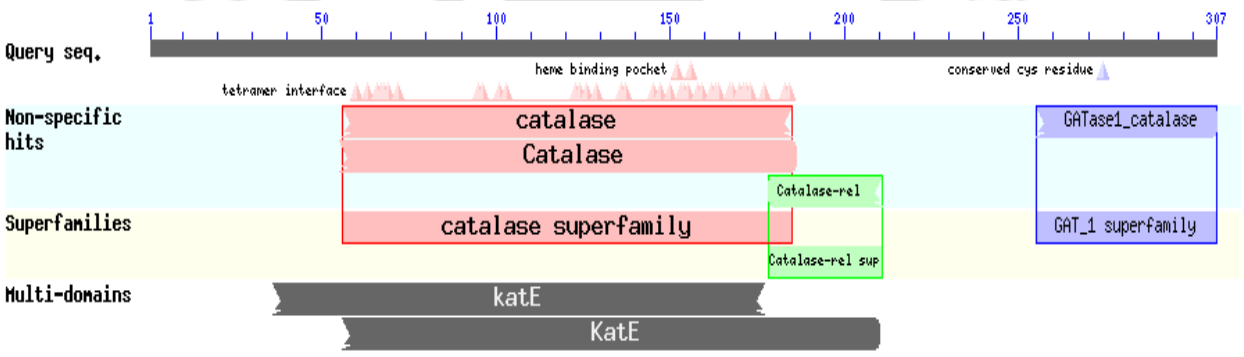

Fig. 3.6.4. Conserved domains of CAT identified after BLAST alignment of peptide fragments obtained after nano LC-MS/MS sequencing of SDS-PAGE band of ~ 90 kDa.

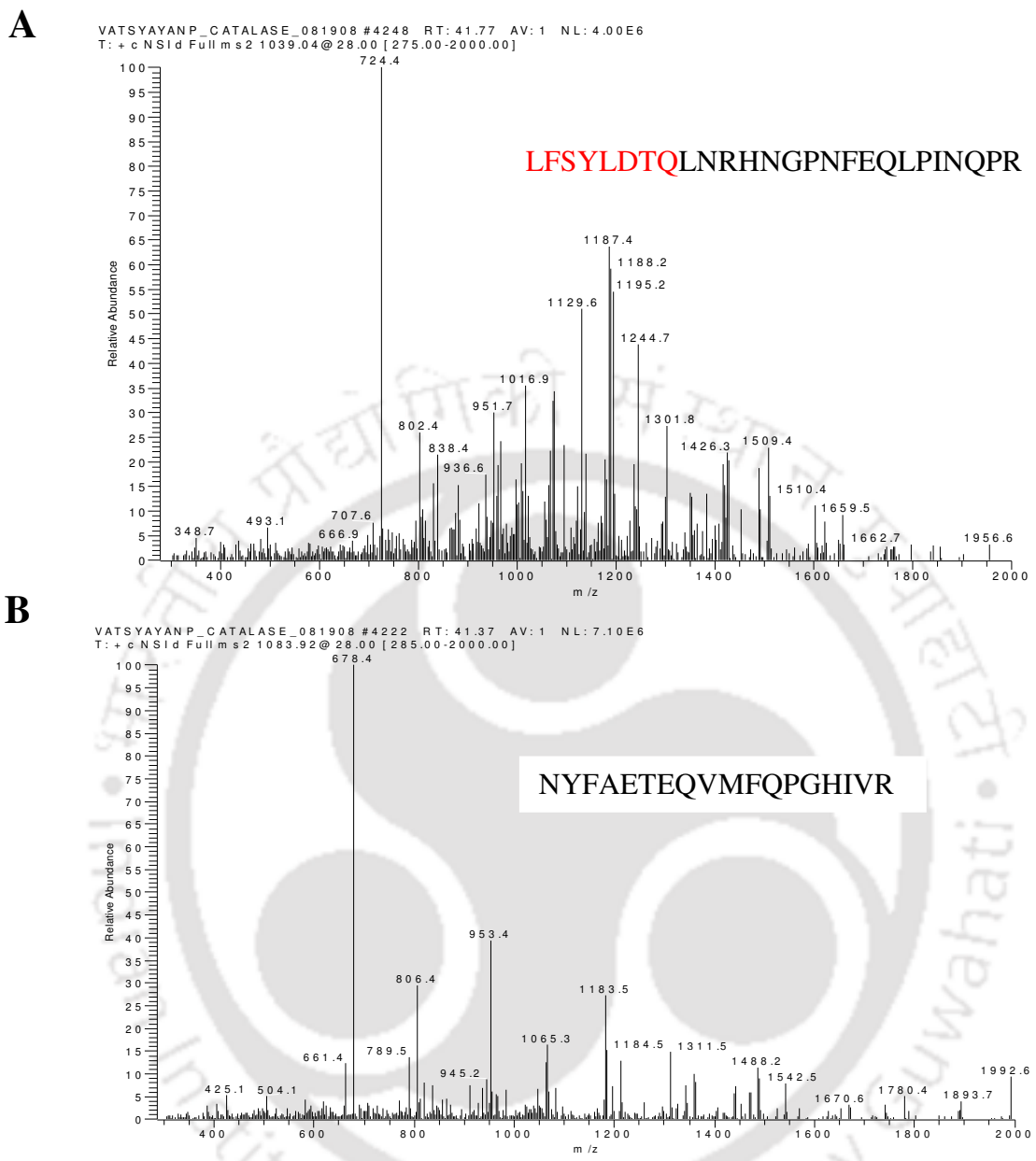

Fig. 3.6.5. **(A)** LC-MS/MS spectrum of "LFSYLDTQLNRHNGPNFEQLPINQPR" peptide. The eight amino acid sequences from left belong to the proximal heme binding domain of CAT. The first residue "R" in the left is missed here due to tryptic digestion, which is however, identified by the overlapping of spectra. The detailed description of proximal heme binding domain is given in the manuscript. **(B)** LC-MS/MS spectrum of "NYFAETEQVMFQPGHIVR" peptide which belong to the tetramer interface domain of CAT.

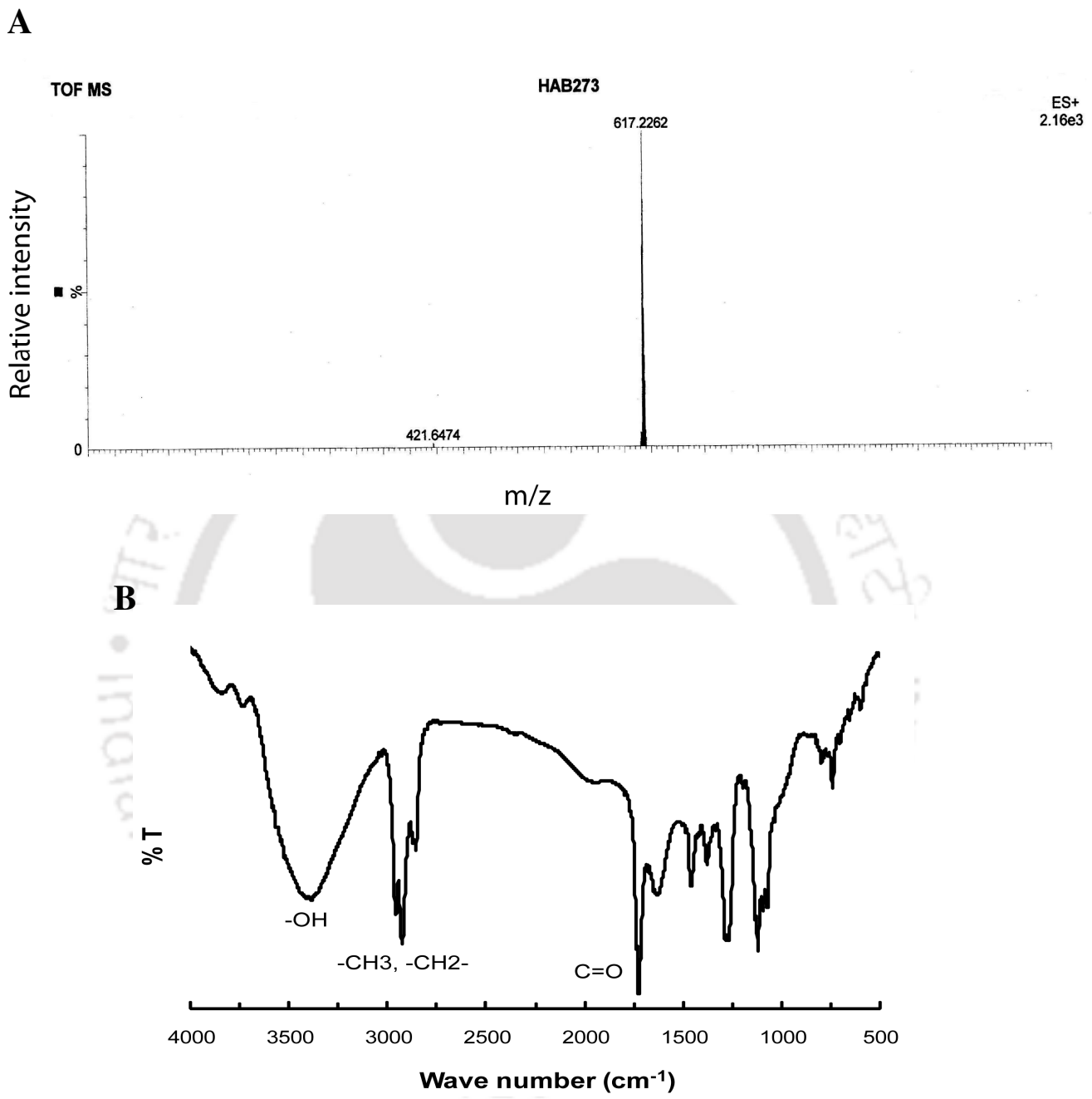

Fig. 3.6.6. **(A)** ESI-MS spectrum of the extracted heme from the native purified CAT. The sample was run in the ESI positive mode. **(B)** FTIR spectrum of the isolated heme. Peaks corresponding to the representative functional groups of heme are shown in the figure.

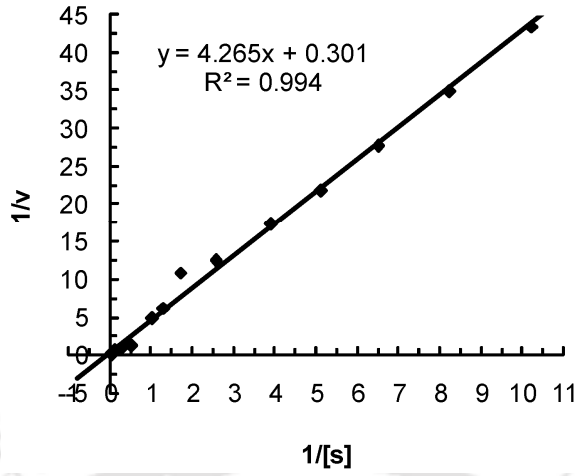

Fig. 3.6.7. Lineweaver-Burk plot for determination of apparent K_m of CAT.

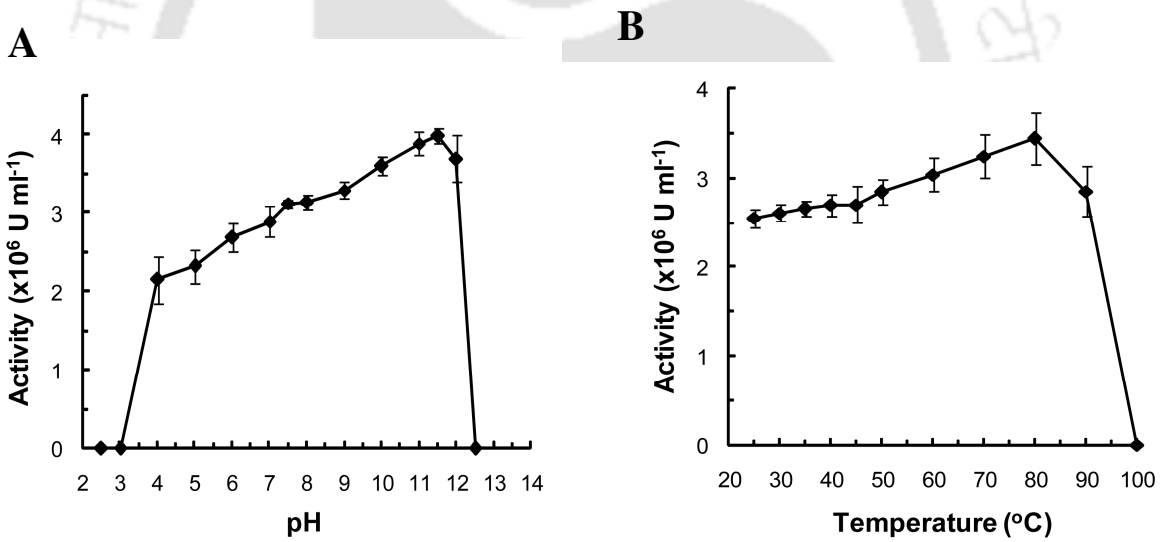

Fig. 3.6.8. CAT activity as a function of pH **(A)** and temperature **(B)**. The different pH buffers (each at a concentration of 50 mM) were trisodium citrate (pH 2.5 to 4.0), sodium acetate (pH 5.0), sodium phosphate (pH 6.0 to 7.5), tris (pH 8.0), ethanolamine (pH 9.0) and sodium phosphate (pH 10.0 to 12.5). Each datum point represents the average of the analysis of triplicate values.

3.7. Tables

Table 3.7.1. Purification table for CAT.

Fractions	Activity ($\times 10^5$ U ml^{-1})	Protein (mg ml^{-1})	Specific activity ($\times 10^5$ U mg^{-1})	Fold Purification	Yield %
crude extract	1.2±0.5	2.9±0.8	0.41±0.10	1.0	100
sup-1[a]	1.7±0.3	1.8±0.5	0.94±0.20	2.3	88.6
pellet-1[a]	2.7±0.8	5.4±1.0	0.50±0.09	1.2	10.8
sup-2[b]	2.3±0.4	1.4±0.3	1.64±0.60	4.0	75.0
pellet-2[b]	0.3±0.1	7.2±1.2	0.04±0.01	0.1	12.4
50% pellet[c]	2.4±0.7	7.2±1.9	0.33±0.10	0.8	10.1
80% pellet[c]	3.3±1.2	1.4±0.5	2.36±0.50	5.8	62.5
HIC purified[d]	14.7±1.4	0.5±0.1	29.40±1.42	71.7	54.4
SEC purified	39.6±2.0	0.6±0.1	66.00±3.97	160.9	47.0

[a] sup-1 and pellet-1 are supernatant and pellet of 10,000×g centrifugation.

[b] sup-2 and pellet-2 are supernatant and pellet of 20,000×g centrifugation.

[c] 50% and 80% pellet are $(NH_4)_2SO_4$ precipitated fractions.

[d] HIC purified fraction was eluted at 250 mM $(NH_4)_2SO_4$ concentration.

Each value represents the mean±standard error at $p<0.05$.

Table 3.7.2. Multiple sequence alignment of amino acid residues of proximal heme binding domain of CAT with other known catalases.

Catalase source organism	Amino acid sequence	Accession code
Aspergillus terreus MTCC 6324	R L F S Y L D T Q	This work
Aspergillus terreus NIH 2624	R L F S Y L D T Q	XP_001216098.1
Aspergillus niger	R L F S Y L D T Q	XP_001388621.1
Aspergillus nidulans FGSC A4	R L F S Y L D T Q	XP_682608.1
Aspergillus fumigatus Af293	R L F S Y L D T Q	XP_748550.1
Penicillium marneffei ATCC 18224	R L F S Y L D T Q	XP_002153601.1
Neurospora crassa OR74A	R L F S Y L D T Q	XP_957826.1
Pseudomonas stutzeri A1501	R L F S Y A D T Q	YP_001174038.1
Escherichia coli SE11	R L F S Y T D T Q	YP_002293177.1
Mycobacterium vanbaalenii PYR-1	R L F S Y L D T Q	YP_954009.1
Candida dubliniensis CD36	R L F S Y A D T H	dbj|BAD77826.1
Arabidopsis thaliana	R V F S Y A D T Q	emb|CAA64220.1
Rattus norvegicus	R L F A Y P D T H	NP_036652.1
Bos taurus	R L F A Y P D T H	NP_001030463.1
Homo sapiens	R L F A Y P D T H	NP_001743.1

Chapter 4

Stability and heme dissociation studies of CAT

4.1. Overview

The *typical* catalases are important heme containing antioxidant enzymes known for their ability to degrade H_2O_2 into water and oxygen. The heme is the prosthetic group that consists of an iron atom contained in the center of porphyrin ring. The heme iron in catalase is pentacoordinated, where phenolic side chain of the conserved tyrosine (Tyr) residue acts as the fifth heme iron ligand, the other four being the nitrogens of the porphyrin ring (Zamocky and Koller 1999; Putnam et al. 2000). The protein bound heme provides catalase a characteristic Soret peak at 405 nm and distinct redox properties (Eriksson et al. 1971; Zhang et al. 2002). Catalases, especially large catalases, are known to be stable over a wide range of pH and temperatures (Switala and Loewen 2002; Diaz et al. 2005). However, the relation between the heme stability in the protein matrix and the stability of catalase activity are not yet clearly known. Studies on the stability of heme in the protein matrix of redox enzymes may unearth important information useful not only for elucidating the structure-function relationships but also for the practical applications of these heme-based enzymes, like development of biosensors and biofuel cells where effective electronic communication between the heme centre and the electrode is a critical factor that dictate the efficiency of these bioelectronic devices (Spiro and Jarzecki 2001; Garcia et al. 2005; Gonzalez and Gonzalez 2005; Karlsson and Nilsson 2005). Notably, to improve the electron transfer from the redox centre across the insulating protein

matrix, reconstitution of heme with the apo-protein or protein has been identified as a possible approach for developing efficient enzyme electrodes for biosensor and biofuel cell applications (Das and Hecht 2007; Hong et al. 2007; Fruk et al. 2009). The purified CAT from *A. terreus* MTCC 6324 had broad pH (pH 4.0 to 12.0) and temperature optima (25ºC to 90ºC) as described in chapter 3. Enticed with the ideas discussed above, we investigate the stability of CAT isolated over a wide range of pH. The stability of the heme in the protein matrix under broad pH was investigated following absorption spectroscopy as well as electrochemical analysis. We conducted further studies on the separation of heme from the CAT protein and its reconstitution with the generated apo-CAT to a functionally active CAT. The stability of the CAT activity was also studied under different temperature conditions and was correlated with the integration of heme inside the protein matrix. Detailed findings on these studies are described in this chapter.

4.2. Literature Review

Many proteins contain a non-diffusible cofactor, often termed a prosthetic group, which is a nonpeptidic molecular moiety bound in the active site of the protein (Degtyarenko et al. 1998). Such a cofactor is required for the protein to conduct its function, such as the binding of substrates and other reaction partners as well as for the catalytic conversion and are often involved in electron-transfer reactions. Prominent examples of such prosthetic groups are porphyrin and flavin derivatives (Fruk et al. 2009). Among porphyrin derivatives, iron containing porphyrins (heme) form a large class of proteins actively involved in various biological functions.

Heme, an essential molecule, is widely distributed among all organisms. Besides cytochromes (e.g. cytochrome b5, cytochrome c; Lemberg and barrett 1973) and globins (e.g. myoglobin, hemoglobin; Antonini and Brunori 1971) responsible for electron transfer and transport and storage of oxygen inside the cells, respectively, a major class of heme proteins is involved in the catalysis of physiologically important reactions. Some of the representatives of the later are catalases, cytochrome P450 and peroxidases etc. (Dawson and Sono 1987), where heme as the redox center plays vital role in catalysis.

Large catalases are a minor subgroup of typical heme containing catalases which possess an extra flavodoxin-like C-terminal domain (Melik-Adamyan et al. 1986; Bravo et al. 1995; Zamocky and Koller 1999). Interestingly, members of this subgroup are found both in bacteria and fungi (Vainshtein et al. 1986; Fowler et al. 1993; Lopez-Medrano et al. 1995; Navarro et al. 1996; Kawasaki et al. 1997; Klotz et al. 1997; Garre et al. 1998; Takasuka et al. 1999; Calera et al. 2000; Switala and Loewen 2002; Klotz and Loewen 2003). They all share high sequence similarity/identity. This situation could be explained by horizontal gene transfer between evolutionary independent organisms sharing a common habitat, but an endosymbiotic origin of peroxisomes is also discussed (Klotz et al. 1997).

Few of these enzymes have been studied from the molecular and kinetic point of view. Conspicuous features of these large catalases are: withstanding molar concentrations of H_2O_2 (Lardinois et al. 1996; Diaz et al. 2001), thermoresistance (≥70°C) (Wasserman 1981; Lopez-Medrano et al. 1995; Diaz et al. 2001; Switala and Loewen 2002), enhanced resistance to denaturants (Lopez-Medrano et al. 1995; Diaz et al. 2001; Switala and Loewen 2002; Calera et al. 2000), and lower sensitivity to inactivation by azide than other catalases (Gruft et al. 1978;

Kikuchi-Torii et al. 1982; Lardinois and Rouxhet 1996). Limited studies have been carried out on the pH stability of these large catalases with a very few recent reports (Diaz et al. 2005)

There are several speculations for the exceptional chemical and temperature stability of large catalases, e.g. in addition to the extra carboxy-terminal `flavodoxin-like' domain, these catalases also have extended N-terminal regions (50-70 residues long), and both these extensions are thought to contribute to the increased chemical and thermal stability of these large- subunit catalases (Zamocky and Koller 1999). Similarly, the conversions of heme b to d are also speculated to contribute to the stability of these large catalases (Zamocky and Koller 1999; Switala and Loewen 2002). Though, it remains to be seen whether these hold true for large catalases from other unexplored sources also. Later works on two isoforms of large catalases from *Neurospora crassa* (Cat-1a and Cat-1e containing heme-b and d, respectively) have however ruled out the possibility for the involvement of the heme-b to d conversion for imparting the chemical, thermal or pH stability to the large catalases (Diaz et al. 2005). There are several other aspects which are required to be explored to completely understand the exceptional stability of large catalases. The linkage of heme inside the protein matrix is always highly specific for all heme containing enzymes which imparts them their characteristic properties (Mitra 1994; Wang et al. 2003). Soret absorption peaks usually reflect the ligand state and environment of the heme and have been efficiently utilized since past to study heme protein matrix interactions or to predict the influence of different denaturing treatments on such interactions (Eriksson et al. 1971; Yoshida and Kikuchi 1978). Similarly, the Fe^{3+}/Fe^{2+} redox center of heme has been recently utilized to study the changes surrounding the redox environment of the heme enzymes (Mie et al. 2006; Panicco et al. 2008)

Several studies have been done on removal of these heme derivatives from the enzyme by chemical methods or biological manipulations, their modifications and reinsertion in the protein matrix to obtain enzymes with different catalytic properties (Fruk et al. 2009). This process is termed enzyme reconstitution. The process includes the preparation of apo-proteins. These are folded proteins which lack their respective prosthetic group, but into which naturally occurring or synthetic cofactors can be introduced (Hill and Wharton 1978; Harris et al. 1993). This approach represents a versatile method for investigating the reaction mechanisms of or introducing novel chemical functions into a given protein. In a broader sense, the term "reconstitution" also refers to the addition of metal cofactors (not only prosthetic group) into apo-enzymes, such as in the case of FeMo centers of nitrogenases (Shah et al. 1994; Hu et al. 2005; Curatti et al. 2007) or NiFe centers of hydrogenases (Fu and Maier 1992). The reconstitution of an apoprotein with a non-natural cofactor moiety can be used for several applications in biotechnology, for example, the preparation of complex novel devices, such as nanoscaled scaffolds, addressable catalysts, or the fabrication of micro- and nanoarrays of semisynthetic proteins (Hamachi et al. 1993; Sakiyama-Elbert and Hubbell 2001; Wong and Bronzion 2003). Additionally, removal and re-insertion of a cofactor has been proven to be a powerful tool for structural enzymology (Neya et al. 1994; Neya et al. 1996), such as studying the role of specific atoms of the cofactor or of distinct amino acids in proximity to the prosthetic group in the active site of the protein. The latter is particularly interesting in the case of heme enzymes, since the environment of the prosthetic group usually plays a crucial role in the enzymes activity.

In the past 30 years the reconstitution of, in particular, flavo and heme enzymes has been harnessed to enable electrical communication between enzymes and electrodes (Hong et al.

2007). This has allowed the elucidation of catalytic mechanisms as well as protein–protein and protein–ligand recognition processes, and the creation of novel biomaterials. From a synthetic chemistry and biocatalysis point of view, there is great interest in the design of novel, semisynthetic metalloenzymes which possess high selectivity and reactivity under mild conditions. Exciting progress has been made on the development of semisynthetic metalloenzymes that mimic their native counterparts (Das and Hecht 2007). For example, heme enzymes with their metal containing porphyrin cofactors are excellent scaffolds for the introduction of novel functions through reconstitution with artificial cofactors. Thus, the reconstitution method can be utilized as a tool to elucidate structure–activity relationships of enzymes and also to design novel biosensors and biomaterials (Fruk et al. 2009).

4.3. Experimental approaches

4.3.1. Reagents

CAT was isolated, purified and characterized from *A. terreus* MTCC 6324, as described in section 3.3. MWCNT with 95% purity (10–15 nm outer diameter, 2-6 nm inner diameter and 0.1-10 µm length and PEI (50%) were obtained from Sigma, NF from Du Pont (USA), and H_2O_2 (30%) was obtained from Merck.

4.3.2. CAT activity assay

CAT activity was assayed by the method of Beers and Sizer (1952) with a partial modification as described in section 3.3.5. The activity was assayed using 50 mM SPB (pH 7.5) and 4.9 mM H_2O_2 (ε_{240} = 43.6 M^{-1} cm^{-1}). One unit (U) of enzyme activity is the amount of enzyme that consumes 2 µmol H_2O_2 in one minute at room temperature.

4.3.3. pH and temperature stability of CAT

For pH stability measurements, the purified CAT samples were incubated for different time periods in different pH buffers namely, trisodium citrate (pH 3.0 to 4.0), sodium acetate (pH 5.0), sodium phosphate (pH 6.0 to 7.5), tris (pH 8.0), ethanolamine (pH 9.0), and sodium phosphate (pH 10.0 to 12.5) each at a concentration of 50 mM at 4ºC and the residual CAT activity was determined at room temperature in SPB (50 mM, pH 7.5). For determination of temperature stability, enzyme samples were incubated at different temperatures (4ºC to 80ºC) in circulating water bath (Julabo SW22, Germany) for different time periods followed by measurement of residual activity of CAT at room temperature in SPB (50 mM, pH 7.5).

The $t_{½}$ was calculated from the value of 0.693/k, where 'k' is the first order rate constant. The value of 'k' was calculated from the slope of a curve obtained by plotting ln a_0/a_t vs time (t), where a_0 is the initial CAT activity and a_t is the residual CAT activity obtained after incubating CAT for different time periods at said pH and temperatures.

4.3.4. pH effect on redox potential and electro-catalytic activity of CAT

Redox potential of CAT immobilized on MWCNT-NF/PEI modified GCE was determined by CV in a conventional three-electrode cell with an Ag/AgCl/saturated KCl reference electrode and platinum wire as counter electrode. Prior to the surface modification, the GCE (5 mm diameter) was polished with 3 µm alumina slurry, and then ultrasonically cleaned successively in distilled water and ethanol to remove adsorbed alumina particles and finally, air dried. The MWCNT-NF film was prepared by method described by others (Tsai et al. 2004). 10 mg MWCNT was added to 1 ml of 5% NF and sonicated for about 3.5 h to obtain a stable and uniform suspension. 10 µl of this suspension was layered on GCE and allowed to dry under clean air at room temperature. Once dried, 15 µl of CAT solution (0.5 mg ml^{-1}) was layered on the MWCNT-NF nano-composite and kept overnight at 4ºC. Finally, 5 µl of PEI (10%) was layered and dried at room temperature. To study the effect of pH, the CV experiments were carried out in different pH buffers in absence and presence of 1.5 mM H_2O_2, respectively. The buffer systems used were similar as used for the determination of pH stability of CAT in section 3.3.6. Electrochemical experiments were performed with a computer - controlled- Autolab modular electrochemical system (Eco Chemie, Utrecht, Netherlands), driven with GPES software (Eco Chemie). All experiments were carried out at room temperature of 25°C.

4.3.5. Heme dissociation and re-association studies

Extraction of heme from purified CAT was carried out by 2-butanone/HCl method (Teale 1959) as described in section 3.3.7. The aqueous fraction containing apo-CAT was dialyzed

against one liter of distilled water to remove remaining ketone, followed by subsequent dialysis against two changes of 500 ml of SPB (50 mM, pH 7.5) first containing 2 mM DTT for one hour and then without DTT overnight and concentrated. Re-association of heme inside the protein matrix was carried out by mixing 100 µl of the isolated heme preparation in 0.1 N NaOH and 400 µl of apo-CAT (0.5 mg ml^{-1}) added with 180 mg of urea (6 M final concentration) followed by incubation at 4ºC for 30 min or heating at 40ºC for 15 min. The reconstituted enzyme was then passed through Sephadex G25 column to remove urea and unbound heme. Fractions containing apo-CAT, reconstituted CAT and native CAT were analyzed for change in their characteristic absorbance spectra and catalytic activity as described in earlier section.

Protein was estimated by Bradford's method using BSA as standard (Bradford 1976).

4.4. Results and discussion

The stability of CAT from *A. terreus* over a broad pH range was investigated and a higher stability towards alkaline side than the acidic side was observed (Fig. 4.6.1). The stability was rapidly diminished with decreasing the incubating pH starting from neutral pH and eventually lost at pH 3.0. The overall stability of CAT, though decreased from its optimum stability at pH 7.5 ($t_{½}$ of nearly 30 months) towards alkaline side, was leveled of beyond pH 10 until the stability was completely lost at pH 12.5. However, this reduction in stability towards acidic side was comparatively much higher than the alkaline side. The stability ($t_{½}$) of CAT within the pH 9.0 to 12.0 fell in the range of 18.5 to 15 months, whereas, the highest stability of CAT in the studied acidic range was 8.5 months (at pH 6.0), which was less than 50% of the average value obtained in the alkaline pH range. Considering the central role of the prosthetic

heme group on the activity of CAT, the effect of pH on the integration of heme within the protein matrix was investigated to understand any possible relation between the pH stability of CAT and its association with the heme. The purified CAT was incubated separately for one week at different test pH and the Soret peak at 405 nm of heme-integrated catalase for the treated CAT samples was monitored. The intensity of the Soret peak of CAT incubated at pH 7.5 was higher than the rest of CAT samples incubated at different pH and was used as reference (Fig. 4.6.2). The intensity of the Soret peaks of CAT treated at pH 4.0, and 3.0 were decreased by 32% and 51%, respectively, whereas, the intensity of the peak of CAT treated at pH 12.0 was decreased only by nearly 10% of the reference. This indicates higher disintegration of heme from the CAT protein matrix in acidic pH than the alkaline pH, and the level of the disintegration was increased with increasing the acidic environment for CAT. Hence, it may be inferred that the linkage of heme prosthetic group with the protein matrix is significantly stable in alkaline environment until pH 12.0 and unstable in acidic environment. At pH 12.5, both the 405 nm and 280 nm peaks were completely disappeared and instead, a curvature with background absorbance throughout the spectral window was observed. This indicates a drastic change of the protein architecture along with the associated breakdown of heme from the CAT protein matrix. At pH 3.0, though the stability of the CAT activity was completely diminished yet the characteristic protein peak at 280 nm was retained. This indicates that the protein architecture of CAT was not much impaired under the acidic condition even down to pH 3.0. Corresponding to the reduction of the Soret peak, a marginal increase in intensity at 280 nm was observed at pH 3.0, which is attributed to the exposure of aromatic amino acid moieties of protein upon splitting the heme from the protein matrix. A minor blue shift of the Soret peak at pH 3.0 was observed, the exact reason for this

shifting is however, not yet known. The blue shift of the Soret peak at acidic pH has been reported for other heme proteins as well (Eriksson et al. 1971).

Since the heme of CAT is chemically linked to the protein matrix through its Fe^{3+}- centre, the redox behavior of heme Fe^{3+}/Fe^{2+} couple of CAT under different pH conditions is expected to throw light on the integration of heme in the CAT protein matrix. A pair of well defined and nearly reversible CV peaks for Fe^{3+}/Fe^{2+} redox couple of immobilized CAT on GCE/MWCNT-NF/PEI with formal potential ($E°$) of about -0.45 V (vs. Ag/AgCl reference electrode) was observed at pH 7.5 (Fig. 4.6.3A; curve a). A negative shift in the formal potential as a function of pH was observed at alkaline pH (pH 8.0 to 12.0) (Fig. 4.6.3A; curves b and c), whereas, a positive shift of the redox potential moving towards zero as a function of pH was observed at acidic pH (Fig. 4.6.3A; curves d, e and f). Although these shifts in potentials of Fe^{3+}/Fe^{2+} redox couple of the immobilized CAT were alike free heme (Fig. 4.6.3B; curves a to f), a significant increase in current of the redox peaks of CAT in comparison to the free heme under the acidic pH was observed (Fig. 4.6.3A and B; curves d, e and f). This increased Fe^{3+}/Fe^{2+} redox current of CAT implies increased electron transfer between the heme and the electrode under the acidic pH conditions. This is possible only when the heme prosthetic groups are largely released from the CAT protein matrix and come closer to the electrode surface by crossing the diffusion barrier usually caused by the insulating protein matrix under the applied potential. A low redox current was observed at highly acidic pH of 3.0 as compared to the current obtained at other acidic test pH. It is suggested that at such high acidic pH the heme is disintegrated fast and released from the protein matrix to the bulk electrolyte solution that led to decrease the heme concentration on the electrode surface resulting in poor charge transfer. The effect of pH on the electrochemical behavior of some heme-based protein has been reported (Liu et al. 2004) while, such studies

directed to elucidate the effect of pH on the stability of heme prosthetic group in catalase are not adequately known. Immobilized CAT on GCE/MWCNT-NF/PEI showed electro-catalysis in a broad range of pH (3.0 to 12.0) (Fig. 4.6.3C), similar to the catalytic activity of CAT. The decrease in electro-catalytic current towards acidic pH can be correlated to the less stability of the heme in protein matrix as explained earlier.

Heme may be isolated from the catalase by extraction at acidic pH (Teale 1959). The weak association of the heme with the protein matrix at acidic pH demonstrated through this investigation validated the extraction of the heme from the native CAT at low pH. The absorbance spectra of the separated apo-CAT was recorded and compared with the spectra of the native CAT (Fig. 4.6.4). In apo-CAT the Soret peak for protein-bound heme at 405 nm was vanished while, the protein peak at 280 nm was retained. The spectral data obtained in this investigation using these Soret peaks demonstrate the successful preparation of apo-CAT from the native CAT of *A. terreus.* The reconstitution study was carried out to understand the nature of association of the heme within this large catalase. An attempt to reconstitute the functionally active CAT by simple mixing of the heme (dissolved in DMSO or buffer) and apo-CAT at room temperature and pH 7.5 was not successful. However, when this reconstitution was carried out under alkaline (0.1 N NaOH) and denaturing environment in presence of 6 M urea or heat (40ºC, 15 min) (Fig. 4.6.5), the CAT activity, though low, was detected (Table 4.7.1). A Soret peak at around 405 nm with albeit low intensity was regenerated in the reconstituted CAT (Fig. 4.6.4). It is likely that removal of the heme resurrects the weak van der Walls forces in the heme-binding pocket of the apo-protein as evident from the requirement of denaturing agents like, urea or heat for exposing the pocket and re-insertion of heme in the protein matrix. The method of reconstitution, however, needs to be optimized for regenerating the entire activity of CAT.

The dissociation of heme in acidic pH can be attributed to the protonation of phenolate side chain of Tyr that weakens the Tyr→Fe^{3+} (heme) bond in the proximal heme binding domain of the protein matrix. Notably, a Tyr residue is known to involve as fifth ligand of the heme iron in catalase through Tyr→Fe^{3+} bond (Putnam et al. 2000). Stable heme-Tyr linkage in the alkaline pH provides better stability to CAT towards the alkaline environment, whereas, protonation of this linkage initiated in acidic environment may cause overall instability to CAT. The protein free heme independently could not function like native CAT as evident from the lack of detectable catalase activity of the free heme. The assembly of the heme with the protein matrix seems to be important for proper catalytic activity of CAT, and this assembly needs to be through proper chemical bonding rather than a mere physical interaction as also suggested by others (Mitra 1994; Wang et al. 2003). Thus Tyr→Fe^{3+} linkage between heme and the protein matrix as reflected through the Soret absorbance is critical for functional stability of CAT. Through this investigation we have reported that the chemical stability of the prosthetic heme in the protein matrix is vital for the functional stability of this large catalase and this stability is increasingly affected by increasing acidity of the medium. This disintegration of heme from the protein matrix likely to influence the secondary structures of the protein, hence the possibility of combined effect of the heme dissociation and shifting of the secondary structure on the functional instability of CAT could not be ruled out. However, though less, the regeneration of the functional activity of the apo-CAT after reconstitution with the heme implies the possible reversibility of these structural shifts, if any.

The stability of CAT diminished steadily with the increasing temperature from 25ºC to 80ºC (Fig. 4.6.6A and B) with $t_{½}$ around 54 days at 25ºC, 15 days at 40ºC, 20 h at 60ºC and 42 min at 80ºC. The effect of temperature on the disintegration of heme was also investigated to

understand any correlation between them. The native CAT when incubated at 80ºC for 3 h 30 min, the heme was completely dissociated as evident from the disappearance of the Soret peak at 405 nm (Fig. 4.6.7). The dissociation rate was, however, found to be initially fast (3.14±0.20 h^{-1}) and then declined after 5 min to a rate of 0.39±0.07 h^{-1} at pH 7.5, 80ºC.

4.5. Conclusions

The stability of CAT from *A. terreus* was decreased with decreasing pH and eventually lost at pH 3.0. The highest stability ($t_{½}$) in the acidic range was at pH 6.0 and it was 38% less than the lowest $t_{½}$ obtained in the alkaline pH range. The intensity of the Soret peak (405 nm) of the heme integrated CAT incubated at pH 12.0, 4.0, and 3.0 were decreased by 10%, 32% and 51%, respectively, from the value obtained at pH 7.5 where the highest CAT stability was recorded. Typical cyclic voltammetric peaks for Fe^{3+}/Fe^{2+} redox couple of CAT immobilized on GCE/MWCNT-NF/PEI with formal potential ($E°$) -0.45 V (vs. Ag/AgCl reference) were detected at pH 7.5. Negative and positive shifts of $E°$ towards alkaline- and acidic-pH, respectively, were detected. A significant increase in redox current of CAT in the acidic pH range was observed. This upsurge current is attributed to the increased electron transfer between the electrode and the heme released on the surface of the electrode as a result of its disintegration from the insulating protein matrix. The heme isolated from CAT at acidic pH was again reconstituted with apo-CAT only at alkaline denaturing conditions to a detectable Soret peak and CAT activity. These findings revealed that the acidic pH promotes disintegration of the heme prosthetic group in the CAT protein and thereby destabilize CAT under acidic environment, though additional investigation is warranted to understand pH induced other impairment of CAT

that may affect its functional stability. The preliminary finding on the effective reconstitution of heme to this large catalase protein matrix is expected to pave the way for the potential application of the heme reconstitution approach on the construction of large catalase-based bioelectrode for biosensor or biofuel cell applications. CAT was also found to be exceptionally stable at wide range of temperatures with $t_{½}$ of 15 days at 40°C, 20 h at 60°C and 42 minutes at 80°C. The CAT activity was completely lost when boiled. The thermal dissociation rate of the heme from protein matrix at 80℃ was 3.14±0.20 h^{-1} for first 5 min followed by 0.39±0.07 h^{-1}.

4.6. Figures

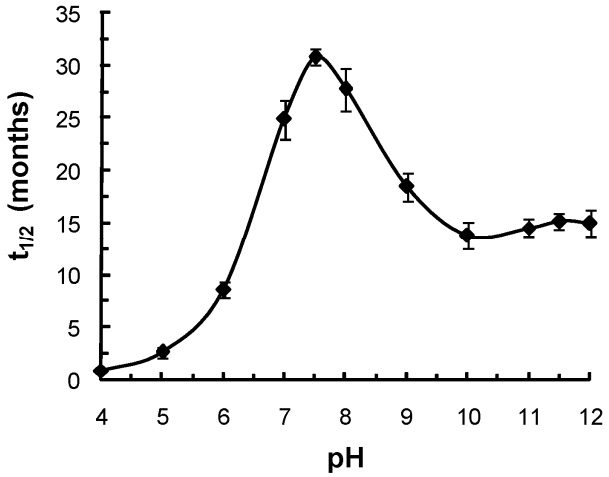

Fig. 4.6.1. Stability studies ($t_{½}$) for CAT activity at different pH. The buffer systems (each at a concentration of 50 mM) were trisodium citrate (pH 4.0), sodium acetate (pH 5.0), sodium phosphate (pH 6.0 to 7.5), tris (pH 8.0), ethanolamine (pH 9.0) and sodium phosphate (pH 10.0 to 12.0). The reactions were carried out at room temperature. The activity of the sample (under standard condition of assay) used for this study was 27.5×10^5 U ml^{-1}.

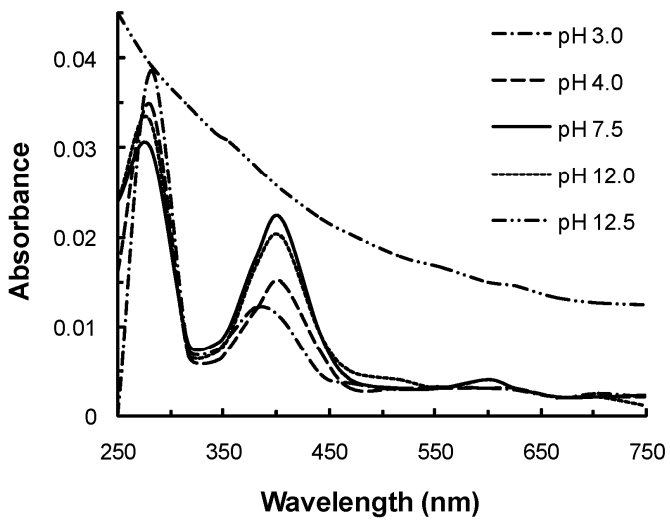

Fig. 4.6.2. Heme dissociation profile as a function of pH. 10 µg ml^{-1} CAT protein was incubated separately in 50 mM trisodium citrate buffer (pH 3.0 and pH 4.0), 50 mM SPB (pH 7.5, 12.0 and 12.5) for one week at 4ºC. All data were recorded at a scan rate of 100 nm min^{-1}.

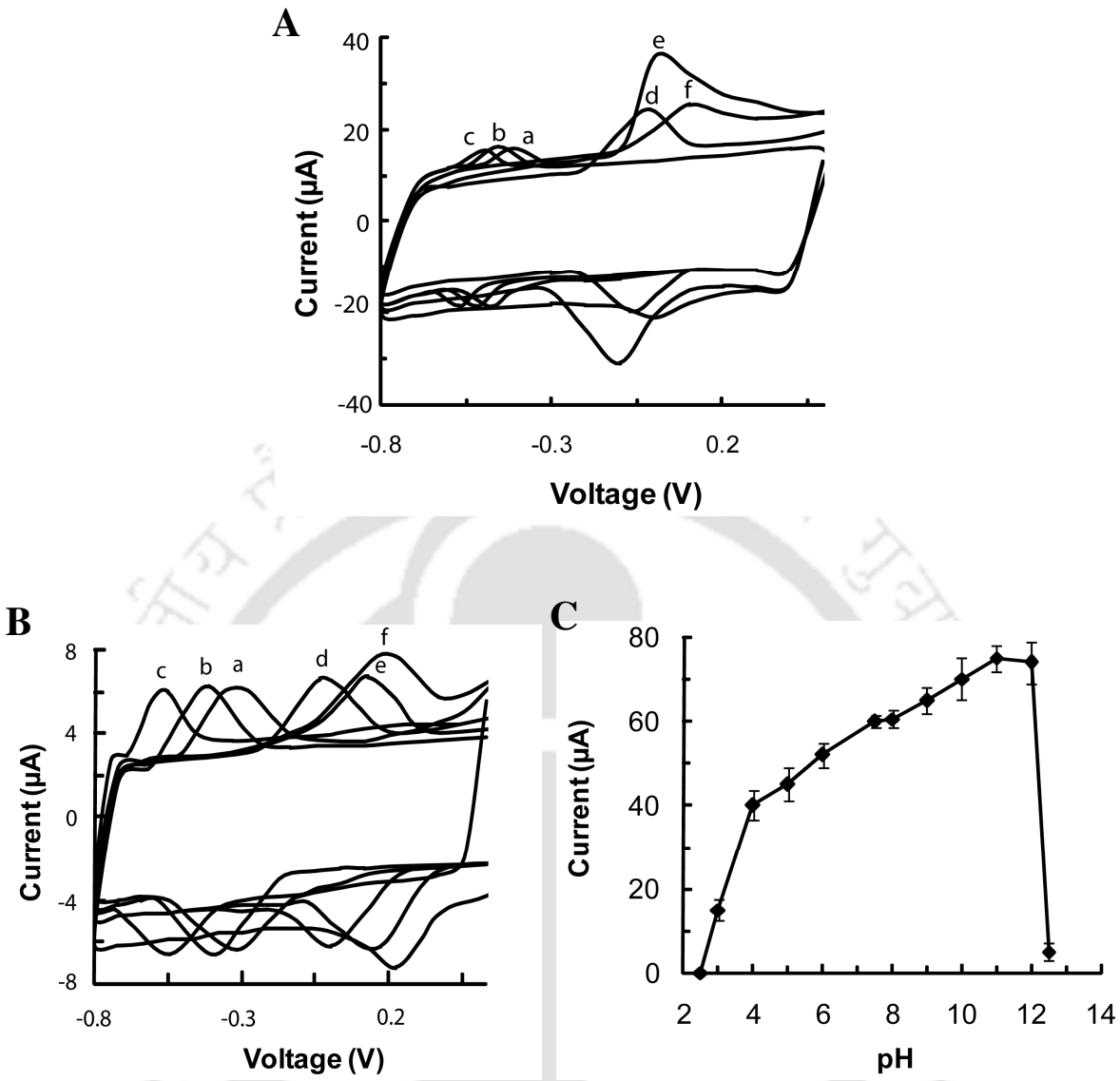

Fig. 4.6.3. **(A)** Cyclic voltammograms of CAT immobilized on GCE/MWCNT-NF/PEI at different pH. **(B)** Cyclic voltammograms of free heme in solution at different pH. Curve a: pH 7.5, curve b: pH 9.0, curve c: pH 12.0, curve d: pH 5.0, curve e: pH 4.0, curve f: pH 3.0. **(C)** Electro-catalytic activity of CAT immobilized on GCE/MWCNT-NF/PEI at different pH in presence of 1.5 mM H_2O_2. The buffer systems (each at a concentration of 50 mM) were trisodium citrate (pH 3.0 to 4.0), sodium acetate (pH 5.0), sodium phosphate (pH 6.0 to 7.5), tris (pH 8.0), and sodium phosphate (pH 9.0 to 12.0). The scan rate used was 100 mV s^{-1}.

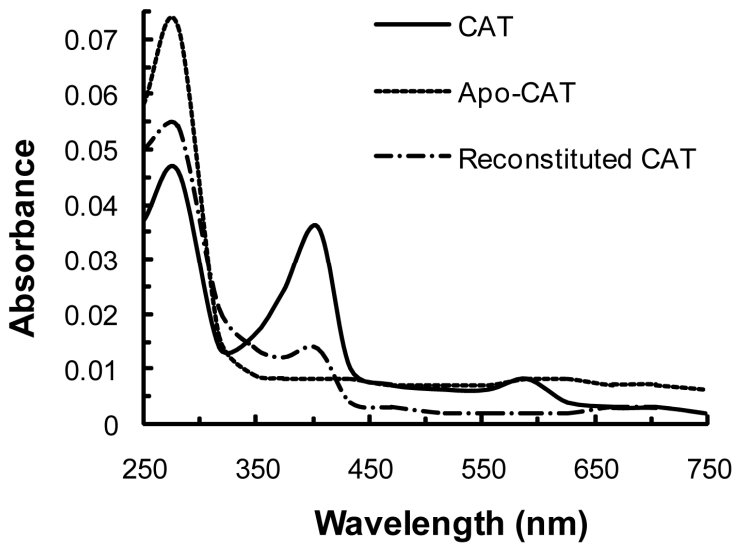

Fig. 4.6.4. UV-Vis absorption spectra of CAT, apo-CAT and heme reconstituted apo-CAT. The scan rate used was 100 nm min^{-1}.

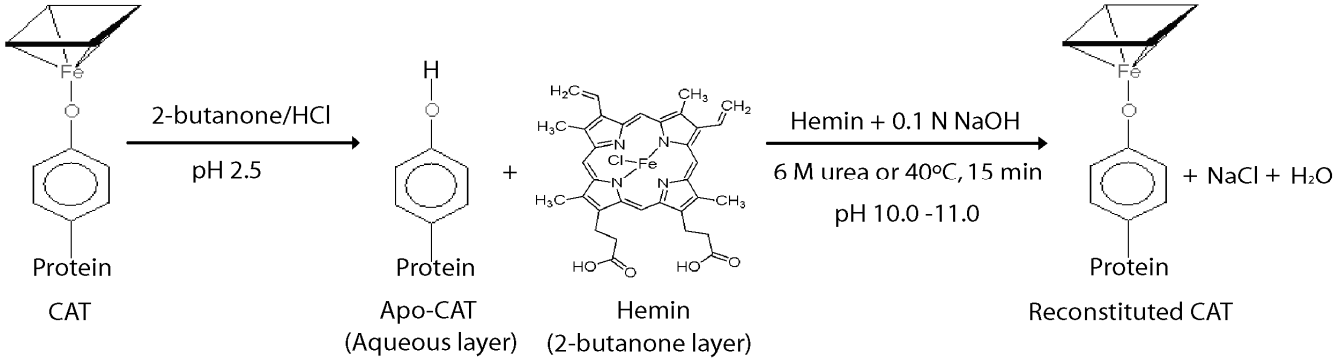

Fig. 4.6.5. Schematic representation of the steps involved in the dissociation of heme from CAT and re-association of heme with the separated apo-CAT.

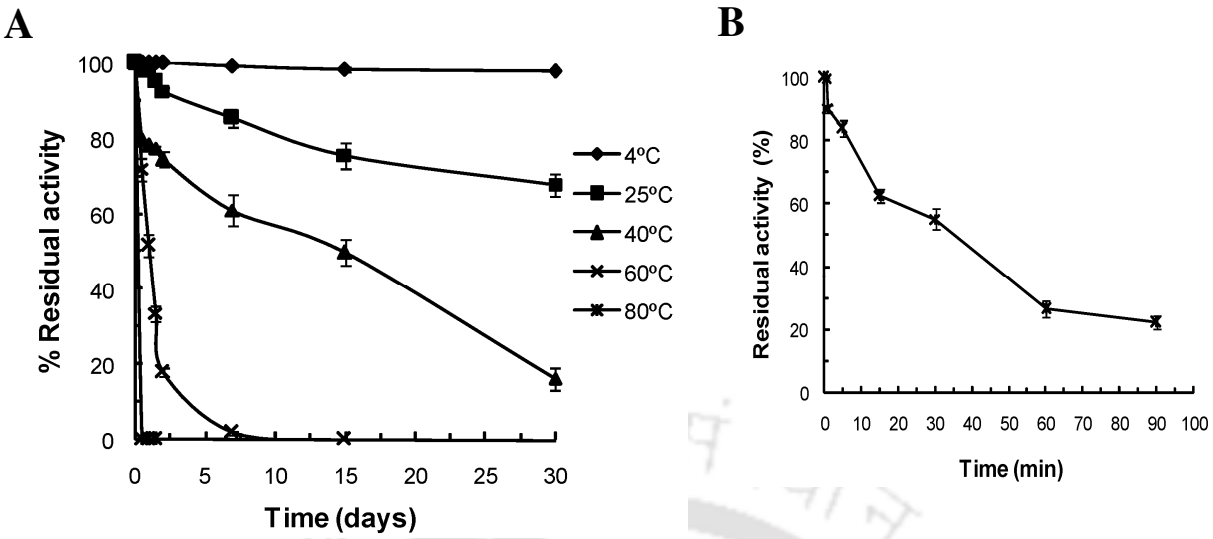

Fig. 4.6.6. **(A)** Temperature stability of CAT activity in 50 mM SPB, pH 7.5. **(B)** Temperature stability of CAT activity at 80°C in 50 mM SPB, pH 7.5. 100% activity corresponds to 34.9×10^5 U ml^{-1}. Each datum point represents the average of the analysis of triplicate values.

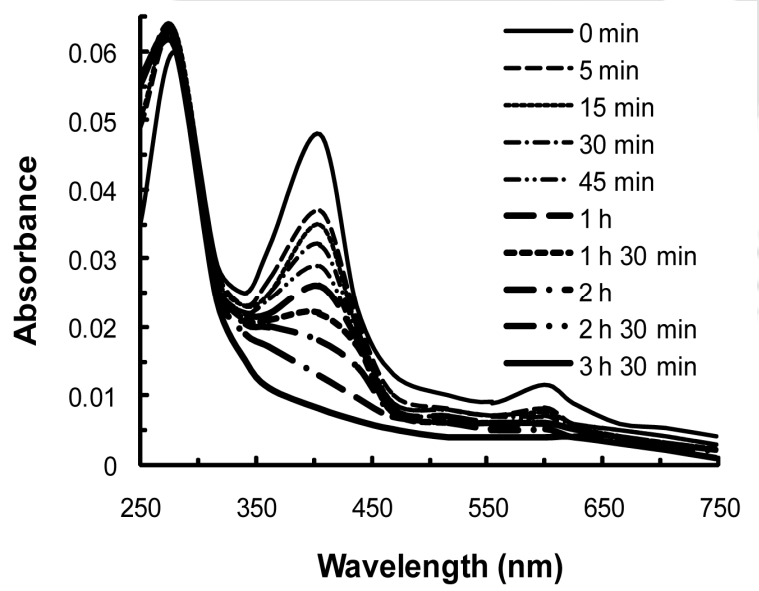

Fig. 4.6.7. Heme dissociation profile as a function of time at 80ºC. Concentration of CAT protein used was 18 µg ml^{-1} in 50 mM SPB (pH 7.5). The spectra recorded in the interval of 0-5 min are omitted here for clarity. All data were recorded at a scan rate of 100 nm min^{-1}.

4.7. Tables

Table 4.7.1. Activity profile of reconstituted CAT.

Fraction	Activity ($\times 10^5$ U ml^{-1})	Protein (mg ml^{-1})	Specific activity ($\times 10^5$ U mg^{-1})
CAT	32.6±1.8	0.69±0.03	47.2±2.7
Apo-CAT	NA	0.05±0.01	NA
Reconstituted CAT	1.3±0.2	0.05±0.01	26.0±1.4

NA- No Activity

Chapter 5

Fabrication and characterization of CAT bioelectrode

5.1. Overview

Catalase is a heme protein which functions in two ways: 'catalytically' decomposing hydrogen peroxide (H_2O_2) into water and oxygen, and 'peroxidatively' oxidizing alcohol, formate or nitrite using H_2O_2 (Zamocky and Koller 1999). CAT from *A. terreus* is a tetramer, containing four identical subunits, each of ~90 kDa, equipped with a high spin ferriprotoporphyrin (heme b). It thus, belongs to the family of large catalases (the others being smaller catalases with subunit mol wt ~60 kDa) and is shown to has high catalytic efficiency and excellent stability as described earlier in chapters 3 and 4. These properties make CAT a potential candidate for the biosensor applications using electrochemical transducer where stability, sensitivity and response time are the most desired features. The electrochemical behavior of large catalases is still largely unexplored. This may be partly due to the fact that electrochemical studies on biocatalysts for biosensor or biofuel cell applications are mostly done on the relatively small redox protein and enzymes (Lotzbeyer et al. 1996; Hu 2001) as direct electrical contact between the electrode surfaces and the redox centers of large proteins are often inhibited by the thick insulating protein matrix and complex molecular structures (Bullen et al. 2006; Murphy 2006). With the advent of new biocompatible matrices, e.g. nanomaterials, polymers, composite metal complex, sol-gel etc. as reviewed by us (Sarma et al. 2009), it has been possible to establish DET between the redox centers of various enzymes with the electronic

units, thus expanding the possibility to develop stable and sensitive bioelectrode for biosensor and biofuel cell applications. MWCNT have been reported as the excellent material for DET between the redox centers of many enzymes and the electrode surfaces due to their large surface area, high conductivity and high chemical stability (Gooding 2005; Wang et al. 2002; Agui et al. 2008). In the current study, MWCNT dispersed in NF with PEI as the encapsulating material have been used for CAT immobilization on GCE. PEI is a water soluble polycationic polymer (Rochefort et al. 2008) and is used here as an encapsulating matrix for CAT adsorbed on MWCNT-NF coated GCE. Although, PEI has been used previously in combination with MWCNT for other enzymes (Rubianes and Rivas 2007; Arribas et al. 2007; Jia et al. 2008), mostly for its dispersion, we have used PEI as an encapsulating matrix in combination with MWCNT-NF composite for immobilization of CAT. We have observed that the PEI layer provides an excellent stability to the bioelectrode by electrostatic interaction with negatively charged CAT adsorbed on MWCNT-NF composite and prevents CAT from leaching. The fabricated bioelectrode using this large catalase has been characterized and a detailed account on the findings is presented here.

5.2. Literature Review

The study of free radicals and antioxidants in biology and food technology has been widely recognized. The prevention of the oxidative reactions in foods, pharmaceutical and cosmetics as well the role of reactive oxygen species (ROS) in chronic degenerative diseases are issues that continue to be investigated due to the difficulties associated to the methods used in the evaluation of antioxidant status in these systems (Mello and Kubota 2007). Electrochemical

biosensors are the foremost tools used for determination of ROS in such analyses (D'Orazio 2003; Mello et al. 2005; Prieto-Simon et al. 2008). The development of biosensor employs different strategies like direct analysis of compounds with characteristics antioxidants, measuring the antioxidant enzymes activity and detection of free radicals (Mello and Kubota 2007; Prieto-Simon et al. 2008). Most of them use immobilized antioxidant enzymes (e.g. catalase, glutathione peroxidase, superoxide dismutase, peroxidase etc.) in combination with electrochemical transducer, in particular, amperometric devices (Campanella et al. 2001; Rover et al. 2001; Akyilmaz et al. 2003; Mello et al. 2005). Enzyme-based biosensors are very suitable since they show excellent selectivity for biological substances and can directly determine and/or monitor ROS in a complex media such as biological or nonbiological samples without needing a prior separation step (Mello and Kubota 2007). The study of direct electrochemistry of redox enzymes or proteins can thus provide a working model to study the mechanism of electron transfer between enzymes in biological systems, and establish a foundation for fabricating new kinds of biosensors, enzymatic bioreactors and biomedical devices (Armstrong et al. 1988; Chaplin and Bucke 1990).

Catalase is a heme containing antioxidant enzyme with a heme ($Fe^{3+/2+}$) prosthetic group at its redox centre (Zamocky and Koller 1999). It is present in almost all aerobic living organisms, where it catalyzes the disproportionation of H_2O_2 into oxygen and water without forming free radicals. The catalytic ability of catalase to reduce H_2O_2 has been applied in the development of H_2O_2 sensors for food, pharmaceutical, cosmetics and clinical applications (Campanella et al. 1998; Buleandra et al. 2000; Campanella et al. 2001; Li et al. 2005; Modrzejewska et al. 2007; Chen et al. 2008; Akyilmaz and Kozgus 2009).

In order to investigate this catalytic ability of catalase in detail, the direct electrochemistry of catalase at the transducer surface (electrode) has to be examined. However, earlier studies showed that immobilization of catalase directly on the bare electrode surface lead to poor electron transfer (Lai and Bergel 2002). This may be due to the fact that the $Fe^{(3+/2+)}$ group is usually deeply buried inside the huge structure of catalase. In order to achieve better electron transfer, catalase has been immobilized on various modified electrode surfaces. The electrode surfaces were modified either with surfactants, biopolymers, organic polymers, hydrogels, sol-gels or dendrimers, respectively (Gebicka and Gebicki 1998; Chen et al. 2001; Huang et al. 2002; Lu et al. 2003; Li et al. 2004; Shen and Hu 2004; Li et al. 2005; Di et al. 2006; Wu et al. 2006; Sun and Wang 2007; Wang et al. 2007). Though noticeable electron transfer was observed with a few modified electrodes, the majority of them fail to promote the electron transfer process. This might be due to the diminished contact between catalase and such modified matrices. The bioelectric contact between catalase and the bare electrode was likely to be improved with the implementation of nanomaterials (Wang et al. 2004). It is a well known fact that, with large surface area and highly porous network, nanomaterials are well suited for the entrapment of biological molecules (Salimi et al. 2007; Wan et al. 2007, 2008). Further, proteins or enzymes can be easily immobilized at these nanomaterials without any damage. In recent years, many researchers have attempted to immobilize catalase on various nanomaterial modified electrode surfaces. Their results ultimately illustrate that catalase immobilized on nanomaterial matrices possesses enhanced electron transfer and excellent catalytic activity. A comparative study on different catalase bioelectrodes are presented in Table 5.2.1 (source: Prakash et al. 2009a). Although the direct electrochemistry of catalase has been studied to a greater extent, the source of catalase is mostly limited to bovine liver (Prakash et al. 2009a). Large catalases from

different sources have been reported to be highly efficient and stable within wide range of pH and temperature conditions (Calera et al. 2000; Diaz et al. 2001; Switala and Loewen 2002). The innate efficiency and stability of large catalase have not been tapped till date for their application in bioelectronic devices like biosensors where sensitivity and stability of the electrode are the major criteria for their successful applications.

Table 5.2.1. The electrochemical parameters of various catalase-modified electrodes.

Modified Electrode	**Techniques**	E_{pa}[a] **(or)** E_{pc}[b] **(V)**	**Linear range (mM)**	**Sensitivity (μA mM^{-1} cm^{-2})**	**Detection limit (μM)**	**References**
Catalase-PAM	CV	-0.5[b]	0.4 - 0.8	-	-	Lu et al. 2003
Catalase-MC	CV	-0.4[b]	0.02-0.12	-	-	Li et al. 2004
Catalase-SF	i-t	-0.2[b]	0.003-0.158	-	-	Wu et al. 2006
Catalase-PNM	i-t	-0.25[b]	0.002-0.035	-	-	Sun and Wang 2007
Catalase/cysteine/Si sol–gel	i-t	0.1[b]	0.001-0.03	-	0.4	Di et al. 2006
Catalase-agarose	CV	-0.24[b]	0.001-0.818	-	-	Wang et al. 2007
Catalase-SWCNT	CV	-0.4[a]	0.7-1.1	-	4.0	Wang et al. 2004
Catalase-SWCNT-CS	CV	-0.52[b]	5–50	6.32	2.5	Jiang et al. 2008
NF-MWCNT-Catalase–GNP	CV	-0.29[a]	1-5	-	-	Zhou et al. 2008a
Catalase-MWCNT	i-t	-0.3[b]	0.01-0.1	3.3	1.0	Salimi et al. 2005
Catalase-MWCNT	CV	-0.56[b]	1.0 - 4.8	-	-	Zhou et al. 2008b
Catalase-NiO	i-t	-0.3[b]	0.001-1.0	15.9	0.60	Salimi et al. 2007
MWCNT-NF-(DDAB/Catalase)	CV	-0.38[b]	0.5 – 1.2	35.62	150	Prakash et al. 2009b

[a] :Anodic peak potential (E_{pa}); [b]: cathodic peak potential (E_{pc}); CS: Chitosan; DDAB: Didodecyldimethylammonium bromide; GNP: Gold nanoparticles; i-t: Chronoamperometry; MC: Methyl cellulose; NiO: Nickel oxide; PAM: Polyacrylamide; PNM: Poly (N-isopropylacrylamide-co-3-methacryloxypropyltrimethoxysilane); SF: Silk fibroin; SWCNT: Single walled carbon nanotubes.

5.3. Experimental approaches

5.3.1. Reagents

CAT was isolated, purified and characterized from *A. terreus* MTCC 6324, as described in section 3.3. The specific activity of purified CAT was $66.00\pm3.97\times10^5$ U mg^{-1} protein. MWCNT with 95% purity (10–15 nm outer diameter, 2-6 nm inner diameter and 0.1-10 µm length) and PEI (50%) were obtained from Sigma, NF from Du Pont (USA), and H_2O_2 (30%) was obtained from Merck. 50 mM SPB, pH 7.5 was used throughout the experiment. The stock solutions of CAT and BSA (1 mg ml^{-1}) were prepared by dissolving the lyophilized protein in 50 mM SPB. All solutions were prepared with deionized water (Milli Q). Solutions were de-aerated by bubbling high-purity (99.99%) argon gas through them prior to the experiments, and the electrochemical cell was kept under argon gas atmosphere throughout the experiments.

5.3.2. Fabrication of MWCNT-NF/CAT/PEI modified GCE and apparatus

Prior to the surface modification, the GCE (5 mm diameter) was polished and cleaned following the procedure described in section 4.3.4. The MWCNT-NF film was prepared by method described by others (Tsai et al. 2004). 10 mg MWCNT was added to 1 ml of 5% NF and sonicated for about 3.5 h to obtain a stable and uniform suspension. 10 µl of this suspension was layered on GCE and allowed to dry under clean air at room temperature. Once dried, 15 µl of CAT solution (0.5 mg ml^{-1}) was layered on the MWCNT-NF nano-composite and kept overnight at 4ºC. Finally, 5 µl of PEI (10%) was layered and dried at room temperature. Separate GCE with each layer as control were prepared simultaneously and dried as earlier. Electrochemical experiments were performed with a computer - controlled- Autolab modular electrochemical

system (Eco Chemie, Utrecht, Netherlands), driven with GPES, FRA and NOVA softwares (Eco Chemie). A conventional three-electrode cell was used with an Ag/AgCl/saturated KCl reference electrode, a platinum wire as counter electrode, and a glassy carbon disk (modified and unmodified) as working electrode. All experiments were carried out at room temperature of 25°C.

5.3.3. Stability studies of the fabricated bioelectrode

To determine the effect of PEI layer on bioelectrode stability, leaching studies were carried out in presence and absence of the PEI layer. The GCE/MWCNT-NF/CAT and GCE/MWCNT-NF/CAT/PEI were stored in SPB, pH 7.5 at 4°C and the residual current was measured at different time intervals. The storage buffer was changed after each reading to avoid any re-adsorption of CAT on the surface of electrode. For determination of operational stability, the bioelectrode was kept in operating condition and current generated was recorded for 48 h. For storage stability, the bioelectrode was stored at 4°C and residual current was measured at different time intervals. A fixed substrate concentration (1 mM H_2O_2) was used throughout the experiments for all stability studies.

5.3.4. EDX Characterization of fabricated bioelectrode

GCE fabricated with each layer were mounted on the specimen holder with electro-conductive tape and sputter coated under vacuum with gold in a sputter coater (SC 7620 Polaron Range). The elemental analysis was done using a LEO 1430 VP variable pressure scanning electron microscope equipped with INCA Oxford EDX facility.

5.4. Results and discussion

5.4.1. Characterization of the self-assembled GCE/MWCNT-NF/CAT/PEI bioelectrode

5.4.1.1. Energy dispersive X-ray spectroscopy

EDX measurements were performed to obtain the elemental composition of the self-assembled films in the stepwise course in order to confirm the immobilization of each layer. Fig. 5.6.1 presents the schematic representation of the layer by layer assembly and parallel EDX scans of the surface for the GCE (A), GCE/MWCNT-NF (B), GCE/MWCNT-NF/CAT (C), and GCE/MWCNT-NF/CAT/PEI (D) in the range of 0-10 keV. GCE surface shows only element C (Fig. 5.6.1A). The main elements of GCE/MWCNT-NF surface are C and F, where C is from GCE, MWCNT and NF whereas, F stems from NF. Other trace elements O and S are also visible in the spectra (Fig. 5.6.1B). The observed elements Fe and N in Fig. 5.6.1C are due to the self-assembly of CAT on the MWCNT-NF modified GCE. The electrostatic self-assembly of PEI on the GCE/MWCNT-NF/CAT film can be further demonstrated by the elements C and N stemming from PEI and underlying layers and a reduced but marked presence of Fe and F from CAT and NF layers, respectively in the EDX survey scan of modified electrode surface (Fig. 5.6.1D).

5.4.1.2. Electrochemical impedance spectroscopy

EIS was employed to further investigate the impedance changes of the electrode surface in the modification process. Fig. 5.6.2A shows the results of the EIS at bare GCE,

GCE/MWCNT-NF, GCE/PEI, GCE/MWCNT-NF/CAT, GCE/MWCNT-NF/CAT/PEI in the presence of equimolar $Fe(CN)_6^{3-/4-}$. To understand clearly the electrical properties of the prepared electrodes/solution interfaces, the Randle's equivalent circuit (inset of Fig. 5.6.2A, top) was chosen to fit the obtained impedance data. In Randle's circuit, it was assumed that the resistance to charge transfer (R_{ct}) is in parallel to the interfacial capacitance (C_{dl}). This parallel combination of R_{ct} and C_{dl} gives rise to a semicircle in the complex plane plot of Z_{im} against Z_{re}, the semicircle diameter equals the R_{ct}. This resistance exhibits the electron transfer kinetics of the redox-probe at the electrode interface. As shown in Fig. 5.6.2A, there is a very low charge transfer resistance for $Fe(CN)_6^{3-/4-}$ at bare GCE (170 Ω). When MWCNT-NF was layered on the electrode surface, R_{ct} increased to about 960 Ω. The increased R_{ct} implies the increased interfacial resistance due to the self-assembly of MWCNT-NF layer. Interestingly, addition of CAT and PEI decreased the R_{ct} to 500 Ω and 280 Ω, respectively. These data suggest that the MWCNT-NF layer here provides a nano-structured matrix for the adsorption of CAT and play an important role similar to a conducting wire or electron conducting tunnel, which makes it easier for the electron transfer to take place to GCE (Gooding 2005; Agui et al. 2008). Further, the decrease in the R_{ct} after the adsorption of CAT implies that the heme Fe^{3+}/Fe^{2+} redox couple of CAT itself is acting as the mediator for the electron transfer between the $Fe(CN)_6^{3-/4-}$ and the layers beneath. Presence of a number of channels for access and vent for substrate and dioxygen, respectively, from the redox center, accompanied by a number of other modifications in the structure, have been reported for the large catalases (Switala and Loewen 2002; Diaz et al. 2009). These properties of large catalases are likely to facilitate the charge transfer across the protein matrix and thereby decrease the overall R_{ct} of the assembled bioelectrode after adsorption of CAT. A control experiment using BSA instead of CAT in the similar self assembled electrode assembly

confirmed our findings, as there was increase in R_{ct} to 1500 Ω (Fig. 5.6.2B). Addition of PEI (polycationic) neutralizes the negative charge of MWCNT-NF composite and CAT (*pI* 4.2, section 3.4) thus preventing the charge repulsion, and thereby supports fast electron transfer due to electrostatic interaction with the underlying layers that cause further decrease in the R_{ct}. Thus, composite MWCNT-NF/CAT/PEI films on the electrode surface provide facile electron transfer which is also supported by the CV results (Fig. 5.6.3A and B). Fig. 5.6.3A shows the increase in the peak currents for $Fe(CN)_6^{3-/4-}$ solution with the addition of CAT layer in the MWCNT-NF modified GCE which were further increased with the addition of PEI layer (inset of Fig. 5.6.3A). In contrast, the addition of BSA layer decreased the corresponding peak currents (Fig. 5.6.3B) thus supporting the fact that addition of CAT and PEI layer mediates the DET process between the $Fe(CN)_6^{3-/4-}$ and electrode (GCE) by decreasing the overall R_{ct} of the fabricated bioelectrode.

5.4.2. Cyclic voltammetry of MWCNT-NF/CAT/PEI modified GCE

The electrochemical behavior of CAT in MWCNT-NF/PEI film was studied by CV. A quasi-reversible CV peak at approximately -0.45 V [$(E_{pa}+E_{pc})/2$], which is the characteristic of catalase heme Fe^{3+}/Fe^{2+} redox couple (Zhang et al. 2002) was observed when MWCNT-NF/CAT electrode was used (Fig. 5.6.4, curve c). Free CAT in SPB (pH 7.5) showed no CV peaks at bare GCE in the same potential window. On the other hand, as shown in Fig. 5.6.4 (curve d) both cathodic and anodic peak currents increased with the addition of PEI layer. The ratio of anodic to cathodic peak currents is approximately 1.0, indicating that CAT undergoes a quasi-reversible redox process at the GCE modified with MWCNT-NF/CAT/PEI film. Where, MWCNT-NF film provides a well graphitized three-dimensional nano-electrode ensemble for sufficient adsorption

of CAT and a suitable environment for electron transfer with underlying GCE. The poly-cationic layer of PEI further adds to the rate of electron transfer by electrostatic interaction with CAT (negatively charged, *pI* 4.2) adsorbed on MWCNT-NF film as evident from the increase in peak currents, and there is no significant shift in the formal potential. The formal potential ($E°$) of CAT estimated as a midpoint of CV reduction and oxidation peak potentials at approximately -420 and -480 mV, respectively is comparable to the catalase formal potential from other modified electrodes (Huang et al. 2002; Lu et al. 2003; Shen and Hu 2004; Rahimi et al. 2010). The separation of cathodic and anodic peak potentials (ΔEp=60 mV) indicates a single electron transfer reaction. The surface coverage (Γ) of electroactive CAT at the modified GCE was calculated to be 2.1×10^{-10} mol cm^{-2}, by using the equation $\Gamma = Q/nFA$, where Q is the charge obtained by integrating the peak current area, n is the number of electrons involved, F is Faraday's constant and A is electrode area. This suggests CAT monolayer formation on MWCNT/NF modified GCE. To obtain the kinetic parameters of CAT redox at MWCNT-NF/PEI modified GCE, the effect of scan rate was investigated. Fig. 5.6.5A shows the CVs at different scan rates. The peak currents (*Ipa* and *Ipc*) versus scan rate plots, shown in Fig. 5.6.5B, exhibits a linear relationship (R^2 = 0.998 and 0.996, respectively), as expected for a surface-confined redox process. The peak-to-peak separation is approximately 60 mV at scan rates of less than 50 mV s^{-1}, suggesting facile charge transfer kinetics over this range of sweep rates. On the other hand, it was found that at scan rates greater than 100 mV s^{-1}, ΔEp increased with the increase of scan rate. The values of peak-to-peak potential separations were proportional to the logarithm of the scan rate for scan rates greater than 100 mV s^{-1} (Fig. 5.6.5C). Based on the Laviron theory, the transfer coefficient (α) and heterogeneous electron transfer rate constant (Ks)

could be estimated by measuring the variation of peak potential with scan rate (Laviron 1979) following these equations.

$$m_{pc} = -\frac{2.3RT}{\alpha nF} \qquad m_{pa} = -\frac{2.3RT}{(1-\alpha)nF}$$

Where, m_{pc} and m_{pa} are the slopes for the cathodic and anodic peak potentials.

α is the charge transfer coefficient.

$$\log K_s = \alpha\log(1-\alpha) + (1-\alpha)\log\alpha - \log\frac{RT}{nF\nu} - \frac{\alpha(1-\alpha)nF\Delta E_p}{2.3RT}$$

Where, R, T and F have their universal values.

ΔE_p is the difference between the *Epc* and *Epa* peak potentials.

n is number of electrons.

v is the scan rate

The α and *K*s of CAT were 0.7±0.1 and 1.05±0.2 s^{-1}, respectively. Similar *Ks* values were reported for smaller catalase (bovine liver) immobilized on other electrodes (Zhang et al. 2001; Zhou et al. 2008a). Thus, by following the current protocol, we are reporting here for the first time, an efficient electrical conductivity between the redox centre of large catalase and electrode.

5.4.3. Electro-catalytic behavior of CAT immobilized on MWCNT-NF/PEI modified GCE

The heme in the redox centre of CAT could be oxidized by H_2O_2 to form an oxyferryl π-cation radical heme intermediate. Subsequently, the enzyme is converted back to its native resting state, ferric porphyrin, by a one-electron/two-proton reduction by electrons from the

electrode. The current obtained from the reduction of oxyferryl π-cation radical heme intermediate is correlated to the concentration of H_2O_2 in the solution. Hence, this current can be used to quantify the peroxidase activity of the immobilized CAT system using chronoamperometry (Scheme 5.4.3.1). This approach enables the direct measurement of the current versus time response to an applied potential step (Armstrong et al. 1997).

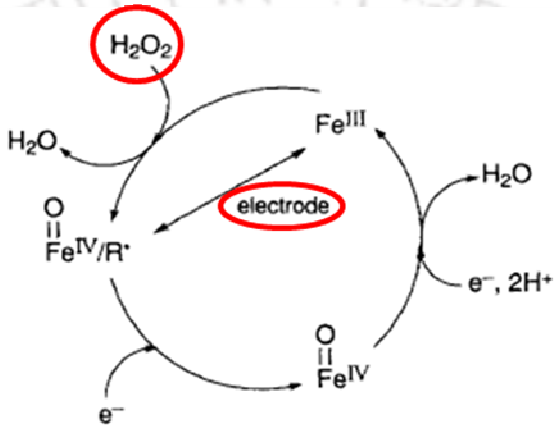

Scheme 5.4.3.1. Schematic representation for electrocatalytic cycle of CAT bioelectrode.

(Adapted from Armstrong et al. 1997)

Fig. 5.6.6A shows the real-time chronoamperometric current vs time curve with subsequent addition of H_2O_2. As can be seen, the current response increases with each addition of H_2O_2 in the testing solution and reaches equilibrium with a response time of ~2 s. A linear response curve (R^2 = 0.993) is obtained within the H_2O_2 concentrations from 10 µM to 5 mM with sensitivity 30 µA mM^{-2} H_2O_2 (Fig. 5.6.6B) where, the intercept on y-axis shows the background current due to immobilization matrix. The detection limit is 1 µM. Furthermore, when H_2O_2 was added to the buffer solution, the voltammetric behavior of the CAT-immobilized

MWCNT-NF/PEI modified GCE changes obviously, with an increase in the reduction peak current and the disappearance of the oxidation peak, where, the reduction peak current increases with the increasing concentration of H_2O_2 in solution (inset of Fig. 5.6.6A). The disappearance of the oxidation peak shows that the oxidation rate of CAT by H_2O_2 is very fast, and increase in reduction peak current indicates the electro-catalytic reduction of CAT immobilized on GCE/MWCNT-NF/PEI. The apparent Michaelis - Menten constant (K_m') for CAT immobilized on GCE/MWCNT-NF/PEI is 3 mM as determined from linear calibration plot (R^2 = 0.975) (Fig. 5.6.6C), where $1/i = 1/i_{max} + K_m'/i_{max}\, C$. The K_m' (3 mM) of fabricated bioelectrode is lower than the biochemically reported K_m values from other large catalases (Switala and Loewen 2002) which suggests the role of MWCNT, NF and PEI in facilitating the electron transfer between substrate and immobilized CAT. Further, the response time and detection limit of the CAT bioelectrode are comparable and even lower than the bioelectrodes fabricated with smaller catalases (Salimi et al. 2005, 2007). Similarly, the sensitivity of the CAT bioelectrode was also found to be higher than some of the reported smaller catalase bioelectrodes (Jiang et al. 2008; Prakash et al. 2009b).

5.4.4. Stability studies for GCE/MWCNT-NF/CAT/PEI bioelectrode

Fig. 5.6.7A shows the effect of encapsulating layer of PEI on the stability of CAT biosensor towards leaching in buffer. Although MWCNT-NF composite provides a well defined structure for the surface adsorption of CAT but a complete loss of residual activity within 48 h of study shows that it is not able to hold CAT for long time. In contrast, with the addition of the PEI layer more than 75% of the residual CAT activity was retained even after 48 h which suggest that PEI

provides the encapsulation of surface confined CAT and prevents its leaching from the surface. It also improves the stability of electrode by neutralizing the charge repulsion between the negatively charged MWCNT-NF and CAT and by making the electrostatic interaction with the underlying layer. The protein stabilizing effect of PEI, which has already been established by other research groups (Andersson and Hatti-Kaul 1999) further aids in the overall stability and efficiency of the fabricated CAT bioelectrode. More than 50% of CAT residual activity was retained when the GCE/MWCNT-NF/CAT/PEI electrode was continuously operated at -480 mV and 25°C for 48 h at fixed substrate concentration (Fig. 5.6.7B). The loss of CAT activity can be attributed to the continuous exposure to high H_2O_2 concentration, effect of temperature and slow leaching of CAT in the solution. The biosensor can be stored for months in dry condition with intermittent use without any significant loss of activity. The high stability of the biosensor in turn is attributed by both innate stability of large CAT from the *A. terreus* and an efficient immobilization technique. Thus, the stability of fabricated CAT bioelectrode also provides it an edge over the other smaller catalase bioelectrodes. The smaller catalase-based bioelectrodes properties had already been reviewed by Prakash et al. (2009a).

5.5. Conclusions

The direct electrochemistry and electro-catalytic properties of CAT from *A. terreus,* immobilized on MWCNT-NF/PEI modified GCE was investigated. A pair of well defined and nearly reversible cyclic voltammetric peaks for Fe^{3+}/Fe^{2+} redox couple of CAT with formal potential ($E°$) of about -0.45 V (vs. Ag/AgCl reference electrode) in pH 7.5 buffer was observed. The surface coverage of CAT immobilized on MWCNT-NF/PEI modified GCE was approximately 2.1×10^{-10} mol cm^{-2}. The electron transfer rate constant (Ks) of 1.05±0.2 s^{-1} was observed for the bioelectrode, indicating facilitation of the electron transfer between CAT and GCE. Assembly of CAT and PEI layer over MWCNT/NF composite showed a considerable decrease in the overall charge transfer resistance (R_{ct}). GCE/MWCNT-NF/CAT/PEI exhibited a remarkable electro-catalytic activity toward the reduction of hydrogen peroxide (H_2O_2). The apparent Michaelis–Menten constant (K_m´) for the fabricated bioelectrode, was calculated as 3 mM H_2O_2. The biosensor response increased linearly with H_2O_2 concentrations from 10 µM to 5 mM. The response time for steady state current and detection limit were ~2 s and 1 µM H_2O_2, respectively. A high operational and storage stability was observed for the self assembled bioelectrode. Thus, the important findings of this chapter are direct electrochemistry and efficient electro-catalytic activity of a large catalase immobilized on MWCNT-NF/PEI modified GCE, and substantially low R_{ct} of this fabricated bioelectrode. High operational and storage stability of the fabricated bioelectrode achieved by using PEI as encapsulating polymer is another interesting finding of this investigation. Further the high sensitivity, low response time and detection limit suggest the potential biosensor application for the fabricated CAT bioelectrode.

5.6. Figures

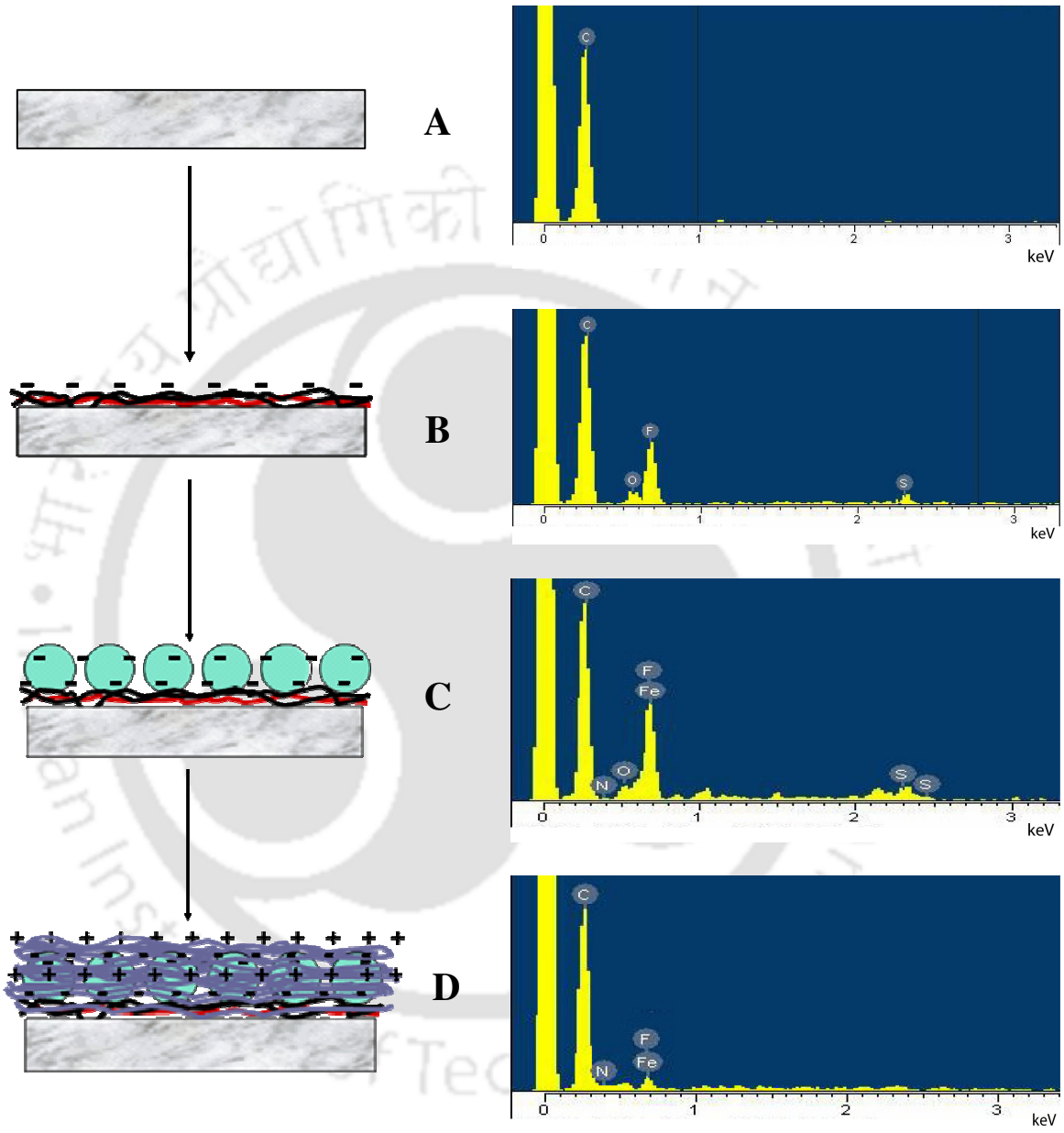

Fig. 5.6.1. Schematic representations and EDX spectra for layer by layer fabrication of CAT bioelectrode. **(A)** Bare GCE, **(B)** GCE/MWCNT-NF, **(C)** GCE/MWCNT-NF/CAT and **(D)** GCE/MWCNT-NF/CAT/PEI.

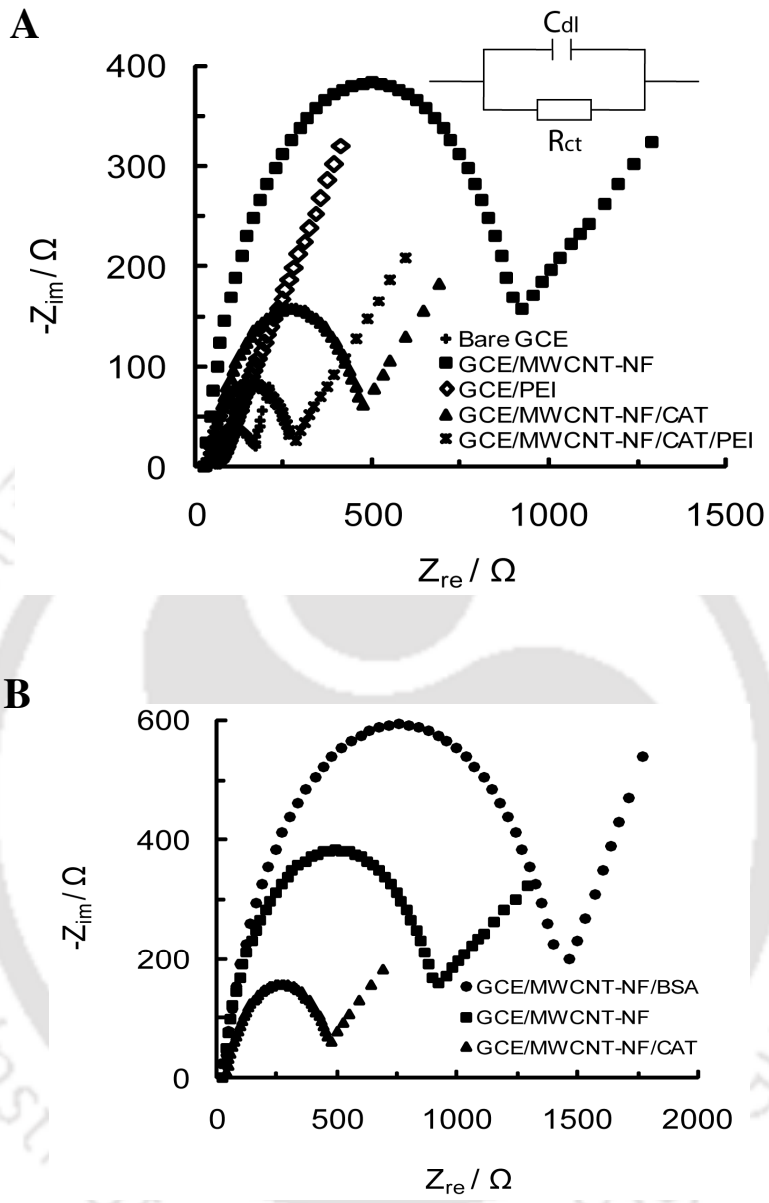

Fig. 5.6.2. Electrochemical impedance plots of **(A)** bare GCE, GCE/MWCNT-NF, GCE/PEI, GCE/MWCNT-NF/CAT and GCE/MWCNT-NF/CAT/PEI; **(B)** GCE/MWCNT-NF/BSA, GCE/MWCNT-NF and GCE/MWCNT-NF/CAT in the presence of 5 mM $Fe(CN)_6^{3-/4-}$ with 0.1 M KCl as supporting electrolyte. The electrode potential was 0.2 V, the frequency range was 0.1 Hz to 100 KHz.

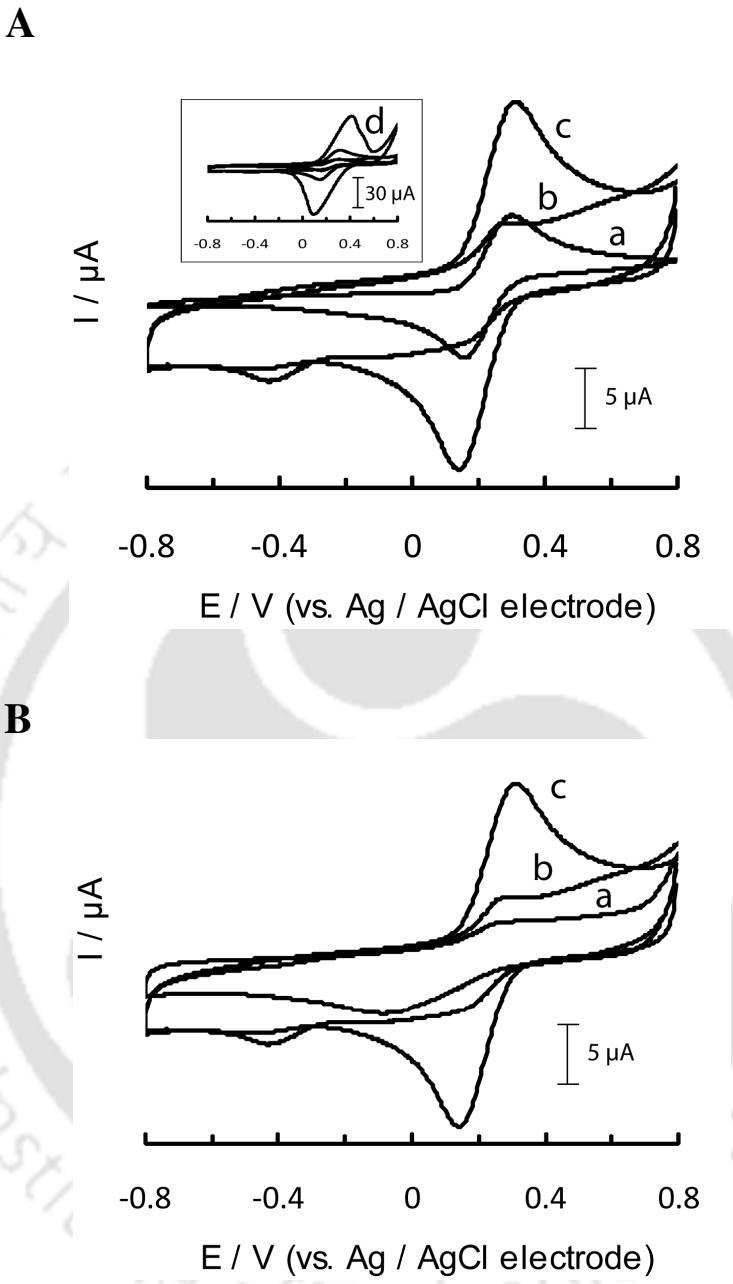

Fig. 5.6.3. Cyclic voltammograms of **(A)** bare GCE (a), GCE/MWCNT-NF (b), GCE/MWCNT-NF/CAT (c) and Inset: GCE/MWCNT-NF/CAT/PEI (d); **(B)** GCE/MWCNT-NF/BSA (a), GCE/MWCNT-NF (b) and GCE/MWCNT-NF/CAT (c) in the presence of 5 mM $Fe(CN)_6^{3-/4-}$ with 0.1 M KCl as supporting electrolyte.

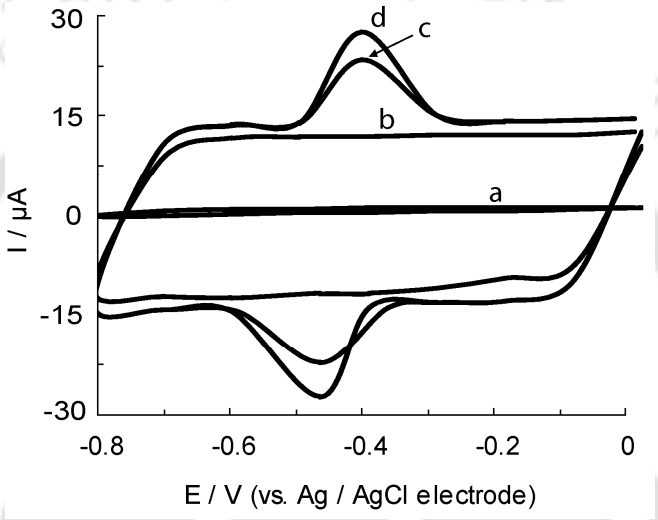

Fig. 5.6.4. Cyclic voltammograms of bare GCE (a), GCE/MWCNT-NF (b), GCE/MWCNT-NF/CAT (c) and GCE/MWCNT-NF/CAT/PEI (d) in 50 mM SPB (pH 7.5) at the scan rate of 100 mV s^{-1}.

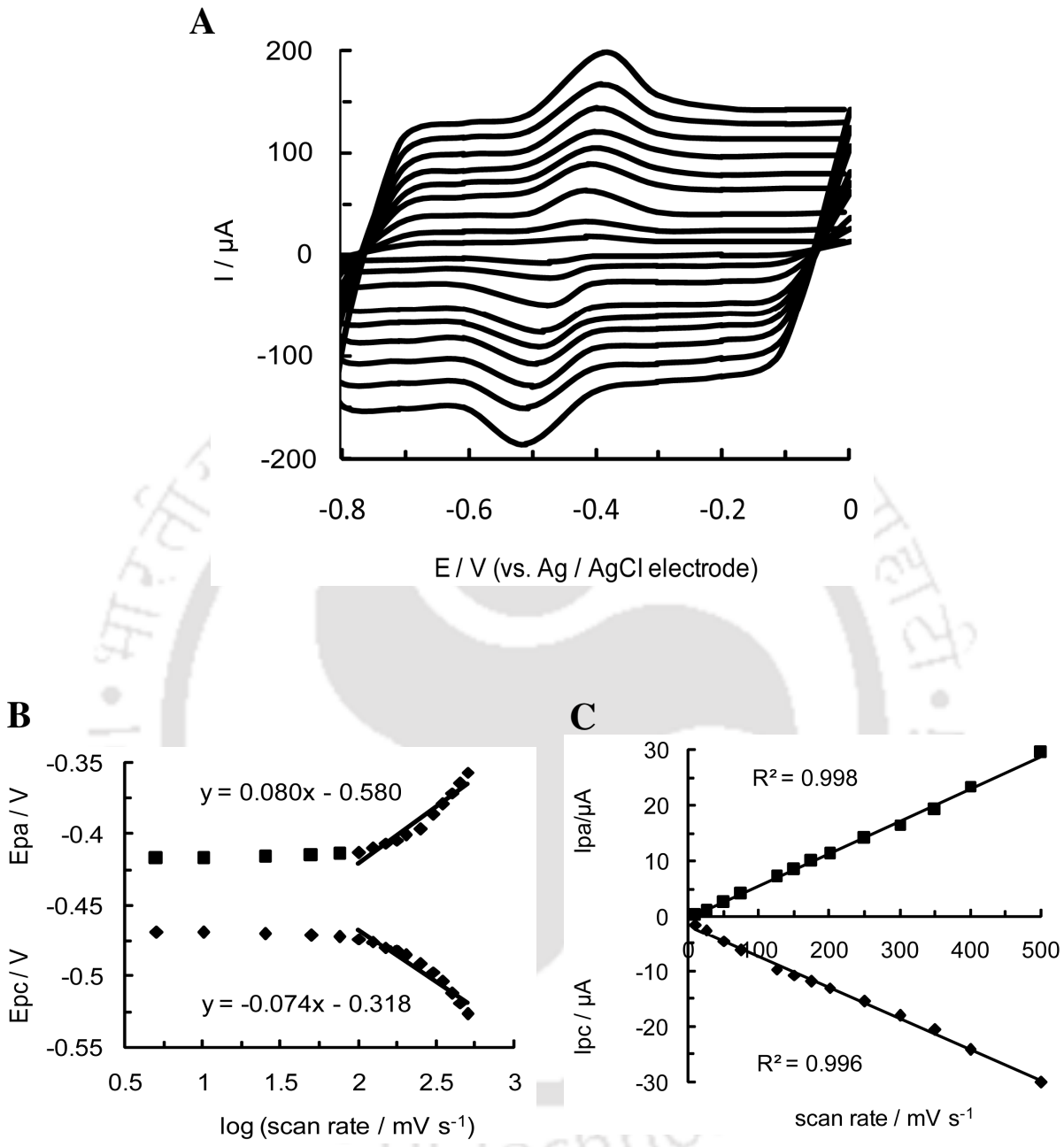

Fig. 5.6.5. **(A)** Cyclic voltammograms of MWCNT-NF/CAT/PEI modified GCE at different scan rates in 50 mM SPB (pH 7.5). The scan rates were 10 to 500 mV s^{-1}. **(B)** Variation of peak potentials vs. the logarithm of the scan rates. **(C)** Plot of peak currents vs. scan rates.

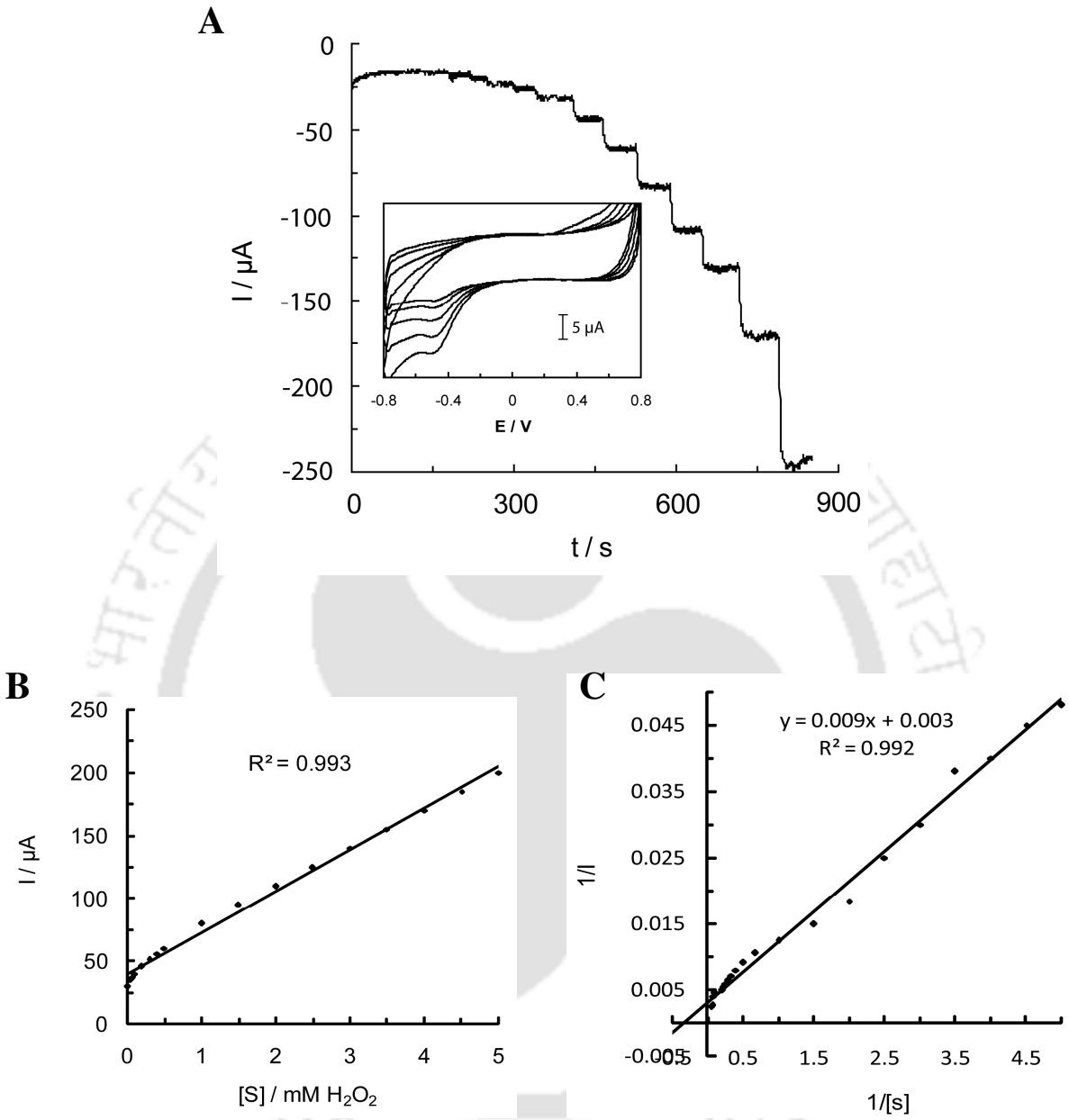

Fig. 5.6.6. (A) Chronoamperometric response of GCE/MWCNT-NF/CAT/PEI bioelectrode to different H_2O_2 concentrations. The operating conditions were: –0.48 V (vs. Ag/AgCl electrode), 50 mM SPB (pH 7.5). Inset: CV of MWCNT-NF/CAT/PEI modified GCE with successive addition of substrates (ranging from 0.1-0.5 mM H_2O_2). **(B)** Response curve of fabricated CAT bioelectrode. **(C)** Linear calibration curve for determination of k_m´ of immobilized CAT.

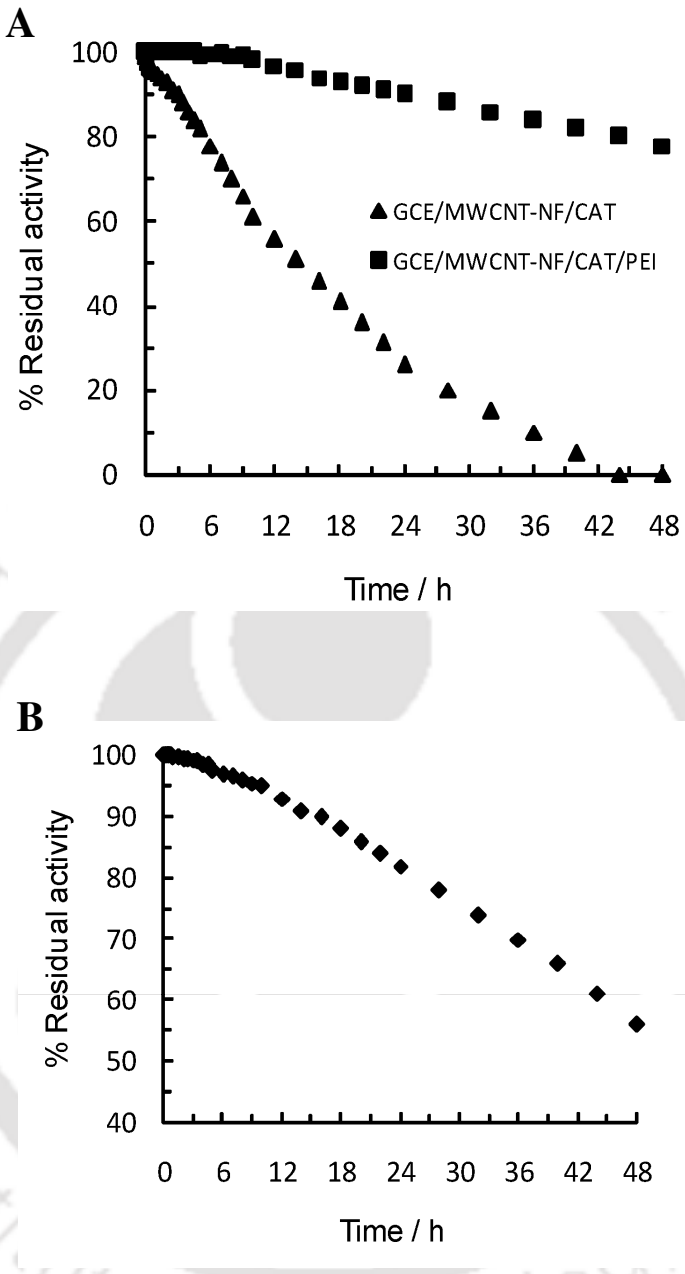

Fig. 5.6.7. Stability studies of fabricated CAT bioelectrode. **(A)** Comparison of stability against leaching for GCE/MWCNT-NF/CAT and GCE/MWCNT-NF/CAT/PEI electrode at 4°C in 50 mM SPB (pH7.5). **(B)** Operational stability of GCE/MWCNT-NF/CAT/PEI electrode. 100% activity corresponds to 80 μA current at substrate concentration of 1 mM H_2O_2 in 50mM SPB (pH 7.5). The operating conditions were: –0.48 V (vs. Ag/AgCl electrode), 50 mM SPB (pH 7.5). Total number of operations: 25.

Chapter 6

Fabrication and characterization of CYP bioelectrode

6.1. Overview

The redox active center of CYP consisting of iron-protoporphyrin IX (heme) is involved in the catalysis of a wide range of redox reactions such as, epoxidation, hydroxylation and heteroatom oxidation (Omura 1999; Beilen and Funhoff 2005). Initially, upon binding of the substrate to CYP, the Fe^{3+} in the native heme acquires an electron from a redox co-factor, usually NAD(P)H, through an electron transport chain in the cells and is subsequently reduced to $Fe^{(II)}$ – heme state. This reduced heme is re-oxidized to a state containing $Fe^{(III)}$ O-$O^{\cdot}$ radical after binding with molecular oxygen and eventually rearranged to a high-energy oxidizing species $Fe^{(IV)}$=O-heme after gaining another electron from the redox co-factor. The substrate already bound to the CYP is oxidized by this oxyferryl species with the concomitant regeneration of the native $Fe^{(III)}$–heme and thus completing the catalytic cycle. One common example of CYP catalyzed oxidation is the oxyfunctionalization of hydrocarbons through hydroxylation of an inactive C–H bond using oxygen molecule (Ortiz de Montellano and De Voss 2005). It has been possible to establish the CYP catalyzed redox reactions electrochemically that eliminate the need of reductant co-factors in the reactions (Bistolas et al. 2005; Shumyantseva et al. 2005). Some of the promiscuous examples include reduction of molecular oxygen, epoxidation of styrene, hydroxylation of fatty acids, steroids, and sensing of a wide range of physiologically relevant drugs as reviewed recently (Fleming et al. 2006). The major driving force for studying CYP

catalyzed reactions electrochemically is their scope for applications for developing amperometric biosensors, bioreactors, and biofuel cells (Djuricic et al. 2004). The success for developing such bioelectrochemical devices depends largely upon the efficiency of the enzyme and the method of fabrication of the bioelectrode, which in turn influence the electron transport kinetics between the redox centre of the enzyme and the electronic unit and also the stability of the construct. Investigations on the enzymes from the sources that have not been adequately studied may unearth efficient enzymes applicable to these potential technological ventures. The sources of CYP so far used for electrochemical studies are mostly limited to bacteria and higher eukaryotic organisms (Bistolas et al. 2005; Shumyantseva et al. 2005), while such studies on CYP from fungal sources are yet to be pursued passably. In this chapter, we are reporting the direct electrochemistry of a CYP from fungus *Aspergillus terreus* MTCC 6324. The CYP from *A. terreus* is highly active towards *n*-hexadecane and many other organic compounds like, methylated organic solvents, steroids, aromatic hydrocarbons etc. as already described in chapter 2. This broad substrate specific property of the CYP supports its catalytic flexibility towards various chemical substrates and thus, offers potential scopes for its applications in areas like, bioelectrocatalytic transformations and biofuel cells. Considering this importance we have investigated further to understand the bioelectrocatalytic response of the CYP towards *n*-hexadecane substrate and the findings on these studies are also incorporated here. The bioelectrode used for these studies was constructed by immobilizing the microsomal CYP on an electro-active surface over GCE prepared with nanocomposite of MWCNT-NF. The enzyme adsorbed on the nanocomposite was encapsulated with PEI to stabilize the construct against leaching as described experimentally in chapter 5 for CAT bioelectrode. Notably, MWCNT have been reported as an excellent material for electron transport between redox centre of enzymes

and the electrode surface as reviewed recently by us (Sarma et al. 2009). Although, immobilization of CYP in multilayer of PEI has been reported earlier (Lvov et al. 1998; Rusling et al. 2000; Munge et al. 2003), the excellent electrostatic interaction among MWCNT-NF nanocomposite (anionic), enzyme (anionic) and PEI (cationic) has not been exploited previously for CYP immobilization.

6.2. Literature Review

CYP are redox enzymes found widely across nature in many living organisms. The catalytic reactions performed by these enzymes (typically monooxygenation) require the transfer of electrons from the reduced cofactors mostly NAD(P)H (Poulos 1995; Lewis 1996; Ortiz de Montellano and De Voss 2005). The requirement for these reduced cofactors can be obviated by electrochemical reduction of CYP at electrode surface (Djuricic et al. 2004).

The electrochemistry of CYP has been investigated using a variety of metal electrodes such as gold (Au) (Lvov et al. 1998; Davis et al. 2000; Bistolas et al. 2004; Fantuzzi et al. 2004), platinum (Pt) (Estabrook et al. 1996) and tin oxide (Reipa et al. 1997; Mayhew et al. 2000; Reipa et al. 2002), as well as non-metal electrodes such as glassy carbon (GCE) (Iwuoha et al. 1998; Lei et al. 2000; Gilardi et al. 2002; Iwuoha et al. 2004; Shumyantseva et al. 2004), pyrolytic graphite (PG) (Zhang et al. 1997; Munge et al. 2003), edge-plane graphite (EPG) (Aguey-Zinsou et al. 2003; Fleming et al. 2003), and carbon cloth (CC) (Zu et al. 1999; Estavillo et al. 2003). Considering obvious advantage of DET over the mediated or other indirect methods of electron transfer, electrochemical studies on CYP have largely focused on the former approach. Although, DET has been observed on bare electrodes (Kazlauskaite et al. 1996; Lo et al. 1999;

Fantuzzi et al. 2004) as reviewed by Bistolas et al. (2005), a variety of other methods for confining CYP at an electrode surface have been attempted (Table 6.2.1). Modifying the electrode with appropriate polymers, polyelectrolytes or other modifiers in order to attain increased electron transfer between the enzyme and the electrode has been very popular in recent years (Table 6.2.1). The design and features of such functional P450 films, with particular applications to biosensing and bioreactors has been summarized recently (Rusling and Zhang 2003; Bistolas et al. 2005; Shumyantseva et al. 2005; Udit and Gray 2005). Considerable success has been reported with the reductive dehalogenation of a variety of halogenated hydrocarbons (Zhang et al. 1997; Wirtz et al. 2000); reduction of molecular oxygen (Scheller et al. 1979; Fleming et al. 2003; Udit and Gray 2005; Udit et al. 2005) and nitric oxide (Xuan et al. 2004); epoxidation of styrene (Lvov et al. 1998; Mayhew et al. 2000; Estavillo et al. 2003; Munge et al 2003); hydroxylation of fatty acids (Estabrook et al. 1996; Udit et al. 2004), steroids (Estabrook et al. 1996; Iwuoha et al. 1998) and camphor (Reipa et al. 1997; Iwuoha et al. 1998; Sugihara et al. 1998); and the demethylation and dealkylation of drugs (Estabrook et al. 1996; Shumyantseva et al. 2000; Joseph et al. 2003; Iwuoha et al. 2004; Shumyantseva et al. 2004), as well as sensing of a wide range of physiologically relevant drugs (Iwuoha et al. 1998; Joseph et al. 2003; Iwuoha et al. 2004; Paternolli et al. 2004; Shumyantseva et al. 2004), organic substances (Shumyantseva et al. 2004) and gases (Xuan et al. 2004). However, the efficiency of most of these processes (turnover rate, number, operating time, etc.) is yet to be optimized for their practical applications.

Although mechanism of CYP catalyzed reactions are known to a greater extent, the parallel bioelectrocatalytic mechanism is yet to be understood adequately. Interpretations of the reaction mechanism are complicated by the fact that substrate conversion requires oxygen whilst the reduction of the CYP heme is overshadowed by the cathodic oxygen reduction. Most

probably, both reductions of the prosthetic group and of oxygen proceed in parallel at the electrode (Scheme 6.4.3.1). To unravel the complexity, the influence of catalase and of CYP inhibitors is a useful diagnostic criterion. First, substrate conversion by the by-product H_2O_2 is suppressed by the addition of catalase. Second, Substrate hydroxylation via the two-electron-reduction of the iron–oxygen complex is effected by the presence of inhibitors. These criteria have not yet been strictly applied in the majority of investigations (Honeychurch et al. 1999).

Table 6.2.1. CYP bioelectrodes based on direct electron transfer (DET) approach.

References	**CYP species**	**Technique**	**Electrode/ modification**	***E*° (formal potential)**	**Substrates tested– catalysis**	**Comments**
Kazlauskaite et al. 1996	Recombinant CYP 101	CV	EPG	−526 mV and −390 mV	Binding of camphor seen. Catalysis not described here	---------
Lo et al. 1999	CYP 101 WT, mutants	CV	EPG, Au	−428 mV to −449 mV	No catalysis	Electrochemistry due to O_2 reduction to a certain extent.
Fantuzzi et al. 2004	CYP 2E1	CV, i-t	GCE, Au	−334 mV	*p*-nitrophenol	One electron transfer, catalysis with different modifications
Iwuoha et al. 1998	CYP 101	CV, i-t	DAB-BSA glutaraldehyde-GCE	−260 mV	Catalysis with camphor, adamantanone and fenchone, DET	Calibration curve done with amperometry. K_m' = 1.41–3.9 mM. Also use of $Co(Sep)^{3+}$
Zhang et al. 1997	CYP 101	CV, SWV	DMPC—PG, DDAB - PG	−250 mV (DDAB), −357 mV (DMPC)	Catalysis seen with O_2 and TCA	Γ = 7.2 mol cm^{-2} (DMPC), Γ = 4.9 mol cm^{-2} (DDAB), Ks =25 (DMPC) s^{-1}, Ks=26 (DDAB) s^{-1}
Fantuzzi et al. 2004	CYP 2E1	CV, i-t	Bare, thiol, DDAB – GCE, Au	−334 mV	Catalysis with *p*-nitrophenol	Electrochemistry and catalysis with different electrodes and modifications
Oku et al. 2004	CYP 119	CV	DDAB-plastic formed carbon electrode	−250 mV (20°C), −50 mV	No catalysis	Electrochemistry observed at 80°C, ΔE (at 20°C) = 90 mV, ΔE (at 80°C) = 30 mV

				(80°C)		
Aguey-Zinsou et al. 2003	CYP 176A1	CV, V-t	DDAB-EPG electrode	−360 mv	No catalysis	Fe^{2+}/Fe^{3+} redox potential unaffected by substrate binding. pH dependence −59 mV/pH unit
Fleming et al. 2003	CYP 102	CV	DDAB-EPG electrode	−250 mV	Catalysis with O_2 and H_2O_2	Ks=221 s^{-1}, no shift of E° with substrate. Slope of pH change (3–8): −33 mV/pH unit, (8–10): −126 mv/pH unit
Estavillo et al. 2003	CYP 1A2	CV (DET), electro-cat (mediated)	Multilayer with PSS - CC	−310 mV	Catalysis with styrene	Electro-cat done at −600 mV at 4°C. Catalase inhibited catalysis.
Lvov et al. 1998	CYP 101	CV, QCM, product analysis	Multilayer with PEI, PDDA, PSS—Au	−250 mV	Catalysis with styrene	Cationic PEI and PDDA and anionic PSS films were used. Au-MPS-(PEI/PSS-CYP101)- CYP101, pH 5.2
Munge et al. 2003	CYP 101	QCM, CV, electro-cat' product analysis	Multilayer with PEI - PG	−250 mV	Catalysis with styrene	Optimization of multilayer conditions. Influence of pH studied. Γ = 0.1 nmol cm^{-2}, turnover rate = 6.3 h^{-1}
Rusling et al. 2000	CYP 101	CV, SWV	PEI multilayer – rough PG electrode	−270 mV	Catalysis with O_2 and H_2O_2	Γ = 0.15 nmol cm^{-2}
Lei et al. 2000	CYP 101	CV	Clay—GCE	−368 mV	No catalysis	Γ = 3.54 pmol cm^{-2}, Ks = 5–152 s^{-1}.
Zu et al. 1999	CYP 101	CV, electro-cat, product analysis	Au-MPS—PDDA, DDAB, multilayer CC	−250 mV	Catalysis with styrene and *cis-β*-methylstyrene	CYP101 immobilized and in solution, product turnover rates higher in multilayer than in solution
Shumy-antseva et al. 2004	CYP 2B4	CV, i-t	Clay/detergent-GCE	−292 to −305 mV	Catalysis with aminopyrine, benzphet-amine	Product analysis, Γ = 40.5 pmol cm^{-2}, K_{cat} = 1.54 min^{-1}
Joseph et al. 2003	CYP 3A4	QCM, CV, SWV, i-t, electro-cat, product analysis	Au – MPS – PDDA multilayer	342 mV (CV), 335 mV (SWV)	Catalysis with verapamil and medazolam	Amperometry done at −500 mV , Response time = 15–25 s, K_m' = 271–1082 µM.
Nicolini et al. 2001	CYP 11A1	CV	Langmuir Blodgett films (mono- and	−295 to −318 mV	No catalysis	Ks = 0.45 s^{-1}, E°'= −470 mV, Binding of cholesterol seen.

			multilayer), ITO glass plate			
Iwuoha et al. 2004	CYP 2D6	CV, i-t	Polyaniline doped GCE	−120 mV	Catalysis with fluoxetine	K_m' = 3.7 µM, $E°$' shifted anodically in the presence of substrate.
Bistolas et al. 2004	CYP 101	Spectroelectrochemistry	Dithionite and aldrithiol-Au	−380 mV	No catalysis	Native state of enzyme during electro-cat.
Davis et al. 2000	CYP 101 (K334C mutant)	CV, SWV	Polycrystalline Au electrode	None mentioned	No catalysis	K334C mutant greater affinity for Au, and enhanced electrochemistry compared to the WT.

CC: Carbon cloth; CD: Cyclodextrin; DAB: 3,3'-diaminobenzidine; DDAB: Didodecyldimethylammonium bromide; DMPC: Dimeristoyl-l-α-phosphatidylcholine; electro-cat: Electrocatalysis; EPG: Edge-plane graphite; i-t: Chronoamperometry; ITO: Indium Tin Oxide; MPS: Mesoporous Silica; PDDA: poly(diallyldimethylammonium chloride); PG: Pyrolytic graphite; PSS: Poly(styrenesulfonate); QCM: Quartz crystal microbalance; STM: Scanning Tunneling microscope; SWV: Square wave voltammetry; SWV: Square wave voltammetry; V-t: Chronopotentiometry; WT: Wild type .

6.3. Experimental approaches

6.3.1. Reagents

Microsomal CYP (EC 1.14.14.1) was isolated from *A. terreus* MTCC 6324 as described elsewhere (section 2.3.2). MWCNT with 95% purity (10–15 nm outer diameter, 2-6 nm inner diameter and 0.1-10 µm length), PEI (50%) and *n*-hexadecane were obtained from Sigma, NF from Du Pont (USA), and PBO was obtained from Fluka. 50 mM tris buffer, pH 8.0 was used throughout the experiment. Stock (300 µM) of hydrocarbon substrate (*n*-hexadecane) was prepared in tris buffer with triton X-100 (5%) and sonicated for 0.5 h. The maximum

concentration of triton X-100 in buffer did not exceed the final concentration of 0.25% at any point in the substrate sensitivity assays. CAT was isolated and purified from the same strain of *A. terreus*, similar to the procedure described elsewhere (section 3.3.2). The stock solution of CAT (1 mg ml^{-1}) was prepared by dissolving in 50 mM SPB (pH 7.5). All solutions were prepared with deionized water (Milli Q). Solutions were de-aerated by bubbling high-purity (99.99%) argon gas through them prior to the experiments.

6.3.2. Fabrication of MWCNT-NF/CYP/PEI modified GCE and apparatus

Prior to the surface modification, the GCE (5 mm diameter) was polished and cleaned by the procedure as described in section 4.3.4. The layering of GCE with MWCNT-NF nanocomposite was carried out by similar procedure described in section 5.3.2. Once dried, 15 µl of CYP solution (0.5 mg ml^{-1}, specific activity 2.2±0.07 U mg^{-1} of microsomal preparation) was layered on the MWCNT-NF nanocomposite and kept overnight at 4ºC. Finally, 5 µl of PEI (10% in tris buffer pH 8.0) was layered and dried at room temperature. Separate GCE with each layer as control were prepared simultaneously and dried as earlier. Electrochemical experiments were performed by similar instrument and softwares as described in section 5.3.2.

6.3.3 Surface morphology studies of the fabricated bioelectrode by atomic force microscopy (AFM)

GCE fabricated with each layer were mounted on the specimen holders with electro-conductive tape and were placed in standard sample plates. AFM was performed using an ambient air scanning probe microscope (Agilent Technologies 5500). Images were recorded with typical contact mode using PicoScan 5 software.

6.4. Results and discussion

6.4.1. Surface morphological characterization of the fabricated bioelectrode by AFM

AFM was used to characterize the surface morphology of the fabricated GCE. Fig. 6.6.1A shows the bare and smooth GCE surface. Fig. 6.6.1B shows the MWCNT-NF nanomatrix on the GCE providing sufficient cavities for the uniform adsorption of CYP (Fig. 6.6.1C). Further, the addition of PEI on the nanomatrix- adsorbed CYP layer squeezed the enzyme effectively within the cavity of the nano-matrix as evident from the Fig. 6.6.1D, thus providing additional physical stability to the immobilized CYP on the electrode. It is suggested that the electrostatic interaction developed between the negatively charged MWCNT-NF-enzyme with the positively charged PEI tightly packed the CYP layer closer to the electrode surface and thereby impart additional stability to the immobilized CYP.

6.4.2. Cyclic voltammetry of MWCNT-NF/CYP/PEI modified GCE

The electrochemical behavior of microsomal CYP in MWCNT-NF/PEI film was studied by CV. A well defined quasi-reversible CV peak at approximately -0.53 V [(*Epa*+*Epc*)/2], characteristic of heme Fe^{3+}/Fe^{2+} redox couple of CYP (Kazlauskaite et al. 1996) was observed when GCE/MWCNT-NF/CYP/PEI electrode was used in anaerobic condition with continuous argon gas purging (Fig. 6.6.2). The ratio of anodic to cathodic peak currents (*Ipa* and *Ipc*) was approximately 1.0 (Fig. 6.6.2, background subtracted CV), indicating that CYP undergoes a quasi-reversible redox process at the GCE modified with MWCNT-NF/CYP/PEI film. Thus,

MWCNT-NF film provides a three-dimensional nano-electrode ensemble for sufficient adsorption of CYP and a suitable environment for electron transfer with underlying GCE. The poly-cationic layer of PEI further adds to the rate of electron transfer by electrostatic interaction with the CYP (negatively charged, as at pH 8.0 most of the proteins are negatively charged) adsorbed on MWCNT-NF film. The formal potential ($E°$) of CYP was estimated as a midpoint of CV reduction and oxidation peak potentials (*Epc* and *Epa*) at approximately -565 mV and -500 mV, respectively. The separation of *Epc* and *Epa* (ΔEp=65 mV) indicates a single electron transfer reaction. The surface coverage (Γ) of 3.45×10^{-10} mol cm^{-2} was calculated for CYP at the modified GCE using the equation $\Gamma = Q/nFA$, where Q is the charge obtained by integrating the peak current area, n is the number of electrons involved, F is Faraday's constant and A is electrode area. To obtain the kinetic parameters of CYP redox at MWCNT-NF/PEI modified GCE, the effect of scan rate was investigated. Fig. 6.6.3A shows the CVs at different scan rates. The peak current (*Ip*) versus scan rate plot, shown in the Fig. 6.6.3B, exhibits a linear relationship (R^2=0.9935), as expected for a surface-confined redox process. The peak to peak separation is approximately 60 mV at scan rates of less than 50 mV s^{-1}, suggesting facile charge transfer kinetics over this range of sweep rates. On the other hand, it was found that at scan rates greater than 100 mV s^{-1}, ΔEp increased with the increase of scan rate. The values of peak to peak potential separations were proportional to the logarithm of the scan rate for scan rates greater than 100 mV s^{-1} (Fig. 6.6.3C). Based on the Laviron's theory, the transfer coefficient (α) and heterogeneous electron transfer rate constant (*Ks*) were estimated by measuring the variation of peak potential with scan rate (Laviron 1979), following the similar procedure described in section 5.4.2. The α and *Ks* of CYP were calculated as 0.6±0.1 and 1.0±0.2 s^{-1}, respectively showing a sufficiently fast electron transfer kinetics between the redox center of immobilized

CYP and the electronic unit. Thus, by following the current protocol, we are reporting here for the first time, an efficient electrical conductivity between the redox centre of microsomal CYP from fungal source and electrode.

6.4.3. Electro-catalytic behavior of CYP immobilized on MWCNT-NF/PEI modified GCE

In well oxygenated solution and in presence of specific substrate (here *n*-hexadecane), a positive shift of ~55 mV was observed in the redox peak for MWCNT-NF/CYP/PEI bioelectrode ($E^{\circ\prime}$ = -0.475, ΔEp = 62 mV). The increase in *Ipc* is also evident from the background subtracted CV accompanied by a decrease of *Ipa* (Fig. 6.6.4). Further with increasing concentration of *n*-hexadecane in the buffer solution, the voltammetric behavior of the CYP-bioelectrode changes obviously, with an increase in the *Ipc* and the subsequent disappearance of the *Ipa* (Fig. 6.6.5A) which, indicates the electro-catalytic reduction of CYP immobilized on GCE/MWCNT-NF/PEI and the increases in the rate of dioxygen binding to the heme.

The positive shift in the redox potential of CYP can be explained in terms of the affinity of CYP towards the binding of the substrate and molecular oxygen leading to some of the critical reorganization in the redox center which makes the whole process more facile. In substrate-free CYP, the transition from a low spin form (six co-ordinate complex) to a high spin form (five co-ordinate complex) upon reduction is likely to result in larger inner sphere reorganization energy, than in substrate-bound CYP which is in high spin form in both oxidation states (Scheme 6.4.3.1). Therefore, relative to substrate bound CYP, the substrate-free form has a less favorable spin state which is stated as one of the reason for the potential shift on substrate binding (Honeychurch et al. 1999). Further, oxygen is the natural co-substrate of CYP and binds to the

ferrous iron (Fe^{2+}) at a very fast rate (Iwuoha et al. 1998, Joseph et al. 2003), thus making the overall process more thermodynamically favorable. The change in $E°$ following substrate binding thus gave birth to the idea of a substrate-dependent thermodynamic switch being present in P450 enzyme systems which may be speculated as the nature's way of preventing the futile cycling of electrons (Daff et al. 1997). Early voltammetric works with $P450_{cam}$ at a graphite electrode (Kazlauskaite et al. 1996) and in biomembrane-like films (Zhang et al. 1997) have shown that the presence of a substrate/inhibitor results in a significant shift in the value of $E°$ to more positive values (in a range of 45 mV-100 mV). However, voltammetric studies in the presence of substrate (or inhibitors) with CYP from other sources have not provided as conclusive or consistent results. Thus, the response profile of the CYP bioelectrode shown in Fig. 6.6.4 is similar to the one from the bacterial sources and is first of its kind for CYP from fungal source.

Although, the increase in *Ipc* was observed with increasing substrate concentration by CYP bioelectrode but the outcome was more significant when CAT was co-adsorbed with CYP in a concentration which can effectively neutralize the H_2O_2 generated on the electrode (by the electrochemical reduction of oxygen) and can thus effectively inhibit the peroxide shunt pathway (Scheme 6.4.3.1), without having an interference in the redox of CYP. The *Ipc* thus generated (Fig. 6.6.5B) can be used to co-relate the complete CYP activity. Saturation and linear response curves were obtained within the *n*-hexadecane concentration from 0.1 µM to 350 µM (Fig. 6.6.5C) and 10 µM to 100 µM (R^2 = 0.975) (Fig. 6.6.5D), respectively by using DPV at -0.51 V. The detection limit was 0.1 µM.

Further, to confirm the correlation between increasing *Ipc* and CYP activity, inhibitor studies with PBO (specific inhibitor of CYP; Hodgson and Levi 1998) was carried out where

different concentration of PBO was layered on the enzyme layer on the electrode and was allowed to dry after which it was washed. DPV with different inhibitor concentrations in presence of a fixed concentration of substrate at -0.51 V showed a linear decrease in *Ipc* with increasing PBO concentration (Fig. 6.6.6A). IC_{50} for CYP activity was observed at 2.7±0.3 µM concentration of PBO (Fig. 6.6.6B).

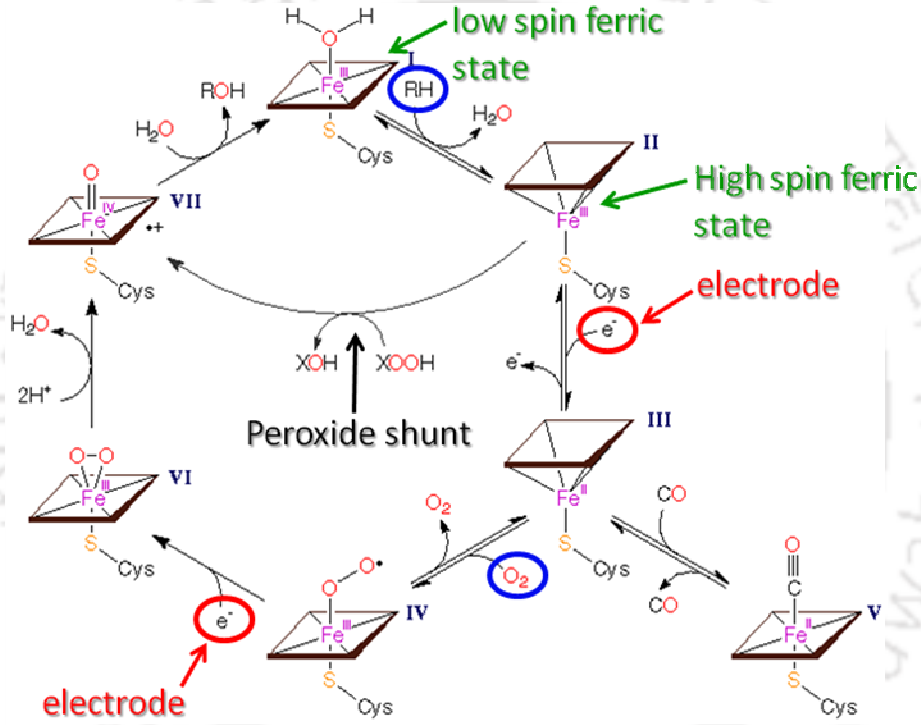

Scheme 6.4.3.1. Electrocatalytic cycle of CYP.

(Adapted and modified from http://metallo.scripps.edu/promise/CYTOCHROMES.html)

6.5. Conclusions

The direct electrochemistry and electro-catalytic properties of microsomal CYP from *A. terreus* MTCC 6324 immobilized on MWCNT-NF/PEI modified GCE were investigated. A pair of well defined and nearly reversible cyclic voltammetric peaks for Fe^{3+}/Fe^{2+} redox couple of CYP with formal potential ($E°$) of about -0.53 V (vs. Ag/AgCl reference electrode) in pH 8.0 buffer was observed under deoxygenated condition. In the presence of oxygen and substrate, the redox potential of the bioelectrode was shifted to -0.475 V. Electro-catalytic current with *n*-hexadecane and inhibition studies with PBO confirmed the involvement of $Fe^{3+/2+}$ system of CYP in the redox process. The bioelectrode exhibited a remarkable electro-catalytic activity towards the *n*-hexadecane substrate. The current response increased linearly from 1 µM to 100 µM of substrate with detection limit 0.1 µM *n*-hexadecane. The IC_{50} for PBO was 2.7 µM. The surface coverage of CYP immobilized on MWCNT-NF/PEI modified GCE was approximately 3.45×10^{-10} mol cm^{-2}, suggesting enzyme monolayer formation. The electron transfer rate constant (*Ks*) was 1.0 ± 0.2 s^{-1}, indicating facilitation of the electron transfer between CYP and GCE. A significant positive shift in the redox potential of CYP in the presence of oxygen and substrate is one of the interesting findings, which supports the theory of thermodynamic switch present in CYP catalytic systems. The results have established the potential of the CYP from *A. terreus* and their fabrication procedure for their application in bioelectronic devices, such as bio-fuel cells.

6.6. Figures

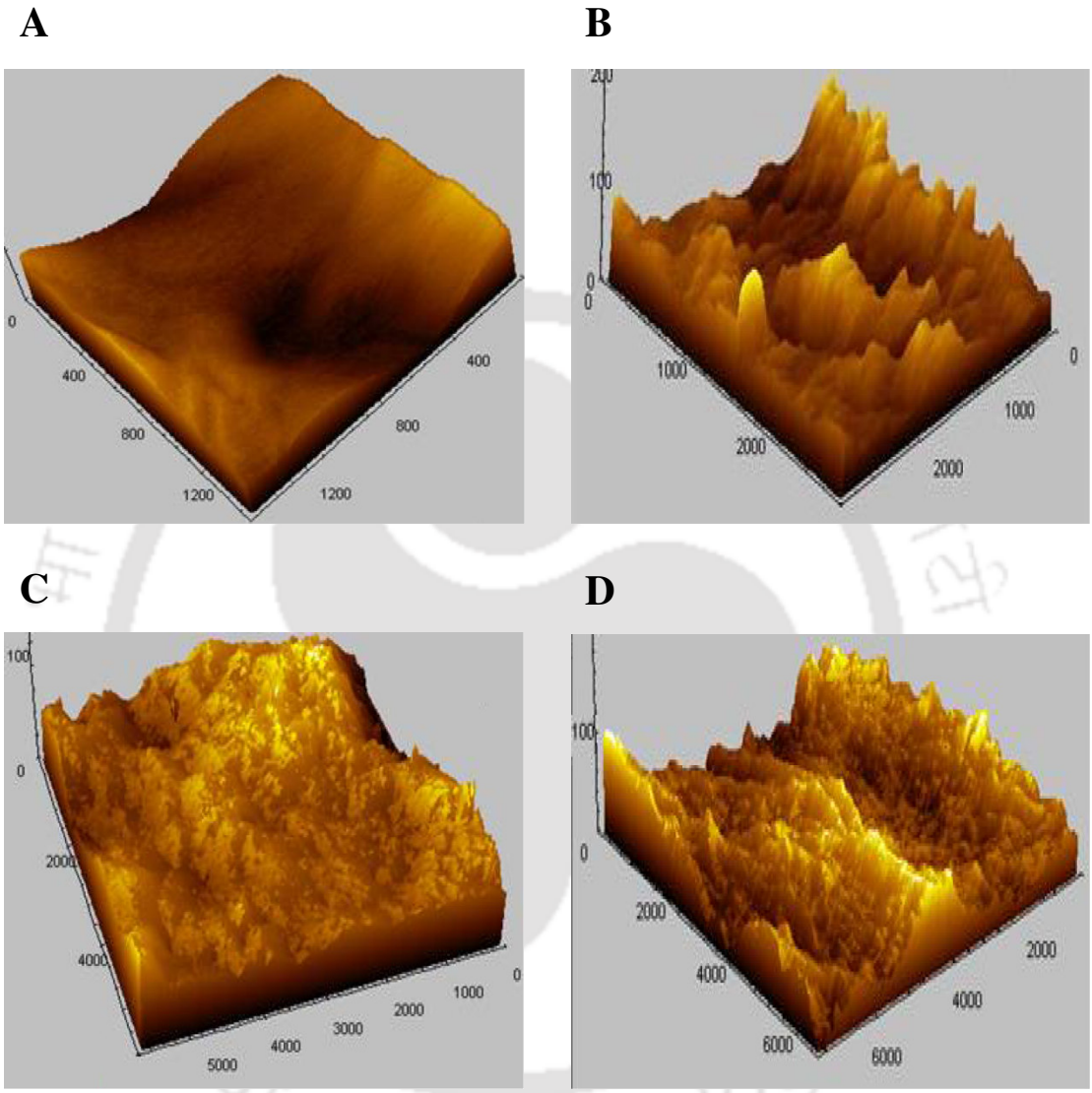

Fig. 6.6.1. AFM images of different layers of modifications of GCE for immobilization of CYP. **(A)** Bare GCE, **(B)** GCE/MWCNT-NF, **(C)** GCE/MWCNT-NF/CYP and **(D)** GCE/MWCNT-NF/CYP/PEI. Scales in all axes are in nm.

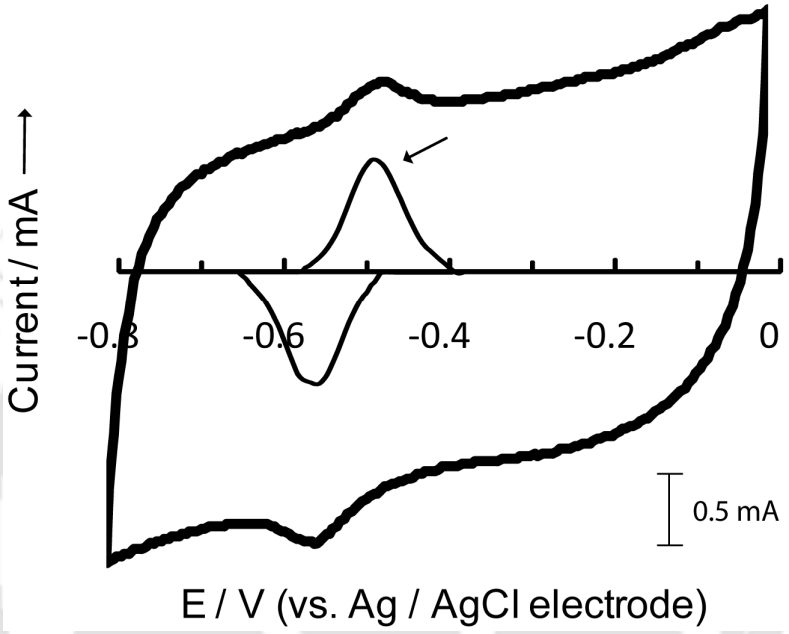

Fig. 6.6.2. The cyclic voltammogram of microsomal CYP immobilized on MWCNT-NF/PEI modified GCE in absence of oxygen. Arrow head points to the background subtracted redox peaks. Background subtraction was carried out by GPES software tool. The voltammogramms were recorded in 50 mM tris buffer (pH 8.0) and scan rate of 100 mV s^{-1}.

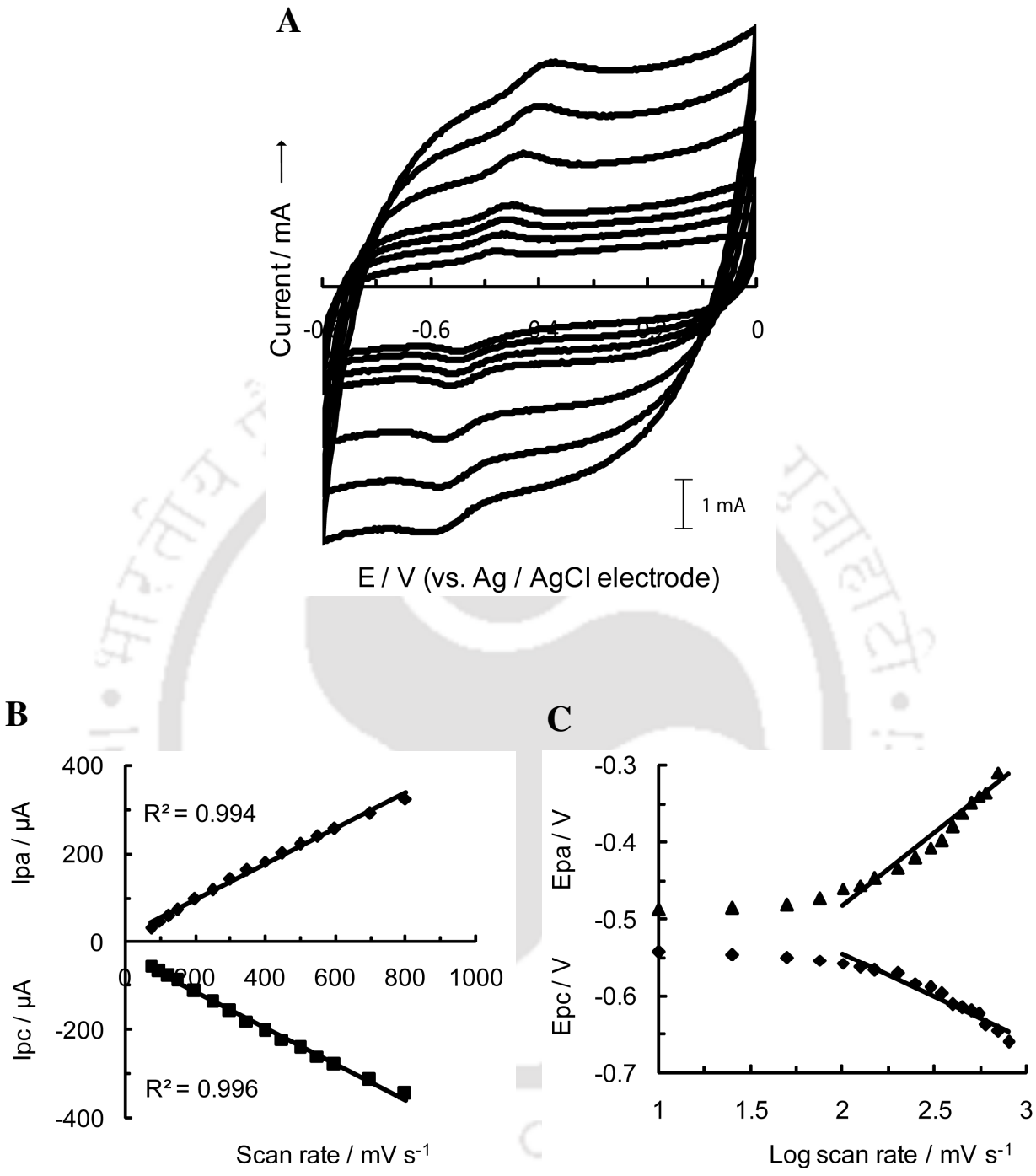

Fig. 6.6.3. **(A)** Cyclic voltammograms of MWCNT-NF/CYP/PEI modified GCE at different scan rates in 50 mM tris buffer (pH 8.0). The scan rates were 10-800 mV s^{-1}. **(B)** Plot of peak currents vs. scan rates. **(C)** Variation of peak potentials vs. the logarithm of the scan rates.

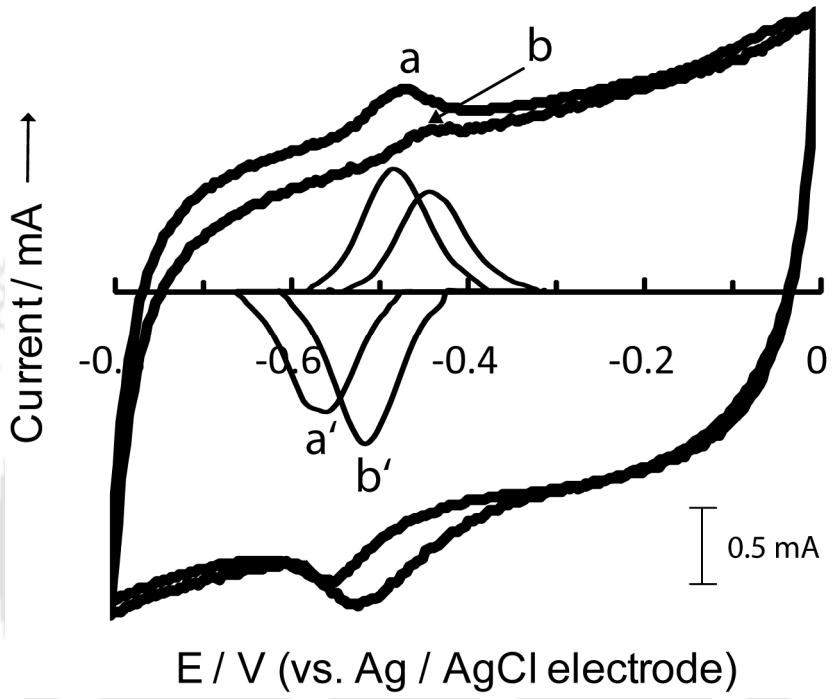

Fig. 6.6.4. Cyclic voltammograms of GCE/MWCNT-NF/CYP/PEI in absence (a) and presence (b) of oxygen and *n*-hexadecane. (a') and (b') depicts the background subtracted peaks of (a) and (b), respectively. Voltammograms were recorded in 50 mM tris buffer (pH 8.0) and scan rate of 100 mV s^{-1}.

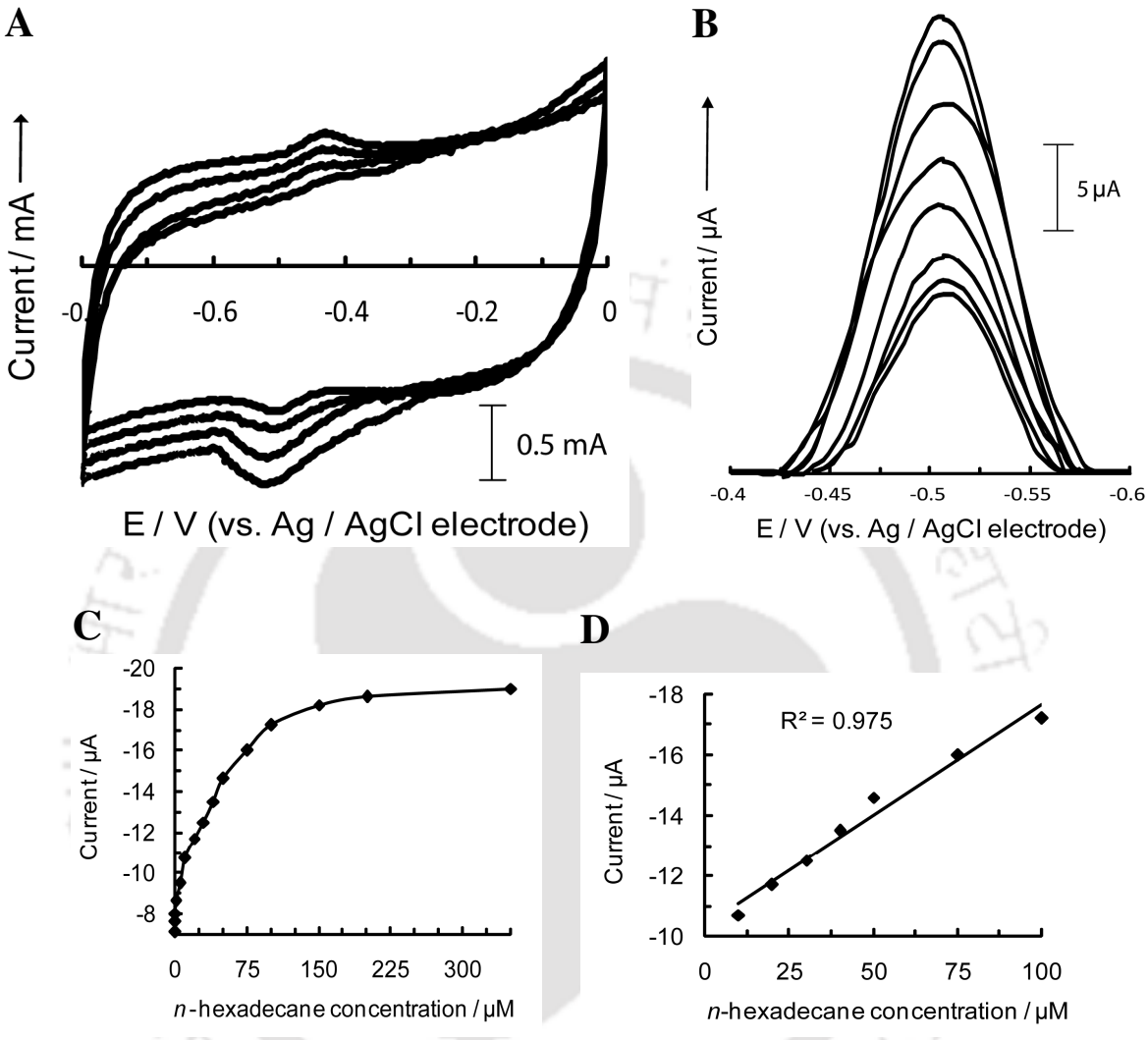

Fig. 6.6.5. Substrate dependent response of fabricated CYP bioelectrode to different *n*-hexadecane concentration. **(A)** Cyclic voltammograms of MWCNT-NF/CYP/PEI modified GCE with successive addition of substrate (ranging from 10-100 µM *n*-hexadecane). **(B)** Differential pulse voltammetric (DPV) curves of GCE/MWCNT-NF/CYP-CAT/PEI with different substrate concentration at -0.51 V. **(C)** Response curve of CYP immobilized on MWCNT-NF/PEI GCE. **(D)** Linear calibration curve for determination sensitivity of immobilized CYP.

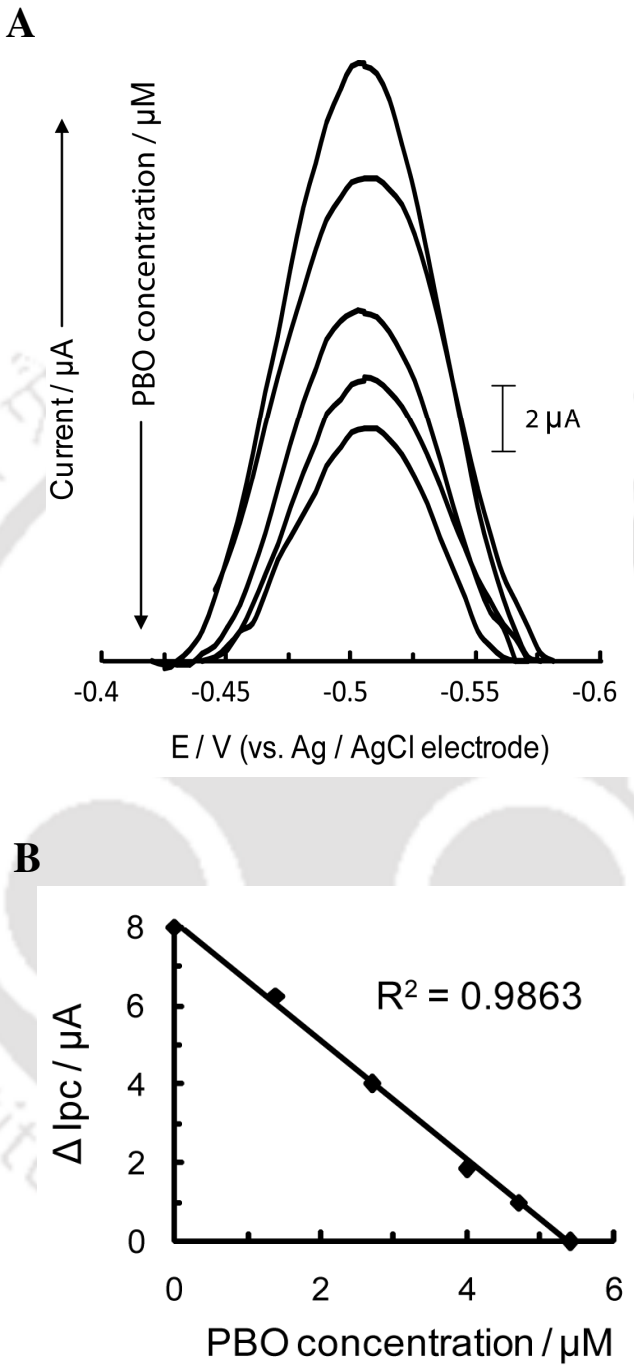

Fig. 6.6.6. Inhibitor studies with PBO. **(A)** DPV curves at different PBO concentrations (at fixed substrate concentration of 100 µM and -0.51 V). **(B)** Linear curve for determination of IC_{50}.

Chapter 7

Outline of the thesis and suggested future directions for the work

7.1. Outline of the thesis

- A membrane bound CYP (Cytochrome P450 monooxygenase) activity was detected in the cells of *A. terreus* MTCC 6324.
- The CYP activity in the *n*-hexadecane grown cells was largely associated with lipid granules in the cytosol.
- The CYP was active with various substrates namely, alkanes, alkane derivatives, alcohols, aromatic compounds, organic solvents, and steroids.
- Detection of CYP activity using methanol, acetone, or dimethylsulphoxide as substrate is appealing. Since report on microbial CYP active on these methylated organic solvents as substrate was not available in the open literature.
- The CYP was found to catalyze both terminal and sub-terminal oxidations of long-chain hydrocarbon substrates.
- Following the heme staining method in SDS–PAGE gel the detected molecular weight of the CYP was ~110 kDa.
- The *Aspergillus terreus* MTCC 6324 had produced very high level of cellular catalase (CAT) during growth on *n*-hexadecane substrate.

- CAT was purified to 160-fold and was found to be a homotetramer with subunit molecular mass of ~90 kDa. The isoelectric pH (pI) of the purified CAT was found to be 4.2.
- Peptide mass fingerprinting studies of the CAT protein showed its highest similarity with the CAT B protein. The fully conserved positions for tyrosine (Y) and arginine (R) residues in the proximal heme binding domain of CAT were detected.
- CAT was active in a broad range of pH 4.0 to 12.0 and temperature 25ºC to 90ºC. The catalytic efficiency (K_{cat}/K_M) of 4.7×10^8 M^{-1} s^{-1} of CAT was considerably higher than most of the extensively studied catalases from different sources.
- The heme from CAT was isolated, purified and identified as heme b.
- High stability in a broad alkaline pH range and high temperature stability were identified as interesting characteristics of the isolated CAT.
- The stability of CAT was much less in acidic condition than the alkaline environment.
- The heme in the CAT protein matrix was disintegrated more in acidic pH and the level of this disintegration increased with decreasing the incubating pH. This heme disintegration has been correlated to the low stability of CAT in acidic pH.
- Apo-CAT was prepared by dissociation of heme from the CAT protein matrix at acidic pH and was again reconstituted back with the isolated heme at alkaline and partially denaturing condition to a functionally active enzyme. This preliminary finding on the effective reconstitution of heme to this large catalase protein matrix is expected to pave the way for the potential application of the heme reconstitution approach on the construction of large catalase-based bioelectrode for biosensor or biofuel cell applications.

- The high turnover number and excellent stability of CAT was explored for the development of electrochemical-based biosensor. A CAT bioelectrode was fabricated on a GCE using MWCNT, NF and PEI in a layer by layer assembly technique using the adsorption and electrostatic interaction for construction of high electroactive and stable CAT-immobilization matrix. A remarkable electro-catalytic activity of the fabricated bioelectrode towards the reduction of H_2O_2 was detected. The biosensor response increased linearly with H_2O_2 concentration from 10 µM to 5 mM. The response time for steady state current and detection limit were ~2 s and 1 µM H_2O_2, respectively. A high operational and storage stability and stability against leaching were observed for the bioelectrode. A decrease in overall impedance of the bioelectrode upon immobilization of CAT was identified as novel finding.
- The direct electrochemistry and bio-electrocatalytic properties of microsomal CYP immobilized on MWCNT-NF/PEI modified GCE were also investigated. A pair of well defined and nearly reversible cyclic voltammetric peaks for $Fe^{(III)}/Fe^{(II)}$ redox couple of CYP with E^0 of about -0.53 V was observed. A shift of ~53 mV was observed in the presence of oxygen with $E^{0\prime}$ shifting to -0.475. CYP bioelectrode exhibits a remarkable electro-catalytic activity towards the *n*-hexadecane substrate. The response increased linearly with *n*-hexadecane concentration from 1 µM to 100 µM with detection limit 0.1 µM. The *Ks* was 1.0±0.2 s^{-1}, indicating facilitation of the electron transfer between CYP and GCE. Immobilized CYP co-adsorbed with CAT shows linear increase in current with increasing hydrocarbon substrate concentration.
- The fabricated CYP bioelectrode showed a high affinity for oxygen and a positive shift in redox potential in presence of oxygen and substrate. This observation on bio-

electrocatalytic property of the fabricated bioelectrode for the hydrocarbon substrates has suggested the potential application of the CYP for the development of biocathode for biofuel cell applications.

7.2. Suggested future directions for the work

The broad substrate specificities of CYP and high catalytic efficiency and broad pH and thermal stability of CAT are the interesting traits of these redox enzymes produced by the filamentous fungi, *A. terreus* considered in this investigation. Detailed molecular characterization and structural elucidation following conventional molecular biological tools and other techniques like cloning, sequencing, circular dichromism and x-ray crystallography may provide useful structural information of these enzyme proteins which is expected to promote further understanding on the said functional and physical properties of these novel enzymes. The exact location of the redox center (heme in the present case) could also be elucidated with these information that may help the precise wiring of these enzymes either through heme-reconstitution approach or nano-fabrication using suitable ligand chemistry, thus, will advance the scope of promoting better electron-transport kinetics between the redox center of the enzyme and the electronic unit for bioelectronic applications. These are expected to reduce not only the background current and response time but also to increase the current density of the fabricated bioelectrodes. Although, a very low response time and high stability for the CAT biosensor has been achieved, to evaluate the practical application of the fabricated bioelectrode further studies like, analysis of real samples and stability against various parameters such as temperature, pH, salt etc. are essential. The decrease in R_{ct} of the electrode in the presence of immobilized CAT is interesting and has opened up an avenue for detailed structural and electrochemical investigation

of CAT to unfold the observed facts. The other important point need to be considered with respect to CYP is the selection of suitable substrate and media in the cathodic compartment for the proposed fuel cell applications. Highly hydrophobic substrate may cause diffusion limitation; thus, proper medium engineering for better substrate solubilization and its subsequent sequestration are critical for the increased electron density and overall electrocatalytic efficiency of the CYP-based biocathode for biofuel cell applications.

Bibliography

Aguey-Zinsou K-F, Bernhardt PV, De Voss JJ, Slessor KE (2003) Electrochemistry of P 450_{cin}: New insights into P-450 electron transfer. Chem Commun 7:418–419

Agui L, Yanez-Sedeno P, Pingarron JM (2008) Role of carbon nanotubes in electroanalytical chemistry: A review. Anal Chim Acta 622:11–47

Akertek D, Tarhan L (1995) Characteristics of immobilized catalases and their applications in pasteurization of milk. Appl Biochem Biotechnol 50:9555–9560

Akyilmaz E, Kozgus O (2009) Determination of calcium in milk and water samples by using catalase enzyme electrode. Food Chem 115:347–351

Akyilmaz E, Sezginturk MK, Dinc-kaya E (2003) A biosensor based on urate oxidase-peroxidase coupled enzyme system for uric acid determination in urine. Talanta 61:73-79

Allgood GS, Perry JJ (1986) Characterization of a manganese-containing catalase from the obligate thermophile *Thermoleophilum album*. J Bacteriol 168:563-567

Amo T, Atomi H, Imanaka T (2002) Unique presence of a manganese catalase in a hyperthermophilic archaeon*, Pyrobaculum calidifontis* VA1. J Bacteriol 184:3305-3312

Andersson LA, Dawson LA (1991) EXAFS spectroscopy of heme containing oxygenases and peroxidases. Struct Bond 64:1-40

Andersson MM, Hatti-Kaul R (1999) Protein stabilising effect of polyethyleneimine. J Biotechnol 72:21–31

Antonini M, Brunori E (1971) Hemoglobin and myoglobin in their reactions with ligands. Neuberger A, Tatum EL (eds) North-Holland Publishers, Amsterdam, The Netherlands

Armstrong FA, Heering HA, Hirst J (1997) Reactions of complex metalloproteins studied by protein-film voltammetry. Chem Soc Rev 26:169-179

Armstrong FA, Hill HAO, Walton NJ (1988) Direct electrochemistry of redox proteins. Acc Chem Res 21: 407– 413

Arribas AS, Bermejo E, Chicharro M, Zapardiel A, Luque GL, Ferreyra NF, Rivas GA (2007) Analytical applications of glassy carbon electrodes modified with multi-wall carbon

nanotubes dispersed in polyethylenimine as detectors in flow systems. Anal Chim Acta 596:183–194

Azevedo AM, Miguel D, Prazeres F, Cabral JMS, Fonseca LP (2005) Ethanol biosensors based on alcohol oxidase. Biosens Bioelectron 21 235–247

Barynin VV, Vagin AA, Melik-Adamyan WR, Grebenko AI, Changulov SV, Popov AN, Andrianova ME, Vainshtein BK (1986) Three dimensional structure of the Tcatalase with a 3 Å resolution. Dokl Akad Nauk SSSR 288:877-880

Beers RFJr, Sizer IW (1952) A spectrophotometric method for measuring the breakdown of hydrogen peroxide by catalase. J Biol Chem 195:133-140

Beilen JB, Funhoff EG (2005) Expanding the alkane oxygenase toolbox: new enzymes and applications. Curr Opin Biotechnol 16:308–314

Beyer WF, Fridovich I (1985) Pseudocatalase from *Lactobacillus plantarum*: Evidence for a homopentameric structure containing two atoms of manganese per subunit. Biochemistry 24:6460-6467

Bistolas N, Christenson A, Ruzgas T, Jung C, Scheller FW, Wollenberger U (2004) Spectroelectrochemistry of cytochrome $P450_{cam}$. Biochem Biophys Res Commun 314:810–816

Bistolas N, Wollenberger U, Jung C, Scheller FW (2005) Cytochrome P450 biosensors – a review. Biosens Bioelectron 20:2408–2423

Bradford MM (1976) A rapid and sensitive method for the quantification of microgram quantities of protein utilizing the principle of protein dye binding. Anal Biochem 72:248–254

Bravo J, Fita I, Ferrer J, Ens W, Hillar A, Switala J, Loewen PC (1997) Identification of a novel bond between a histidine and the essential tyrosine in catalase HPII of *Escherichia coli*. Protein Sci 6:1016-1023

Bravo J, Verdaguer N, Tormo J, Betzel C, Switala J, Loewen PC, Fita I (1995) Crystal structure of catalase HPII from *Escherichia coli*. Structure 3:491-502

Britton LN (1984) Microbial degradation of aliphatic hydrocarbons. In: Microbial degradation of organic compounds (Gibson DT, ed), Marcel Dekker, New York 5:181-252

Brown-Petersen NJ, Salin ML (1993) Purification of a catalase-peroxidase from *Halobacterium halobium*: Characterization of some unique properties of the halophilic enzyme. J Bacteriol 175:4197-4202

Buleandra M, Radu GL, Tanase I (2000) Redox protein electroanalysis: metalloproteins. Roum Biotechnol Lett 5:423-438

Bullen RA, Arnot TC, Lakeman JB, Walsh FC (2006) Biofuel cells and their development. Biosens Bioelectron 21:2015-2045

Bushnell LD, Haas FF (1941) The utilization of certain hydrocarbons by microorganisms. J Bacteriol 41:653–673

Buzy A, Bracchi V, Sterijades R, Chroboczek J, Thibault P, Gagnon J, Jouve HM, Hydry-Clergeon G (1995) Complete amino acid sequence of *Proteus mirabilis* PR catalase. Occurrence of a methionine sulfone in the close proximity of the active site. J Protein Chem 14:59-72

Calera JA, Sanchez-Weatherby J, Lopez-Medrano R, Leal F (2000) Distinctive properties of the catalase B of *Aspergillus nidulans*. FEBS Lett 475:117-120

Campanella L, Roversi R, Sammartino MP, Tomassetti M (1998) Hydrogen peroxide determination in pharmaceutical formulations and cosmetics using a new catalase biosensor. J Pharmaceut Biomed 18:105–116

Campanella L, Sammartino MP, Tomassetti M, Zannella S (2001) Hydroperoxide determination by a catalase OPEE: application to the study of extra virgin olive oil rancidification process. Sens Actuators B Chem 76:158-165

Carpena X, Wiseman B, Deemagarn T, Singh R, Switala J, Ivancich A, Fita I, Loewen PC (2005) A molecular switch and electronic circuit modulate catalase activity in catalase-peroxidases. EMBO reports 6:1156-1162

Chance B (1947) An intermediate compound in the catalase-hydrogen peroxide reaction. Acta Chem Scand 1:236-267Chance B (1949) The Reaction of Catalase and Cyanide. J Biol Chem 179**:**1299**-**1309

Chandlee JM, Tsaftaris AS, Scandalios JG (1983) Purification and partial characterization of three genetically defined catalases of maize. Plant Sci Lett 29:117-131

Chaplin MF, Bucke C (1990) The large-scale use of enzymes in solution. In: Enzyme Technology, Cambridge University Prees, UK 138-166

Chen H, Mousty C, Chen L, Cosnier S (2008) A new approach for nitrite determination based on a HRP/catalase biosensor. Mater Sci Eng C 28:726–730

Chen X, Xie H, Kong J, Deng J (2001) Characterization for didodecyldimethylammonium bromide liquid crystal film entrapping catalase with enhanced direct electron transfer rate. Biosens Bioelectron 16:115–120

Claiborne A, Fridovich I (1979) Chemical and enzymatic intermediates in the peroxidation of *o*-dianisidine by Horseradish peroxidase 1. Spectral properties of the products of dianisidine oxidation. Am Chem Soc 18:2324–2329

Clayton RK (1959) Purified catalase from *Rhodopseudomonas spheroides*. Biochim Biophys Acta 36:40-47

Cohen G, Rapatz W, Ruis H (1988) Sequence of the *Saccharomyces cerevisiae* CTA1 gene and amino acid sequence of catalase A derived from it. Eur J Biochem 176:159-163

Coon MJ (2005) Cytochrome P450: Nature's most versatile biological catalyst. Annu Rev Pharmacol Toxicol 45:1–25

Curatti L, Hernandez JA, Igarashi RY, Soboh B, Zhao D, Rubio LM (2007) *In vitro* synthesis of the iron molybdenum cofactor of nitrogenase from iron, sulfur, molybdenum, and homocitrate using purified proteins. Proc Natl Acad Sci USA 104:17626- 17631

D'Orazio P (2003) Biosensors in clinical chemistry. Clinica Chimica Acta 334:41–69

Daff SN, Chapman SK, Turner KL, Holt RA, Govindaraj S, Poulos TL, Munro AW (1997) Redox control of the catalytic cycle of flavocytochrome P450 BM3. Biochemistry 36:13816-13823

Das A, Hecht MH (2007) Peroxidase activity of *de novo* heme proteins immobilized on electrodes. J Inorg Biochem 101:1820–1826

Dashti N, Al-Awadhi H, Khanafer M, Abdelghany S, Radwan S (2008) Potential of hexadecane utilizing soil-microorganisms for growth on hexadecanol, hexadecanal and hexadecanoic acid as sole sources of carbon and energy. Chemosphere 70:475–479

Davis JJ, Djuricic D, Lo KKW, Wallace ENK, Wong LL, Hill HAO (2000) A scanning tunnelling study of immobilised cytochrome $P450_{cam}$. Faraday Discuss 116:1–8

Dawson JH, Sono M (1987) Cytochrome P-450 and chloroperoxidase: Thiolate-ligated heme enzymes. Spectroscopic determination of their active site structures and mechanistic implications of thiolate ligation. Chem Rev 87:1255-1276

Day BJ (2004) Catalytic antioxidants: a radical approach to new therapeutics. Therapeutic Focus-Reviews 9:557-566

Degtyarenko KN, North ACT, Perkins DN, Findlay JBC (1998) PROMISE: a database of information on prosthetic centers and metal ions in protein active sites. Nucleic Acids Res 26:376–381

Deutsch HF (1951) A highly active horse erythrocyte catalase. Acta Chem Scand 5:815-819

Di J, Zhang M, Yao K, Bi S (2006) Direct voltammetry of catalase immobilized on silica sol–gel and cysteine modified gold electrode and its application. Biosens Bioelectron 22:247-252

Diaz A, Munoz-Clares RA, Rangel P, Victor-Julian V, Hansberg W (2005). Functional and structural analysis of catalase oxidized by singlet oxygen. Biochimie 87:205–214

Diaz A, Rangel P, Montes De Oca Y, Lledias F, Hansberg W (2001) Molecular and kinetic study of catalase-1, a durable large catalase of *Neurospora crassa*. Free Radical Bio Med 31:1323–1333

Diaz A, Valdes VJ, Rudino-Pinera E, Horjales E, Hansberg W (2009) Structure–function relationships in fungal large-subunit catalases. J Mol Biol 386:218–232

Djuricic D, Fleming BD, Hill HAO, Tian Y (2004) Towards exploiting the electrochemistry of cytochrome P450. In: Trends in molecular electrochemistry (Pombeiro AJL, Amatore C, eds), Marcel Dekker, USA and Fontis Media SA, Switzerland 189-208

Dus K, Katagiri M, Yu CA, Erbes DL, Gunsalus IC (1970) Chemical characterization of cytochrome P-450$_{cam}$. Biochem Biophys Res Commun 40:1423–1430

Eremin AN, Makarenko MV, Drozhdenyuk AP, Moroz IV, Mikhailova RV (2004) Precipitated, coprecipitated, and carbon-mineral sorbents for isolation of extracellular catalase from *Penicillium piceum* F-648. Appl Biochem Microbiol 40:433-440

Eriksson CE, Olsson PA, Svensson SG (1971) Denatured hemoproteins as catalysts in lipid oxidation. J Am Oil Chem Soc 48:442-447

Eschenfeldt WH, Zhang Y, Samaha H, Stols L, Eirich LD, Wilson CR, Donnelly MI (2003) Transformation of fatty acids catalyzed by cytochrome P450 monooxygenase enzymes of *Candida tropicalis*. Appl Environ Microbiol 69:5992-5999

Estabrook RW, Cooper DY, Rosenthal S (1963) The light-reversible carbon monoxide inhibition of the steroid C-21 hydroxylation system of the adrenal cortex. Biochem J 338:741–755

Estabrook RW, Faulkner KM, Shet MS, Fisher CW (1996) Application of electrochemistry for P450-catalysed reactions. Meth Enzymol 272: 44-51

Estabrook RW, Werringloer J (1978) The measurement of difference spectra: application to the cytochromes of microsomes. Methods Enzymol 52:212–220

Estavillo C, Lu Z, Jansson I, Schenkman JB, Rusling JF (2003) Epoxidation of styrene by human cyt P450 1A2 by thin film electrolysis and peroxide activation compared to solution reactions. Biophys Chem 104:291-296

Fantuzzi A, Fairhead M, Gilardi G (2004) Direct electrochemistry of immobilized human cytochrome P450 2E1. J Am Chem Soc 126:5040-5041

Fleisher B (1974) Isolation and characterization of golgi apparatus and membranes from rat liver. Methods Enzymol 31:180–191

Fleming BD, Johnson DL, Bond AM, Martin LL (2006) Recent progress in cytochrome P450 enzyme electrochemistry. Expert Opin Drug Metab Toxicol 2:581-589

Fleming BD, Tian Y, Bell SG, Wong LL, Urlacher V, Hill HA (2003) Redox properties of cytochrome P450BM3 measured by direct methods. Eur J Biochem 270:4082-4088

Folsch J, Less M, Stanley S (1957) A simple method for the isolation and purification of total lipids from animal tissues. J Biol Chem 226:497–509

Fowler T, Rey MW, Vaha-Vahe P, Power SD, Berka RM (1993) The catR gene encoding a catalase from *Aspergillus niger*: primary structure and elevated expression through increased gene copy number and use of a strong promoter. Mol Microbiol 9:989–998

Fraaije MW, Roubroeks HP, Hagen WR, Van-Berkel WJ (1996) Purification and characterization of an intracellular catalase-peroxidase from *Penicillium simplicissimum*. Eur J Biochem 235:192-198

Fruk L, Kuo C-H, Torres E, Niemeyer CM (2009) Apoenzyme reconstitution as a chemical tool for structural enzymology and biotechnology. Angew Chem Int Ed 48:1550–1574

Fu C, Maier RJ (1992) Nickel-dependent reconstitution of hydrogenase apoprotein in *Bradyrhizobium japonicum* Hupc mutants and direct evidence for a nickel metabolism locus involved in nickel incorporation into the enzyme. Arch Microbiol 157:493- 498

Galston AW, Bonnichsen RK, Arnon DI (1952) The preparation of highly purified spinach leaf catalase. Acta Chem Scand 5:781-790

Garcia P, Bruix M, Rico M, Ciofi-Baffoni S, Banci L, Shastry MCR, Roder H, Woodyear T de Lumley, Johnson CM, Fersht AR, Barker PD (2005) Effects of heme on the structure of the denatured state and folding kinetics of cytochrome b562. J Mol Biol 346:331–344

Garre V, Muller U, Tudzynski P (1998) Cloning, characterization, and targeted disruption of cpcat1, coding for an in planta secreted catalase of *Claviceps purpurea.* Mol Plant Microbe Interact 11:772–783

Gebicka L, Gebicki JL (1998) Interaction of sodium bis (2-ethylhexyl) sulfosuccinate (AOT) with catalase and horseradish peroxidase in an aqueous solution and in the reverse micelles of AOT/*n*-heptane. Biochem Mol Biol Int 45:805-811

Gilardi G, Meharenna YT, Tsotsou GE, Sadeghi SJ, Fairhead M, Giannini S (2002) Molecular Lego: design of molecular assemblies of P450 enzymes for nanobiotechnology. Biosens Bioelectron 17:133–145

Gilles-Gonzalez M-A, Gonzalez G (2005) Heme-based sensors: defining characteristics, recent developments, and regulatory hypotheses. J Inorg Biochem 99:1–22

Goldberg I, Hochman A (1989) Three different types of catalases in *Klebsiella pneumoniae*. Arch Biochem Biophys 268:124-128

Gooding JJ (2005) Nanostructuring electrodes with carbon nanotubes: A review on electrochemistry and applications for sensing. Electrochim Acta 50:3049–3060

Goswami P, Cooney JJ (1999) Sub-cellular localization of enzymes involved in oxidation of *n*-alkane by *Cladosporium resinae*. Appl Microbiol Biotechnol 51:860–864

Gruft H, Ruck R, Traynor J (1978) Properties of a unique catalase isolated from *Aspergillus niger.* Can J Biochem 56:916–919

Guan L, Scandalios JG (1995) Developmentally related responses of maize catalase genes to salicylic acid. Proc Natl Acad Sci USA 92:5930-5934

Guengerich FP (1991) Reactions and significance of cytochrome P-450 enzymes. J Biol Chem 266:10019–10022

Hamachi I, Tanaka S, Shinkai S (1993) Light-driven activation of reconstituted myoglobin with a ruthenium tris (2, 2'-bipyridine) pendant. J Am Chem Soc 115:10458-10459

Haraguchi H, Mochida Y, Sakai S, Masuda H, Tamura Y, Mizutani K, Tanaka O, Chou WH (1996) Protection against oxidative damage by dihydroflavonols in *Engelhardtia chrysolepis*. Biosci Biotechnol Biochem 60:945–948

Hargrove MS, Singleton EW, Quillin ML, Ortiz LA, Phillips GNJr, Olson JS (1994) His^{64} (E7) → Tyr apomyoglobin as a reagent for measuring rates of hemin dissociation. J Biol Chem 269:4207-4214

Harris RZ, Newmyer SL, Ortiz de Montellano PR (1993) Horseradish peroxidase-catalyzed two-electron oxidations. Oxidation of iodide, thioanisoles, and phenols at distinct sites. J Biol Chem 268:1637- 1645

Hartig A, Ruis H (1986) Nucleotide sequence of the *Saccharomyces cerevisiae* CTT1 gene and deduced amino-acid sequence of yeast catalase T. Eur J Biochem 160:487-490

Herbert D, Pinsent J (1948) Crystalline bacterial catalase. Biochem J 43:193-202

Hill KE, Wharton DC (1978) Reconstitution of the apoenzyme of cytochrome oxidase from *Pseudomonas aeruginosa* with heme d_1 and other heme groups. J Biol Chem 253:489-495

Hochman A, Goldberg I (1991) Purification and characterization of a catalase-peroxidase and a typical catalase from the bacterium *Klebsiella pneumoniae.* Biochim Biophys Acta 1077:299-307

Hochman A, Shemesh A (1987) Purification and characterization of a catalase-peroxidase from the photosynthetic bacterium *Rhodopseudomonas capsulata*. J Biol Chem 262:6871-6876

Hodgson E, Levi PE (1998) Interaction of piperonyl butoxide with cytochrome P450. In: Piperonyl butoxide: the insecticide synergist. Academic Press, London 41-54

Honeychurch MJ, Hill HAO, Wong LL (1999) The thermodynamics and kinetics of electron transfer in the cytochrome $P450_{cam}$ enzyme system. FEBS Lett 451:351-353

Hong J, Moosavi-Movahedi AA, Ghourchian H, Rad AM, Rezaei-Zarchi S (2007) Direct electron transfer of horseradish peroxidase on Nafion-cysteine modified gold electrode. Electrochim Acta 52:6261–6267

Hu N (2001) Direct electrochemistry of redox proteins or enzymes at various film electrodes and their possible applications in monitoring some pollutants. Pure Appl Chem 73:1979–1991

Hu Y, Fay AW, Ribbe MW (2005) Identification of a nitrogenase FeMo cofactor precursor on NifEN complex. Proc Natl Acad Sci USA 102:3236- 3241

Huang H, Hu N, Zeng Y, Zhou G (2002) Electrochemistry and electrocatalysis with heme proteins in chitosan biopolymer films. Anal Biochem 308:141-151

Igarashi T, Kono Y, Tanaka K (1996) Molecular cloning of manganese catalase from *Lactobacillus plantarum*. J Biol Chem 271:29521-29524

Ikeda T (1992) Electrochemical biosensors based on biocatalyst electrodes. Bull Electrochem 8:145–159

Imai Y (1976) The use of 8-aminooctyl sepharose for the separation of some components of hepatic microsomal electron transfer system. J Biochem 80:267–276

Ito O, Nakamura Y, Tan L, Ishizuka T, Sasaki Y, Minami N, Kanazawa M, Ito S, Sasano H, Kohzuki M (2006) Expression of cytochrome P-450 4 enzymes in the kidney and liver: regulation by PPAR and species-difference between rat and human. Mol Cell Biochem 284:141-148

Iwuoha EI, Joseph S, Zhang Z, Smyth MR, Fuhr U, Ortiz de Montellano PR (1998) Drug metabolism biosensors: electrochemical reactivities of cytochrome $P450_{cam}$ immobilised in synthetic vesicular systems. J Pharm Biomed Anal 17:1101-1110

Iwuoha EI, Wilson A, Howel M, Mathebe NGR, Montane-Jaime K, Narinesingh D, Guiseppi-Elie A (2004) Cytochrome P4502D6 (CYP2D6) bioelectrode for fluoxetine. Anal Lett 37: 929-941

Jia F, Shan C, Li F, Niu L (2008) Carbon nanotube/gold nanoparticles/polyethylenimine-functionalized ionic liquid thin film composites for glucose biosensing. Biosens Bioelectron 24:945–950

Jiang HJ, Yang H, Akins DL (2008) Direct electrochemistry and electrocatalysis of catalase immobilized on a SWNT-nanocomposite film. J Electroanal Chem 623:181-186

Joseph S, Rusling JF, Lvov YM, Friedberg T, Fuhr U (2003) An amperometric biosensor with human CYP3A4 as a novel drug screening tool. Biochem Pharmacol 65: 1817-1826

Kagawa M, Murakoshi N, Nishikawa Y, Matsumoto G, Kurata Y, Mizobata T, Kawata Y, Nagai J (1999) Purification and cloning of a thermostable manganese catalase from a thermophilic bacterium. Arch Biochem Biophys 362:346–355

Kang YS, Lee DH, Yoon BJ, Oh DC (2006) Purification and characterization of a catalase from photosynthetic bacterium *Rhodospirillum rubrum* S1 grown under anaerobic conditions. J Microbiol 44:185-191

Karlsson J, Nilsson T (2005) The C subunit of *Ideonella dechloratans* chlorate reductase: expression, purification, refolding, and heme reconstitution. Protein Expres Purif 41:306–312

Kawasaki L, Wysong D, Diamond R, Aguirre J (1997) Two divergent catalase genes are differentially regulated during *Aspergillus nidulans* development and oxidative stress. J Bacteriol 179:3284–3292

Kazlauskaite J, Westlake ACG, Wong LL, Hill HAO (1996) Direct electrochemistry of cytochrome $P450_{cam}$. Chem Commun 18:2189-2190

Kikuchi-Torii K, Hayashi S, Nakamoto H, Nakamura S (1982) Properties of *Aspergillus niger* catalase. J Biochem (Tokyo) 92:1449–1456

Kim HJ, Chun HS, Yang R (2000) Inhibition of benzo[a]pyreneinduced cytotoxicity and cytochrome P450 1A activity by dietaryflavonoids in human liver cell model: structure–activity relationship. Biotechnol Lett 22:1941–1946

Klingenberg M (1958) Pigments of rat liver microsomes. Arch Biochem Biophys 75:376-386

Klotz MG, Klassen GR, Loewen PC (1997) Phylogenetic relationships among prokaryotic and eukaryotic catalases. Mol Biol Evol 14:951–958

Klotz MG, Loewen PC (2003) The molecular evolution of catalytic hydroperoxidases: evidence for multiple lateral transfer of genes between prokaryota and from bacteria into eukaryota. Mol Biol Evol 20:1098–1112

Kono Y, Fridovich I (1983) Isolation and characterization of the pseudocatalase of *Lactobacillus plantarum.* J Biol Chem 258:6015-6019

Koops DR, Casazza JP (1985) Identification of ethanol-inducible P-450 isozyme 3a as the acetone and acetol monooxygenase of rabbit microsomes. J Biol Chem 260:13607–13612

Kumar AK, Goswami P (2006) Functional characterization of alcohol oxidases from *Aspergillus terreus* MTCC 6324. Appl Microbiol Biotechnol 72:906–911

Kumar AK, Goswami P (2008) Purification and properties of a novel broad substrate specific alcohol oxidase from *Aspergillus terreus* MTCC 6324. Biochim Biophys Acta 1784:1552–1559

Kumar AK, Vatsyayan P, Goswami P (2010) Production of lipid and fatty acids during growth of *Aspergillus terreus* on hydrocarbon substrates. Appl Biochem Biotechnol 160: 1293-1300

Laemmli UK (1970) Cleavage of structural proteins during the assembly of the head of bacteriophage T4. Nature 227:680–685

Lai ME, Bergel A (2002) Direct electrochemistry of catalase on glassy carbon electrodes. Bioelectrochemistry 55:157-160

Lardinois OM, Mestdagh MM, Rouxhet PG (1996) Reversible inhibition and irreversible inactivation of catalase in presence of hydrogen peroxide. Biochim Biophys Acta 1295:222–238

Lardinois OM, Rouxhet PG (1996) Peroxidatic degradation of azide by catalase and irreversible enzyme inactivation. Biochim Biophys Acta 1298:180–190

Laviron E (1979) General expression of the linear potential sweep voltammogram in the case of diffusionless electrochemical systems. J Electroanal Chem 101:19–28

Lei C, Wollenberger U, Jung C, Scheller FW (2000) Claybridged electron transfer between cytochrome CYP101 and electrode. Biochem Biophys Res Commun 268:740–744

Lemberg R, Barrett J (1973) Cytochromes. Academic Press, New York

Lemberg R, Foulkes EC (1948) Reaction between catalase and hydrogen peroxide. Nature 161:131-132

Lentz O, Urlacher V, Schmid RD (2004) Substrate specificity of native and mutated cytochrome P450 (CYP102A3) from *Bacillus subtilis*. J Biotechnol 108:41-49

Levy E, Eyal Z, Hochman A (1992) Purification and characterization of a catalase-peroxidase from the fungus *Septoria tritici*. Arch Biochem Biophys 296:321-327

Lewis DFV (1996) Cytochromes P450: structure, function and mechanism. Taylor & Francis, London

Li M, He P, Zhang Y, Hu N (2005) An electrochemical investigation of hemoglobin and catalase incorporated in collagen films. Biochim Biophys Acta 1749:43-51

Li YM, Chen XT, Li J, Liu HH (2004) Direct voltammetry and catalysis of hemoenzymes in methyl cellulose film. Electrochim Acta 49:3195-3200

Liu HH, Tian ZQ, Lu ZX, Zhang ZL, Zhang M, Pang DW (2004) Direct electrochemistry and electrocatalysis of heme-proteins entrapped in agarose hydrogel films. Biosens Bioelectron 20:294–304

Lo KKW, Wong LL, Hill HAO (1999) Surface-modified mutants of cytochrome CYP101 enzymatic properties and electrochemistry. FEBS Lett 451:342–346

Loew O (1901) Catalase, a new enzym of general occurrence. Report No. 68, US Dept. Agri., Washington, 47-55

Lopez-Medrano R, Ovejero MC, Calera JA, Puente P, Leal F (1995) An immunodominant 90-kilodalton *Aspergillus fumigatus* antigen is the subunit of a catalase. Infect Immun 63:4774–4780

Lotzbeyer T, Schuhmann W, Schmidt HL (1996) Electron transfer principles in amperometric biosensors: direct electron transfer between enzymes and an electrode surface. Sensor Actuat B 33:50–54

Lu AYH, Kuntzman R, West S, Conney AH (1972) Reconstituted liver microsomal enzyme system that hydroxylates drugs, other foreign compounds, and endogenous substrates. I. Determination of substrate specificity by the cytochrome P-450 and P-448 fractions. Biochem Biophys Res Commun 42:1200–1206

Lu HY, Li Z, Hu NF (2003) Direct voltammetry and electrocatalytic properties of catalase incorporated in polyacrylamide hydrogel films. Biophys Chem 104:623-632

Lvov YM, Lu Z, Schenkman JB, Zu X, Rusling JF (1998) Direct electrochemistry of myoglobin and cytochrome $P450_{cam}$ in alternate layer-by-layer films with DNA and other polyions. J Am Chem Soc 120:4073-4080

Mayhew MP, Reipa V, Holden MJ, Vilker VL (2000) Improving the cytochrome P450 enzyme system for electrode-driven biocatalysis of styrene epoxidation. Biotechnol Prog 16:610-616

Melik-Adamyan WR, Barynin VV, Vagin AA, Borisov VV, Vainshtein BK, Fita I, Murthy MR, Rossmann MG (1986) Comparison of beef liver and *Penicillium vitale* catalases. J Mol Biol 188:63-72

Mello LD, Alves AA, Macedo DV, Kubota LT (2005) Peroxidase-based biosensor as a tool for a fast evaluation of antioxidant capacity of tea. Food Chem 92:515–519

Mello LD, Kubota LT (2007) Biosensors as a tool for the antioxidant status evaluation. Talanta 72:335–348

Mfincnerovfi D, Augustin J (1994) Fungal metabolism and detoxification of polycyclic aromatic hydrocarbons: a review. Biores Technol 48:97–106

Mie Y, Kishita M, Neya S, Funasaki N, Mizutani F, Nishiyama K, Taniguchi I (2006) Electrochemical analysis of heme functions of myoglobin using semi-artificial myoglobins. J Electroanal Chem 588:226-234

Mitra S (1994) Stereochemical structure and biochemical activity of heme proteins. Proc Indian Acad Sci (Chem Sci) 106:729-734

Modrzejewska B, Guwy AJ, Dinsdale R, Hawkes DL (2007) Measurement of hydrogen peroxide in an advanced oxidation process using an automated biosensor. Water Res 41:260– 268

Mokrasch LC (1953) Analysis of hexose phosphates and sugar mixtures with the anthrone reagent. J Biol Chem 208:55-59

Monti D, Baldaro E, Riva S (2003) Separation and characterization of two catalase activities isolated from the yeast *Trigonopsis variabilis*. Enzyme Microb Technol 32:596-605

Munge B, Estavillo C, Schenkman JB, Rusling JF (2003) Optimisation of electrochemical and peroxide-driven oxidation of styrene with ultrathin polyion films containing $P450_{cam}$ and myoglobin. Chembiochem 4:82-89

Murphy L (2006) Biosensors and bioelectrochemistry. Curr Opin Chem Biol 10:177–184

Nagao A, Maeda M, Lim BP, Kobayashi H, Terao J (2000) Inhibition of β-carotene-15,15*-dioxygenase activity by dietary flavonoids. J Nutr Biochem 11:348–355

Nagy JM, Cass AE, Brown KA (1997) Purification and characterization of recombinant catalase-peroxidase, which confers isoniazid sensitivity in *Mycobacterium tuberculosis*. J Biol Chem 272:31265-31271

Nakayama N, Shoun H (1994) Fatty acid hydroxylase of the fungus *Fusarium oxysporum* is possibly a fused protein of cytochrome P-450 and its reductase. Biochem Biophys Res Commun 202:586–590

Nakayama N, Takemae A, Shoun H (1996) Cytochrome P450foxy, a catalytically self-sufficient fatty acid hydroxylase of the fungus *Fusarium oxysporum*. J Biochem 119:435–440

Navarro RE, Stringer MA, Hansberg W, Timberlake WE, Aguirre J (1996) *catA,* a new *Aspergillus nidulans* gene encoding a developmentally regulated catalase. Curr Genet 29:352–359

Neya S, Funasaki N, Shiro Y, Iizuka T, Imai K (1994) Consequence of rapid heme rotation to the oxygen binding of myoglobin. Biochim Biophys Acta 1208:31-37

Neya S, Nakamura M, Imai K, Hori H, N Funasaki (1996) Functional comparison of the myoglobins reconstituted with symmetric deuterohemes. Biochim Biophys Acta 1296:245-249

Nicolini C, Erokhin V, Ghisellini P, Paternolli C, Ram MK, Sivozhelezov V (2001) P-450scc engineering and nanostructuring for cholesterol sensing. Langmuir 17:3719–3726

O'Brien KB, Killoran SJ, O'Neill RD, Lowry JP (2007) Development and characterization *in vitro* of a catalase-based biosensor for hydrogen peroxide monitoring. Biosens Bioelectron 22:2994–3000

Obinger C, Regelsberger G, Strasser G, Burner U, Peschek GA (1997) Purification and characterization of a homodimeric catalase-peroxidase from the cyanobacterium *Anacystis nidulans*. Biochem Biophys Res Commun 235:545-552

Ogawa J, Sulistyaningdyah WT, Li QS, Tanaka H, Xie SX, Kano K, Ikeda T, Shimizu S (2004) Two extracellular proteins with alkaline peroxidase activity, a novel cytochrome c and a catalase-peroxidase, from *Bacillus sp.* No.13. Biochim Biophys Acta 1699:65-75

Okado-Matsumoto A, Fridovich I (2001) Subcellular distribution of superoxide dismutases (SOD) in rat liver: Cu, Zn–SOD in mitochondria. J Biol Chem 276:38388–38393

Oku Y, Ohtaki A, Kamitori S, Nakamura N, Yohda M, Ohno H, Kawarabayashi Y (2004) Structure and direct electrochemistry of cytochrome P-450 from the thermoacidophilic crenarchaeon *Sulfolobus tokodaii* strain 7. J Inorg Biochem 98:1194–1197

Omura T (1999) Forty years of cytochrome P450. Biochem Biophy Res Comm 266:690–698

Omura T, Sato R (1962) A new cytochrome in liver microsomes. J Biol Chem 237:1375–1376

Omura T, Sato R (1964a) The carbon monoxide-binding pigment of liver microsomes. I. evidence for its hemoprotein Nature. J Biol Chem 239:2370–2378

Omura T, Sato R (1964b) The carbon monoxide-binding pigment of liver microsomes. II. solubilization, purification, and properties. J Biol Chem 239:2379–2385

Ortiz de Montellano PR, De Voss JJ (2005) Cytochrome P450: Structure, Mechanism and Biochemistry. (Ortiz de Montellano PR, ed), Kluwer Academic/Plenum Publishers, New York, 183–245

Panicco P, Astuti Y, Fantuzzi A, Durrant JR, Gilardi G (2008) P450 versus P420: correlation between cyclic voltammetry and visible absorption spectroscopy of the immobilized heme domain of cytochrome P450 BM3. J Phys Chem B 112:14063–14068

Paternolli C, Antonini M, Ghisellini P, Nicolini C (2004) Recombinant cytochrome P450 immobilization for biosensor applications. Langmuir 20:11706-11712

Porter TD, Kasper CB (1986) NADPH-cytochrome P-450 oxidoreductase: flavin mononucleotide and flavin adenine dinucleotide domains evolved from different flavoproteins. Biochemistry 25:1682–1687

Poulos TL (1995) Cytochrome P450. Curr Opin Struc Biol 5:767–774

Poulos TL (2005) Structural and functional diversity in heme monooxygenases. Drug Met Dispo 33:10–18

Prakash PA, Yogeswara U, Chen SM (2009a) A review on direct electrochemistry of catalase for electrochemical sensors. Sensors 9:1821-1844

Prakash PA, Yogeswaran U, Chen SM (2009b) Direct electrochemistry of catalase at multiwalled carbon nanotubes-nafion in presence of needle shaped DDAB for H_2O_2 sensor. Talanta 78:1414-1421

Prieto-Simon B, Cortina M, Campas M, Calas-Blanchard C (2008) Electrochemical biosensors as a tool for antioxidant capacity assessment. Sensor Actuat B 129:459–466

Putnam CD, Arvai AS, Bourne Y, Tainer JA (2000) Active and inhibited human catalases structures: Ligand and NADPH binding and catalytic mechanism. J Mol Biol 296:295-309

Rahimi P, Rafiee-Pour HA, Ghourchian H, Norouzi P, Ganjali MR (2010) Ionic-liquid/NH_2-MWCNTs as a highly sensitive nano-composite for catalase. Biosens Bioelectron 25:1301–1306

Reipa V, Mayhew MP, Holden MJ, Vilker VL (2002) Redox control of the $P450_{cam}$ catalytic cycle: effects of Y96F active site mutations and binding of a non-natural substrate. Chem Commun 4:318– 319

Reipa V, Mayhew MP, Vilker VL (1997) A direct electrode-driven P450 cycle for biocatalysis. Proc Natl Acad Sci 94:13554-13558

Ro YT, Lee HI, Kim EJ, Koo JH, Kim E, Kim YM (2003) Purification, characterization, and physiological response of a catalase-peroxidase in *Mycobacterium sp.* strain JC1 DSM 3803 grown on methanol. FEMS Microbiol Lett 226:397-403

Rochefort D, Kouisni L, Gendron K (2008) Physical immobilization of laccase on an electrode by means of poly(ethyleneimine) microcapsules. J Electroanal Chem 217:53–63

Rover LJr, Kubota LT, Hoehr NF (2001) Development of an amperometric biosensor based on glutathione peroxidase immobilized in a carbodiimide matrix for the analysis of reduced glutathione from serum. Clin Chim Acta 308:55-67

Rubianes MD, Rivas GA (2007) Dispersion of multi-wall carbon nanotubes in polyethylenimine: A new alternative for preparing electrochemical sensors. Electrochem Commun 9:480–484

Rusling JF, Zhang Z (2003) Designing functional biomolecular films on electrodes. In: Biomolecular Films: Design, Function and Applications (J Rusling, ed), Marcel Dekker Inc, New York, USA

Rusling JF, Zhou L, Munge B, Yang J, Estavillo C, Schenkmann JB (2000) Applications of polyion films containing biomolecules to sensing toxicity. Faraday Discuss 116:1–11

Sakiyama-Elbert S, Hubbell J (2001) Functional biomaterials: Design of novel biomaterials. Annu Rev Mater Res 31:183-201

Salimi A, Noorbakhsh A, Ghadermarz M (2005) Direct electrochemistry and electrocatalytic activity of catalase incorporated onto multiwall carbon nanotubes-modified glassy carbon electrode. Anal Biochem 344:16-24

Salimi A, Sharifi E, Noorbakhsh A, Soltanian S (2007) Direct electrochemistry and electrocatalytic activity of catalase immobilized onto electrodeposited nano-scale islands of nickel oxide. Biophys Chem 125:540-548

Sana TR, Waddell K, Fischer SM (2008) A sample extraction and chromatographic strategy for increasing LC/MS detection coverage of the erythrocyte metabolome. J Chromatogr B 871:314–321

Sarma AK, Vatsyayan P, Goswami P, Minteer SD (2009) Recent advances in material science for developing enzyme electrodes. Biosens Bioelectron 24:2313-2322

Scheller F, Renneberg R, Schwarze W, Strnad G, Pommerening K, Prumke HJ, Mohr P (1979) Electrochemical investigations on the oxygen activation by cytochrome P450. Acta Biol Med Germ 38:503-509

Scheller U, Kraft R, Karl-Ludwig S, Schunck WH (1994) Generation of the soluble and functional cytosolic domain of microsomal cytochrome P450 52A3. J Biol Chem 269:12779–12783

Scheller U, Zimmer T, Kaergel E, Schunck WH (1996) Characterization of the *n*-alkane and fatty acid hydroxylating cytochrome P450 forms 52A3 and 52A4. Arch Biochem Biophys 328:245–254

Schnuck WH, Riege P, Honeck H, Muller HG (1983) Isolation and reconstitution of the alkane monooxygenase system from the yeast *Lodderomyces elongisporus.* Z Allg Mikrobiol 23:653–660

Schonbaum GR, Chance B (1976) Catalase. In: The Enzymes (Boyer PD, ed), Academic Press, New York, USA 13:363-408

Schroeder WA, Shelton JR, Shelton JB, Robberson B, Apell G, Fang RS, Bonaventura J (1982) The complete amino acid sequence of bovine liver catalase and the partial sequence of bovine erythrocyte catalase. Arch Biochem Biophys 214:397-421

Schulz H, Pellicioli EC, Thoeny-Meyer L (2000) New insights into the role of CcmC, CcmD and CcmE in the haem delivery pathway during cytochrome c maturation by a complete mutational analysis of the conserved tryptophan-rich motif of CcmC. Mol Microbiol 37:1379–1388

Segrest JP, Jackson RL (1972) Molecular weight determination of glycoproteins by polyacrylamide gel electrophoresis in sodium dodecyl sulfate. Method Enzymol 28:54-63

Shah VK, Allen JR, Spangler NJ, Ludden PW (1994) *In vitro* synthesis of the iron-molybdenum cofactor of nitrogenase. Purification and characterization of NifB cofactor, the product of NIFB protein. J Biol Chem 269:1154- 1158

Shen L, Hu N (2004) Heme protein films with polyamidoamine dendrimer: direct electrochemistry and electrocatalysis. Biochim Biophys Acta 1608:23–33

Shumyantseva VV, Bulko TV, Archakov AI (2005) Electrochemical reduction of cytochrome P450 as an approach to the construction of biosensors and bioreactors. J Inorg Biochem 99:1051-1063

Shumyantseva VV, Bulko TV, Bachmann TT, Bilitewski U, Schmid RD, Archakov AI (2000) Electrochemical reduction of flavocytochromes 2B4 and 1A2 and their catalytic activity. Arch Biochem Biophys 377:43-48

Shumyantseva VV, Ivanov YD, Bistolas N, Scheller FW, Archakov AI, Wollenberger U (2004) Direct electron transfer of cytochrome P450 2B4 at electrodes modified with nonionic detergent and colloidal clay nanoparticles. Anal Chem 76: 6046-6052

Sichak SP, Dounce AL (1986) Analysis of the peroxidatic mode of action of catalase. Arch Biochem Biophys 249:286-295

Smith GCM, Tew DG, Wolf CR, (1994) Dissection of NADPH cytochrome P450 oxidoreductase into distinct functional domains. Proc Natl Acad Sci USA 91:8710–8714

Spiro TG, Jarzecki AA (2001) Heme-based sensors: theoretical modeling of heme-ligand–protein interactions. Curr Opin Chem Biol 5:715–723

Stern KG (1936) The constitution of the prosthetic group of catalase. J Biol Chem 112:661-669

Stoilov I, Jansson I, Sarfarazi M, Schenkman JB (2001) Roles of cytochrome P450 in development. Drug Metabol Drug Interact 18:33-55

Sugihara N, Ogoma Y, Abe K, Kondo Y, Akaike T (1998) Immobilization of cytochrome P450 and electrochemical control of its activity. Polym Adv Technol 9:307-313

Sumner JB, Dounce AL (1937) Crystalline catalase. J Biol Chem 121:417-424

Sun YX, Wang SF (2007) Direct electrochemistry and electrocatalytic characteristic of heme proteins immobilized in a new sol–gel polymer film. Bioelectrochemistry 71:172-179

Switala J, Loewen PC (2002) Diversity of properties among catalases. Arch Biochem Biophys 401:145–154

Takasuka T, Sayers NM, Anderson MJ, Benbow EW, Denning DW (1999) *Aspergillus fumigatus* catalases: cloning of an *Aspergillus nidulans* catalase B homologue and evidence for at least three catalases. FEMS Immunol Med Microbiol 23:125–133

Teale FWJ (1959) Cleavage of the haem-protein link by acid methylethylketone. Biochim Biophys Acta 35:543

Thompson VS, Schaller KD, Apel WA (2003) Purification and characterization of a novel thermo-alkali-stable catalase from *Thermus brockianus*. Biotechnol Prog 19:1292-1299

Tsai YC, Chen JM, Li SC, Marken F (2004) Electroanalytical thin film electrodes based on a Nafion™ – multi-walled carbon nanotube composite. Electrochem Commun 6:917–922

Udit AK, Gray HB (2005) Electrochemistry of heme-thiolate proteins. Biochem Biophys Res Commun 338:470-476

Udit AK, Hill MG, Bittner VG, Arnold FH, Gray HB (2004) Reduction of dioxygen catalysed by pyrene-wired heme domain cytochrome P450 BM3 electrodes. J Am Chem Soc 126:10218-10219

Udit AK, Hindoyan N, Hill MG, Arnold FH, Gray HB (2005) Protein-surfactant film voltammetry of wild-type and mutant cytochrome P450 BM3. Inorg Chem 44: 4109-4111

Urlacher VB, Eiben S (2006) Cytochrome P450 monooxygenases: perspectives for synthetic application. Trends Biotechnol 24:324-330

Vainshtein BK, Melik-Adamyan WR, Barynin VV, Vagin AA, Grebenko AI, Borisov VV, Bartels KS, Fita I, Rossmann MG (1986) Three-dimensional structure of catalase from *Penicillium vitale* at 2.0 Å resolution. J Mol Biol 188:49–61

Van den Heuvel RHH, Fraaije MW, Mattevi A, Laane C, van Berkel WJH (2001) Vanillyl-alcohol oxidase, a tasteful biocatalyst. J Mol Catal B: Enzym 11:185–188

von Ossowski I, Mulvey MR, Leco PA, Borys A, Loewen PC (1991) Nucleotide sequence of *Escherichia coli* katE, which encodes catalase HPII. J Bacteriol 173:514-520

Wan LS, Ke BB, Wu J, Xu ZK (2007) Catalase immobilization on electrospun nanofibers: effects of porphyrin pendants and carbon nanotubes. J Phys Chem C 111:14091-14097

Wan LS, Ke BB, Xu ZK (2008) Electrospun nanofibrous membranes filled with carbon nanotubes for redox enzyme immobilization. Enzyme Microb Technol 42:332-339

Wang JX, Li MX, Shi ZJ, Li NQ, Gu ZN (2002) Direct electrochemistry of cytochrome c at a glassy carbon electrode modified with single-wall carbon nanotubes. Anal Chem 74:1993–1997

Wang L, Wang J, Zhou F (2004) Direct electrochemistry of catalase at a gold electrode modified with single-wall carbon nanotubes. Electroanal 16:627-632

Wang M, Roberts DL, Paschke R, Shea TM, Masters BSS, Kim JP (1997) Three-dimensional structure of NADPH-cytochrome P450 reductase: prototype for FMN- and FAD containing enzymes. Proc Natl Acad Sci USA 94:8411–8416

Wang SF, Chen T, Zhang ZL, Pang DW, Wong KL (2007) Effects of hydrophilic room temperature ionic liquid 1-butyl-3-methylimidazolium tetrafluoroborate on direct electrochemistry and bioelectrocatalysis of heme proteins entrapped in agarose hydrogel films. Electrochem Commun 9:1709-1714

Wang W-H, Lu J-X, Yao P, Xie Y, Huang Z-X (2003) The distinct heme coordination environments and heme-binding stabilities of His39Ser and His39Cys mutants of cytochrome b5. Prot Eng 16:1047-1054

Warburg O (1923) Experiments on surviving carcinoma tissue. Biochem J 142:317-333

Wasserman BP, Hultin HO (1981) Effect of deglycosylation on the stability of *Aspergillus niger* catalase. Arch Biochem Biophys 212:385–392

White RE, Coon MJ (1980) Oxygen activation by cytochrome P-450. Ann Rev Biochem 49:315–356

Wieland H, Franke W (1927) About the mechanism of Oxidation. XII. The activation of hydrogen peroxide by iron. Liebigs Ann Chem 457:1–70

Wirtz M, Klucik J, Rivera M (2000) Ferredoxin-mediated electrocatalytic dehalogenation of haloalkanes by cytochrome $P450_{cam}$. J Am Chem Soc 122:1047-1056

Wong JY, Bronzion JD (ed) (2003) Biomaterials: Principles and applications. CRC Press, Boca Raton, FL

Wu Y, Shen Q, Hu S (2006) Direct electrochemistry and electrocatalysis of heme-proteins in regenerated silk fibroin film. Anal Chim Acta 558:179-186

Xuan GS, Jung S, Kim S (2004) Electrocatalytic reduction of nitric oxide by cytochrome P450-modified gold electrodes. Bull Korean Chem Soc 25:165-166

Yoshida T, Kikuchi G (1978) Purification and properties of heme oxygenase from pig spleen microsomes. J Biol Chem 253:4224-4229

Zamocky M, Janecek S, Koller F (1997) The area of the main substrate channel is highly conserved among all true catalases. Biologia 52:723-730

Zamocky M, Koller F (1999) Understanding the structure and function of catalases: clues from molecular evolution and *in vitro* mutagenesis. Prog Biophys Mol Biol 72:19–66

Zhang B, Zhang Z, Wang B, Yan J, Li J, Cai SM (2001) Preparation of gold nano-arraied electrode on silicon substrate and its electrochemical properties: Probe into biosensor based on electroluminescence of porous silicon. Acta Chimi Sin 59:1932-1936

Zhang Z, Chouchane S, Magiliozzo RS, Rusling JF (2002) Direct voltammetry and catalysis with *Mycobacterium tuberculosis* catalaseperoxidase, peroxidases and catalase in lipid films. Anal Chem 74:163–170

Zhang Z, Nassar AEF, Lu Z, Schenkman JB, Rusling JF (1997) Direct electron injection from electrodes to cytochrome $P450_{cam}$ in biomembrane-like films. J Chem Soc Faraday Trans 93:1769-1774

Zhou B, Wang J, Gao X, Tian Y (2008a) Attachment of nanoparticles to pyrolytic graphite electrode and its application for the direct electrochemistry and electrocatalytic behavior of catalase. Anal Lett 41:1832-1849

Zhou H, Lu TH, Shi HX, Dai ZH, Huang XH (2008b) Direct electrochemistry and electrocatalysis of catalase immobilized on multi-wall carbon nanotubes modified glassy carbon electrode and its application. J electroanal Chem 612:173-178

Zhu Y, Nomura T, Xu Y, Zhang Y, Peng Y, Mao B, Hanada A, Zhou H, Wang R, Li P, Zhu X, Mander LN, Kamiya Y, Yamaguchi S, He Z (2006) Elongated uppermost internode encodes a cytochrome P450 monooxygenase that epoxidizes gibberellins in a novel deactivation reaction in rice. Plant Cell 18:442-456

Zu X, Lu Z, Zhang Z, Schenkman JB, Rusling JF (1999) Electroenzyme-catalyzed oxidation of styrene and cis-methylstyrene using thin films of cytochrome $P450_{cam}$ and myoglobin. Langmuir 15:7372–7377

List of Publications

I. In Referred Journals

Preety Vatsyayan, A. Kiran Kumar, Papori Goswami, Pranab Goswami, Broad substrate Cytochrome P450 monooxygenase activity in the cells of *Aspergillus terreus* MTCC 6324, Bioresource Technology 99 (2008) 68–75.

Preety Vatsyayan, Sandip Bordoloi and Pranab Goswami, Large catalase based bioelectrode for biosensor application, Biophysical Chemistry, 153 (2010) 36–42.

Preety Vatsyayan and Pranab Goswami, Acidic pH conditions induce dissociation of the haem from the protein and destabilise the catalase isolated from *Aspergillus terreus* MTCC 6324, Biotechnology Letters, DOI: 10.1007/s10529-010-0442-2.

Anil Kumar Sarma, **Preety Vatsyayan**, Pranab Goswami, Shelley D. Minteer, Recent advances in material science for developing enzyme electrodes. Biosensors and Bioelectronics 24 (2009) 2313–2322.

A. Kiran Kumar, **Preety Vatsyayan**, and Pranab Goswami, Production of lipid and fatty acids during growth of *Aspergillus terreus* on hydrocarbon substrates, Applied Biochemistry and Biotechnology 160 (2010) 1293-1300.

Preety Vatsyayan and Pranab Goswami, Highly active and stable catalase from a hydrocarbon degrading *Aspergillus terreus* MTCC 6324 (communicated).

Preety Vatsyayan, Mitun Chakraborty, Sandip Bordoloi and Pranab Goswami, Direct electrochemistry of cytochrome P450 from *Aspergillus terreus* immobilized on MWCNT-NF/PEI modified glassy carbon electrode (communicated).

II. In Conferences

Preety Vatsyayan, A. Kiran Kumar, and Pranab Goswami, Characterization of alkane oxygenase produced by *Aspergillus terreus*. *46th Annual Conference, MICROBIOTECH 2005*, Hyderabad, 8-10 December, 2005, Page no: 103 (Ind 80).

Preety Vatsyayan and Pranab Goswami, Cytochrome-P450-monooxygenase of *Aspergillus terreus* MTCC 6324, *International Conference on design of biomaterials (BIND- 06),* IIT Kanpur, 8-11 December, 2006 (P:55).

A. Kiran Kumar, **Preety Vatsyayan** and Pranab Goswami, Purification and functional characterization of alcohol oxidases of *Aspergillus terreus* MTCC 6324, *SBCI,* JNU New Delhi, 8-11 December 2006 (PI:49).

Preety Vatsyayan, A. Balasubrahmanyam and Pranab Goswami, Electrochemical studies of cytochrome P450 monooxygenase for biofuel cell applications, *DM-ELANTE 2008*, *Indian Society for electroanalytical chemistry* (BARC, Mumbai) held at Munnar, Kerala, 25-28 February, 2008 (RS-6). **The work presented here was acknowledged with first prize.**

Preety Vatsyayan and Pranab Goswami, Studies on catalase for the construction of enzyme electrode for biosensor applications, *International Society of Biotechnology*, 2008, Gangtok, Sikkim, 28-30 December, 2008 (page no:22).

Preety Vatsyayan , A. Kiran Kumar , Pranab Goswami, A potential *Aspergillus terreus* strain for bioremediation of petroleum hydrocarbon, *International Congress of Environmental Research*, BITS – Pilani, Goa Campus, Goa. 18-20 December, 2008.

Preety Vatsyayan, Sandip Bordoloi, Lepakshi Barbora and Pranab Goswami, Direct electrochemistry of large novel catalase from *Aspergillus terreus* Immobilized on MWCNT-NF/PEI modified glassy carbon electrode and its fuel cell application, *Fucetech, 2009*, *International Symposium and Exhibition on Fuel Cell Technologies*, Mumbai, 11-13 November, 2009 (page no:82)

Sandip Bordoloi, **Preety Vatsyayan**, Pranab Goswami, Fabrication of carbon nanotube-based cholesterol oxidase bioelectrode for biosensor and biofuel cell application, *International Conference on Advanced Nanomaterial and Nanotechnology* (ICANN)-2009, Indian Institute of Technology Guwahati, December 9-11, 2009.

Pranab Goswami and **Preety Vatsyayan**, Application potential of large catalase from *Aspergillus terreus* MTCC 6324 for bioelectronic devices, International Conference on Molecular and Functional Catalysis, Singapore, 11-15 July 2010.